BRNO UNIVERSITY OF TECHNOLOGY

VYSOKÉ UČENÍ TECHNICKÉ V BRNĚ

FACULTY OF ELECTRICAL ENGINEERING AND COMMUNICATION

FAKULTA ELEKTROTECHNIKY
A KOMUNIKAČNÍCH TECHNOLOGIÍ

DEPARTMENT OF POWER ELECTRICAL AND ELECTRONIC ENGINEERING

ÚSTAV VÝKONOVÉ ELEKTROTECHNIKY A ELEKTRONIKY

LOSSES IN INDUCTION MACHINES SUPPLIED BY A FREQUENCY CONVERTER

ZTRÁTY V ASYNCHRONNÍCH STROJÍCH Nnapájených Z MĚNIČE FREKVENCE

MASTER'S THESIS

DIPLOMOVÁ PRÁCE

AUTHOR — Bc. Miroslav Lípa
AUTOR PRÁCE

SUPERVISOR — doc. Ing. Jan Bárta, Ph.D.
VEDOUCÍ PRÁCE

BRNO 2024

BRNO UNIVERSITY OF TECHNOLOGY
FACULTY OF ELECTRICAL ENGINEERING AND COMMUNICATION

Master's Thesis

Master's study program **Power Electrical and Electronic Engineering**

Department of Power Electrical and Electronic Engineering

Student: Bc. Miroslav Lípa ***ID:*** 220770

Year of study: 2 ***Academic year:*** 2023/24

TITLE OF THESIS:

Losses in induction machines supplied by a frequency converter

INSTRUCTION:

1. Conduct a literature review and describe the losses in asynchronous machines powered by a frequency converter.
2. Describe methods for measuring and evaluating losses in asynchronous machines powered by a frequency converter.
3. Perform experimental verification of losses on the specified asynchronous machine when powered by a frequency converter with varying switching frequencies.
4. Validate the measured data on an electromagnetic model of the asynchronous machine.

RECOMMENDED LITERATURE:

[1] P. C. Sen: Principles of Electric Machines and Power Electronics, ISBN: 9781118078877 (EN)

[2] Juha Pyrhonen , Valeria Hrabovcova , R. Scott Semken: Electrical Machine Drives Control : An Introduction, ISBN: 9781119260455 (EN)

[3] L. Aarniovuori, H. Kärkkäinen, A. Anuchin, J. J. Pyrhönen, P. Lindh and W. Cao, "Voltage-Source Converter Energy Efficiency Classification in Accordance With IEC 61800-9-2," in IEEE Transactions on Industrial Electronics, vol. 67, no. 10, pp. 8242-8251, Oct. 2020, doi: 10.1109/TIE.2019.2949526

Date of project specification: 5.2.2024 ***Deadline for submission:*** 20.5.2024

Supervisor: doc. Ing. Jan Bárta, Ph.D.

doc. Ing. Ondřej Vítek, Ph.D.
Chair of study program board

Abstract

The master's thesis deals with the measurement of an induction motor with two different power supplies, a frequency converter and a generator. Then these two power supplies were simulated using the finite element method and compared. The first chapter deals with the description of the asynchronous machine powered by the frequency converter and also the recommended modifications for this kind of power supply to avoid as many undesirable phenomena as possible. The second chapter deals with the losses of the asynchronous machine. The third chapter discusses the approach to measuring harmonic losses due to inverter power supply and also the standardized approach according to international standards. The second half of the third chapter also describes the computational analysis which is used in this thesis in the form of finite element analysis. Finally, the measurement uncertainties in the standard input-output method are described. In the fourth chapter, the modeling in ANSYS MAXWELL software is presented, where first the creation of a model of the specified machine is described, then its simulation with sinusoidal power supply, and in the second half the simulation with PWM power supply is explained and how the PWM was replicated using the measured waveforms. In the fifth section, all the measurement results are presented with figures to give a better idea of the results. At the end of the chapter, a comparison of the simulation and measurements and its lack of accuracy is presented.

Keywords

Induction motor, harmonic losses, frequency converter, induction motor losses, measurement of induction motor, electromagnetic model, finite element method, simulation comparison, additional losses.

Abstrakt

Diplomová práce se zabývá měřením asynchronního motoru se dvěma různými zdroji napájení, a to s frekvenčním měničem a generátorem. Tyto dva zdroje napájení byly následně simulovány pomocí metody konečných prvků a porovnány. První kapitola se zabývá popisem asynchronního stroje napájeného frekvenčním měničem a také doporučenými úpravami pro tento druh napájení, aby se předešlo co nejvíce nežádoucím jevům. Druhá kapitola se věnuje ztrátám asynchronního stroje. Třetí kapitola popisuje přístup k měření a vyhodnocování harmonických ztrát způsobených napájením z měniče a také standardizovaný přístup podle mezinárodních norem. Druhá polovina třetí kapitoly také popisuje výpočetní analýzu, která je v této práci použita ve formě analýzy konečných prvků. Nakonec jsou popsány nejistoty měření při použití standardní metody vstup-výstup. Ve čtvrté kapitole je představeno modelování v softwaru ANSYS MAXWELL, kde je nejprve popsána tvorba modelu specifikovaného stroje, poté jeho simulace se sinusovým napájením, a v druhé polovině je vysvětlena simulace s PWM napájením a jak bylo PWM replikováno pomocí naměřených průběhů. V páté kapitole jsou prezentovány všechny výsledky měření s vyhodnocením. Na konci kapitoly je uvedeno srovnání simulace a měření a jeho nedostatečná přesnost.

Klíčová slova

Asynchronní motor, harmonické ztráty, frekvenční měnič, ztráty indukčního motoru, měření asynchronních motorů, elektromagnetický model, metoda konečných prvků, porovnání simulace, přídavné ztráty.

Rozšířený abstrakt

Diplomová práce se zabývala měřením a porovnáním asynchronního motoru se dvěma různými zdroji napájení. Měření je nejprve provedeno s napájením z frekvenčního měniče pro sledování přídavných ztrát vzniklých z PWM, a poté s generátorem, který slouží jako zdroj sinusového průběhu. Měření je provedeno tak, aby oba zdroje byly porovnatelné. Tepelné rozdíly pak ukázaly, kde vznikají další harmonické ztráty. Pro další ověření měření byly provedeny i simulace pomocí metody konečných prvků v softwaru ANSYS MAXWELL. Oba zdroje napájení byly simulovány využitím hodnot z měření a následně srovnány.

První kapitola se zabývá popisem asynchronního stroje napájeného frekvenčním měničem. Nejdříve jsou popsány negativní vlivy takového napájení a také doporučené úpravy pro tento druh napájení, aby se předešlo co nejvíce nežádoucím jevům. Dále se kapitola zabývá moderními přístupy k řízení motoru. Je zde uvedena publikace, která zobrazuje porovnání aktuálně používaných druhů řízení a vysvětluje výhody a nevýhody určitých způsobů.

Druhá kapitola vysvětluje rozložení ztrát v asynchronním stroji. Kromě základního rozdělení jsou uvedeny i typické hodnoty ztrát, kde se vyskytují a jak vznikají z fyzikálního hlediska.

Třetí kapitola popisuje přístup k měření a vyhodnocování harmonických ztrát způsobených napájením z frekvenčního měniče. V další sekci je vysvětlen přístup k měření negativních účinků PWM, ale i standardizovaný přístup pro měření hodnot harmonických ztrát podle mezinárodních norem. Zde uvedené normy byly využity pro měření stroje v laboratoři. Druhá polovina třetí kapitoly ukazuje výpočetní analýzu, která je v této práci použita ve formě analýzy konečných prvků (MKP). Základy této metody byly aplikovány na geometrii stroje. Kapitola je doplněna také o porovnání přesnosti MKP a analytického modelu. Jsou zde uvedeny i nevýhody MKP, jako jsou výpočtová náročnost na hardware, ale i dlouhý čas analýzy. Nakonec jsou popsány nejistoty měření při použití standardní metody vstup-výstup, což souvisí s určováním ztrát u strojů s vysokou účinností.

Ve čtvrté kapitole je představeno modelování v softwaru ANSYS MAXWELL. Nejprve je popsáno vytvoření modelu specifikovaného stroje v RMxprt podle skutečných hodnot z dokumentace stroje a poté jeho simulace se sinusovým napájením. V druhé polovině kapitoly je vysvětlena simulace s PWM napájením a jak bylo PWM replikováno pomocí naměřených průběhů. Bylo zapotřebí provést FFT analýzu naměřených průběhů

a získat tak pracovní harmonické pro stvoření napěťové rovnice, která byla zadána do MKP. Všechny průběhy ze simulací jsou uvedeny a krátký komentář popisuje jejich rozdíly.

V páté kapitole je nejprve vysvětleno, jak byly určeny zátěžové pracovní body a jak bylo měření naplánováno. První test zahrnoval měření mechanických ztrát a poté následovalo měření napájení s měničem frekvence, dále generátorem a nakonec měření motoru naprázdno. Metodologie je vysvětlena s pomocí blokového diagramu. V druhé polovině kapitola prezentuje všechny výsledky měření s vyhodnocením. Výsledky jsou uvedeny chronologicky, jak byla měření provedena, všechny hodnoty jsou uvedeny v tabulkách a také zobrazeny v grafech. Na konci kapitoly jsou porovnána dvě napájení, a to i s výsledky ze simulace.

Bibliographic citation:

LÍPA, Miroslav. *Losses in induction machines supplied by a frequency converter [online].* Brno, 2024. Available also at: https://www.vut.cz/studenti/zav-prace/detail/160033. Master's Thesis. Vysoké učení technické v Brně, Fakulta elektrotechniky a komunikačních technologií, Department of Power Electrical and Electronic Engineering. Supervisor Jan Bárta

Acknowledgement

I would like to thank my thesis supervisor doc. Ing. Jan Bárta, Ph.D., for his constant motivation, guidance and professionalism throughout my studies, but more especially during the realization of my thesis. His friendly mentoring and his way of inspiring me to desire to learn more made my academic journey a unique and valuable experience.

I also thank Assoc. Prof. Lassi Aarniovuori for giving me the opportunity to have an exchange stay at the Finnish LUT University, where he created a welcoming and pleasant environment to carry out the practical part of my thesis.

Last but not least, I would like to thank D. Sc. Hannu Kärkkäinen for his devotion of time and expertise to all parts of my thesis, whether it was in his precious help while conducting the measurements in the laboratory, or during the preparation of my thesis, with his valuable advice under a considerate, helpful and kind attitude.

Contents

List of figures

List of tables

Abbreviations and symbols

Symbol	Variable	Unit
B	Flux density	(T)
B_{m}	Maximum flux density	(T)
B_{r}	Remanent flux density	(T)
ΔB	Flux density differential	(T)
C	Specific heat capacity	($\mathrm{Jkg^{-1}K^{-1}}$)
f	Frequency	(Hz)
f_{diff}	Frequency difference	(Hz)
f_{fund}	Fundamental frequency	(Hz)
f_{n}	Rated frequency	(Hz)
f_{s}	Stator frequency	(Hz)
H	Magnetic field strength	(A/m)
H_{c}	Coercive field strength	(A/m)
H_{max}	Maximal magnetic field strength	(A/m)
ΔH	Magnetic field strength differential	(A/m)
I	Current	(A)
I_{avgfund}	Average fundamental current	(A)
I_{n}	Rated current	(A)
I_{rms}	Effective current	(A)
I_{s}	Stator current	(A)
Δi_{μ}	Magnetizing current differential	(A)
k_{ed}	Eddy current loss coefficient	(-)
k_{h}	Loss hysteresis coefficient	(-)
L_{pa}	Volume level	(dB)
n_{n}	Rated rotational speed	(rpm)
n_{act}	Actual rotational speed	(rpm)
n_{set}	Set rotational speed	(rpm)
P_1	Input power	(W)
P_2	Output power	(W)
p_{ed}	Eddy current loss	(W)
P_{fe}	Iron losses	(W)
$P_{\mathrm{fe,anl}}$	Analyzed iron losses	(W)
$P_{\mathrm{fe,FEM}}$	Calculated iron losses	(W)
P_{fw}	Friction and windage losses	(W)
$P_{\mathrm{fw,anl}}$	Analyzed friction and windage losses	(W)

Symbol	Variable	Unit
$P_{\mathrm{fw,FEM}}$	Calculated friction and windage losses	(W)
P_{h}	Hysteresis losses	(W)
P_{harmPD}	Harmonic power	(W)
P_{in}	Input power	(W)
P_{loss}	Losses	(W)
P_{Lr}	Stray load losses	(W)
$P_{\mathrm{Lr,anl}}$	Analyzed stray load losses	(W)
$P_{\mathrm{Lr,FEM}}$	Calculated stray load losses	(W)
P_{mech}	Mechanical losses	(W)
P_{out}	Output power	(W)
P_{r}	Rotor copper losses	(W)
$P_{\mathrm{r,anl}}$	Analyzed rotor copper losses	(W)
$P_{\mathrm{r,FEM}}$	Calculated rotor copper losses	(W)
P_{s}	Stator copper losses	(W)
$P_{\mathrm{s,anl}}$	Analyzed stator copper losses	(W)
$P_{\mathrm{s,FEM}}$	Calculated stator copper losses	(W)
P_{δ}	Air gap power	(W)
Δp_{fe}	Iron losses	(W)
Δp_{fe1}	Iron losses differential	(W)
Δp_{fe2}	Iron losses differential	(W)
ΔP_{in}	Input power differential	(W)
Δp_{j}	Copper losses differential	(W)
Δp_{j1}	Copper losses differential	(W)
Δp_{j2}	Copper losses differential	(W)
Δp_{loss}	Losses differential	(W)
ΔP_{mech}	Mechanical losses differential	(W)
ΔP_{out}	Output power differential	(W)
Q	Relative power	(W)
q_{m}	Mass flow	(kgs^{-1})
R	Resistance	(Ω)
S	Apparent power	(W)
S_{H}	Hysteresis loop area	(m^2)
ΔS_{H}	Hysteresis loop area differential	(m^2)
t	Time	(s)
T	Torque	(Nm)
T_{act}	Actual time period	(s)
t_{an}	Time of a rising edge	(s)
T_{b}	Breakdown torque	(Nm)
T_{n}	Nominal time period	(s)

Symbol	Variable	Unit
T_{set}	Set time period	(s)
ΔT	Temperature differential	(K)
U	Voltage	(V)
u_1	Voltage vector	(V)
u_2	Voltage vector	(V)
u_3	Voltage vector	(V)
u_4	Voltage vector	(V)
u_5	Voltage vector	(V)
u_6	Voltage vector	(V)
U_{diff}	Voltage difference	(V)
U_{hfud}	Fundamental voltage	(V)
U_{n}	Rated voltage	(V)
U_{rms}	Effective voltage	(V)
U_{s}	Stator voltage	(V)
η	Efficiency	(-)
η_{max}	Maximum efficiency	(-)
η_{min}	Minimum efficiency	(-)
Ψ_{s}	Stator flux linkage	(Wb)
λ	Power factor	(-)

Symbol	Variable
CPU	Central processing unit
DPWM	Symmetrical two-phase pulse width modulation
DTC	Direct torque control
FEA	Finite element analysis
FEM	Finite element method
HDD	Hard Disk Drive
IEC	International Electrotechnical Commission
IM	Induction motor
MS	Magnetostatic
PWM	Pulse width modulation
RAM	Random access memory
SSD	Solid-state drive
SVPWM	Space vector pulse width
TH	Time harmonic
THD	Total harmonic distortion
TM	Transient magnetic

Introduction

The importance of induction machines nowadays is still high despite their lower efficiency compared to synchronous machines. This is mainly because of their simplicity and toughness, which guarantees a lower chance of machine failure and also maintenance. The basic parts of an induction machine are described in [1], where an induction machine is made up of two main parts, like a stator and a rotor. The stator most commonly contains a three-phase winding, and the rotor consists of either a squirrel cage or a wound rotor. Compared to synchronous machines, they are also characterized by the ability to start directly from the grid. The rotor speed then depends on the frequency of the power supply.

Current trends in sustainability present electrical machine manufacturers with constant challenges in designing machines to be more efficient. The publication [2] describes that electrical machines represent a large part of energy consumption, so there has always been a drive to increase efficiency levels in various institutions. According to the publication [3], the production and design of an induction motor is more cost-effective and also more maintenance-friendly due to the wide spare parts market compared to synchronous machines. So, despite increasing international efficiency standards, manufacturers are still trying to push these machines to higher efficiency levels, for example by using different material in the rotor cage. This is also advantageous for market development, where manufacturers form a competition that pushes them further. This is the main objective of the IEC efficiency standards, where the publication [4] explained that the transformation of the market and the reduction of the environmental impact of electrical machines, mainly induction machines, allows for better and better designs. For manufacturers, it is always a question of cash flow, but with a very detailed design, induction machines could match some synchronous machines.

A big step and help for induction machines was the development of power electronics, which allowed the use of frequency converters using pulse width modulation (PWM). Frequency converters became a very popular source for asynchronous machines, mainly because of the change of speed for certain work tasks. This change allows for increased efficiency of the system. Powering an electrical machine with a frequency converter has its negative features as well. The unwanted characteristics are the additional losses occurring in the machine due to higher frequency which affects harmonics and other phenomena. The article [5] explains that the additional losses resulting from frequency converters are still not well studied and their modeling is very challenging. With the further development of power electronics, the switching frequency of inverters is increasing, which also according to the publication [6] reduces negative characteristics such as current harmonics associated with PWM power

supplies. The [7] publication shows that three methods can be used to obtain frequency converter losses, namely input output, calorimetric, and calculation, but for such a calculation the [8] publication describes that there is no general method for calculating the additional losses from the PWM supply and most often these losses are calculated as a percentage of the total losses. Total losses can increase by up to 20 % when using an inverter compared to a generator. The additional losses can also affect the engine running at higher temperature, the temperature affects the operating point, with the [8] publication showing a reduction in the rated machine power of up to 20 %. The correct temperature value is important for the age of the machine. It is important to find a balance between the age of the machine and its performance. When designing and developing an induction machine, it can be advantageous to know if the machine will be powered by a frequency converter. The thermal condition of the machine at work will always be affected by the dimensions of the machine, but special modifications to the machine can achieve better performance. The publication [9] states that these possibilities have not yet been fully explored. Despite this, some are explained in the thesis. According to [10] and [11], the basic tasks of induction motors with frequency converters include pumps, fans, compressors, conveyor belts, robots, and cranes.

The master thesis is a continuation of the semestral thesis. The section on measurement uncertainties is taken from the first semestral thesis [12]. The first, second and third chapters are taken from the second semestral thesis [13].

1 Induction motor fed by frequency converter

1.1 Induction motor with frequency converter

Induction converter-fed motors are very popular. Powering an induction motor with a frequency converter brings several advantages. We can effectively change the rotor speed and thus influence the power required at the shaft under variable loads. For example, during start-up we can spin the induction motor using ramp characteristics [14]. Combination of induction machine and frequency converter became especially popular with the arrival of efficiency standards, when there was a need to increase the efficiency of induction machines, but there are also some disadvantages to powering the motor with a frequency converter like additional harmonic losses. The book [15] defines the occurrence of the lowest harmonic near the switching frequency. In order to approach the ideal sine waveform, high possible switching frequency is required. Modulation methods do not have a constant frequency spectrum because their switching frequency is not fixed. The switching frequency that changes the current in the induction motor is limited by the transient induction of the motor. The transient inductance describes the inductance of the machine during a fast pulse at the output of the inverter. The rotor responds to such a pulse by its leakage inductance. The book [15] goes on to describe that transient inductance can be equated to short circuit inductance, but this is not applicable in practice because there are different magnetic states in the measurement. In modern control methods using the vector method, the pulses do not have to follow a predefined modulation scheme, but in the steady state the pulse pattern is chosen to represent the inductive load as much sinusoidal current as possible. Controlling the induction motor (IM) by a converter is not an easy task. In the development of motor control, the thyristors used, operating at low switching frequencies, created such losses that the rated power of the machine had to be reduced. Thyristor inverters operated at frequencies in the hundreds of hertz, resulting in slow voltage rise. With the low voltage rise, insulation was saved, but the motor wires had to be kept short. However, with today's advances in technology, the switching frequency has moved into the kilohertz range, and filters limit the voltage steepness to protect the windings.

1.1.1 Negative effects

The thesis [14] explains that the high switching frequency of the transistors results in a high steepness of the voltage at the output of the converter. This phenomenon causes higher stress on the insulation of the conductors and is caused by the parasitic capacities of the conductors, where the uneven voltage values in the conductors are distributed to the edges of the motor winding. Another issue is higher dielectric losses, which also

occur due to high voltage gradients. Both problems can be prevented by enhanced insulation. Capacitive currents also happen in winding and motor frame. The center of the winding in the star circuit and the imaginary center of the inverter voltage is at a different potential. The centers are not connected, so there should be no voltage effects, but in the real case there are parasitic capacitances between the winding and the frame. Capacitive currents caused by the potential difference will flow through these points. For this reason, it is important to thoroughly ground the motor and use cable shielding. When using mechanical bearings, bearing currents can occur. Mechanical bearings should never be involved in the transmission of electrical energy. Dissertation [16] explains that the capacitive currents described earlier, which flow through the winding and motor frame, can also flow through mechanical parts such as the shaft and bearings. Capacitive currents reduce the lifespan of bearings. One logical way to prevent bearing currents is to limit capacitive currents, but this is not always possible, so isolating the bearings and using a filter in the inverter is recommended. The dissertation [16] outlines that the above mentioned arising problems when powering an IM from a frequency converter can be avoided by design modifications and in terms of popularity of IM with frequency converter, these modifications are done in almost all IMs. Design modifications shown below in the table 1.1 can affect the magnitude of motor losses, but cannot be overly relied upon. The cost of the motor is also important to the motor manufacturer, which means that a poorly designed motor cannot be saved by such modifications. The main modifications that should be emphasized are modifications to winding insulation and the highest possible symmetry in all respects. This section of negative effects also includes additional harmonic losses, but these will be described in the next chapter.

Table 1.1: Methods to reduce additional losses caused by PWM supply according to [16].

Modification	Description
Winding and insulation system modifications	
Reinforcement of insulation (threaded, interphase and slotted)	Respecting surge spikes in the machine power supply
Reinforcement of the winding input coil insulation	Respecting the change in voltage distribution
Use of non-conductive bandages	Avoiding heating by induced currents
Use of semiconductive varnishes for impregnation	Avoiding surface and sliding discharges
Winding with parallel conductors and distribution in parallel branches	Respecting the increased influence of the skin effect
Change in winding scheme	Better suppression of harmonics
Modification of the bearing assembly	
Use of insulated bearing	Avoiding low frequency bearing currents
Using a hybrid or ceramic bearing	Avoiding the effect of bearing currents on the bearing
Installing brushes at bearings and maintaining perfect brush to shaft contact	Limiting the effect of shaft voltage and shaft voltage on the bearings
Generally inserting insulation into each anticipated current path	
Other possible modifications	
Insulating motor components	Preventing uncontrolled current flow from induced voltages
External ventilation	Improve machine cooling with greater depth of regulation
Number of slots per pole chosen as an integer and the slots rotated by one slot spacing	Suppressing design harmonics and induction of current generated by bearings
All components designed and manufactured with maximum possible symmetry	
Air gap tolerances of ±10% maintained	

1.1.2 Drive characteristics

The learning text [17] describe that although induction motors are usually designed for 50 hz, they are capable of operating at twice that frequency without further modification. This capability decreases with rotor size, where the mechanical properties of the rotor tend to be more critical and more stressed. The fan cooling the motor will also get faster, and so will its noise. Three frequency ranges are described for the IM thermal performance limit with a transducer. If the stator frequency is greater than the rated frequency, then the motor is in the flux weakening region. As the name implies, this is the region where the flux linkage is reduced, the motor operates at rated current, and cooling is more efficient because the fan spins at a higher speed despite increased additional losses. There is no temperature problem in this mode. In constant torque mode, the temperature problem does not occur because as the speed decreases at constant current, the iron losses decrease with square of speed, but the cooling air from the fan drops linearly. In the reduced torque mode, below half the rated motor speed, the motor does not cool well because the airflow is not as efficient. Copper losses must be regulated by stator current, the machine torque drops. As the speed decreases, the breakdown torque also decreases, which compensates for the overload ratio.

1.1.3 Control and modulation methods

The motor is powered by the voltage generated at the inverter output by PWM modulation. Typical PWM modulation waveform at the inverter output.

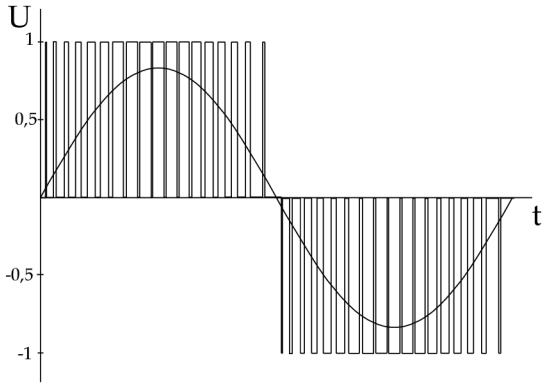

Figure 1.1: Pulse width modulation, redrawn from [18].

Several methods are used for induction motor control, depending on the application. Article [19] shows that the additional losses arising from the inverter cannot be influenced too much by the control method, therefore, there is generally no best control method chosen. An older but popular style of motor control includes scalar control. The bachelor thesis [20] shows the advantages of this method, where simplicity and cheapness can account for its popularity. The control principle is based on changing the amplitude and

frequency of scalar quantities such as voltage, current, and magnetic flux. The thesis [21] adds that the scalar control must change the magnitude of the voltage as the frequency changes. This maintains the ratio of stator voltage to frequency, so that the magnetic flux of the motor remains constant. Thesis [20] then explains that the constant flux region is capable of varying the rotational speed from zero to nominal speed. No sensing of the position or speed of the rotor is required for such control, which may also appear to be a disadvantage. Simple motor speed control is an advantage, but this method achieves some inaccuracies and can only work effectively at steady state. The dynamic properties of the controlled system are problematic for such control, due to transients that do not affect the position of the space vectors [20]. In the constant power region, the frequency increases above the nominal power, the voltage remains constant, and the motor torque decreases as the motor flux decreases.

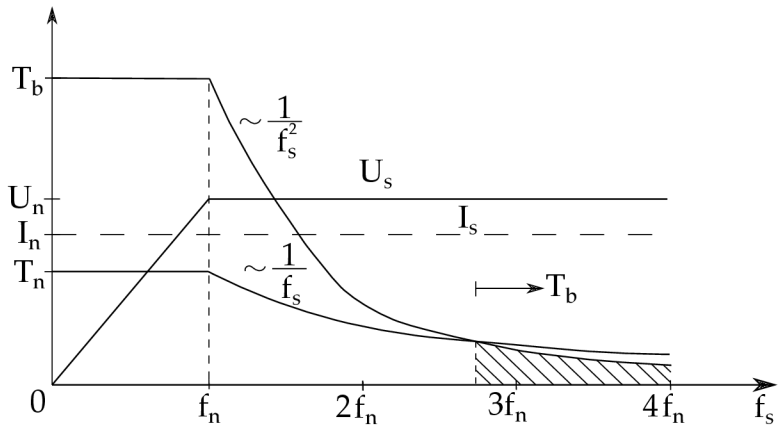

Figure 1.2: Voltage control of induction motor with area of constant flux and constant power, redrawn from [17].

Vector control is explained in thesis [22], which describes that the principle is a feedback control of the position of the magnetic flux in the machine. The feedback loops of the current make it possible to achieve good dynamic control characteristics. The induction motor is controlled by the magnitude of voltage, current, and coupled stator magnetic flux. The control is performed in the d-axis and q-axis using DC values and is dependent on the rotor speed and angle information. In the d-axis, the desired and actual coupled magnetic flux is compared and in the q-axis the speed or torque controller is overridden. In practice, the use of rotor flux control is preferred. The publication [23] shows that different types of voltage modulation affect the output shape of the voltage waveform that reaches the motor input. Three different commercially used voltage converters, each using a different modulation method. Before moving on to the definition of the three main modulations, we need to define the term carrier frequency. The carrier frequency is a fixed frequency that defines the potential of the switching instants. In carrier-based modulation, the maximum switching frequency is the carrier frequency

and the actual switching frequency is smaller.

Direct torque control (DTC) is a kind of PWM control that has the advantage of fast machine torque control, robustness, and simple design. Disadvantages include high torque ripple and variable switching frequency. DTC has a different effect on harmonic losses due to the use of carrier-based switching in comparison to the constant switching frequency. Thesis [22] defines the principle as controlling magnetic flux and torque by direct control of relay controllers with hysteresis without current loops. The stator current and voltage are indirectly here, and this means that there is no need to transform the parameters. The magnetic field of the stator is formed by voltage vectors. The torque here is therefore controlled by the angle of the stator and rotor vectors of the flux linkage. Increasing the angle between these vectors decreases or increases the value of the motor torque. The values of the flux linkage angle vary by selecting the voltage vector depending on the sector in which it is located. In DTC, unlike PWM methods, the switching frequency is not fixed but depends on the desired average value dependent on the torque hysteresis bands. This means that there is no predefined switching pattern. This achieves minimization of the pulsation and frequency variation.

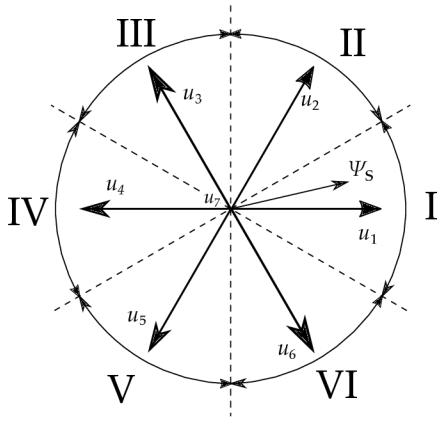

Figure 1.3: Direct torque control, redrawn from [22].

Publication [23] further describes that space vector pulse width modulation (SVPWM) is the standard for switching power converters. For SVPWM, the output voltage is defined by the turn-on time of the vectors, the sampling time, and the voltage vectors themselves. SVPWM schemes are defined using the zero-voltage vector. The zero voltage vector is chosen on the basis of the least number of switching operations. Symmetrical Two-Phase Modulation (DPWM) is another vector-controlled method. It uses two-phase modulation and the third phase is switched 60° to the DC bus to increase the efficiency of the converter. Theoretically, the modulation frequency is reduced by one-third, which also reduces the switching losses by one-third compared to the previous method. The disadvantage is high current harmonics at low modulation.

1.1.4 Comparison of modulation methods

The analysis of a 37 kW induction motor fed by a frequency inverter was described in a publication [23] using the three methods mentioned in the previous section. This publication compared the measured converter-fed IM losses with the modeled ones. Using a software with FEM, the recorded voltage waveforms of three different modulation methods were input into the model. Furthermore, the study monitored the THD of the voltage and current waveforms as the motor load changed for the three modulation methods. THD values for carrier-based modulation, such as SVM and DPWM are close to each other compared to the THD of the DTC method, which is significantly higher. The highest THD value occurs at the load 25% and then decreases. The different value of these methods arises because of the actual switching frequency, which is different from the theoretical one. The the second one is lower because of over-modulation when there is excess voltage, whereas DTC has a variable switching frequency, and this is constant for different load values. For comparison, the figure 1.4 shows the measured losses of IM fed by different methods.

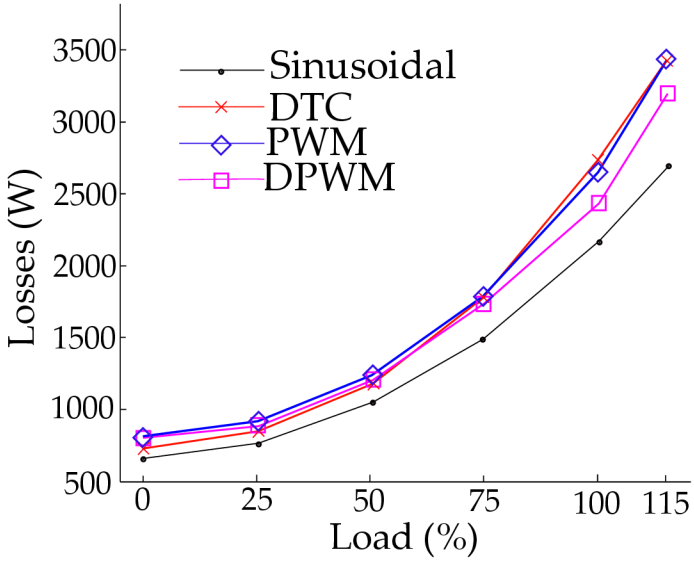

Figure 1.4: Comparison of modulation methods with total losses for 37 kW motor, redrawn from [24].

The results of the publication show that when the measured losses of all three modulations are compared with those simulated by FEM, the simulation results are quite consistent with the measured results. The differences arise at very low load values and most so for the DPWM. For the differences in the individual loss components from the analyzed measurement data versus the FEM, the publication describes the small differences and why they occurred. For the stator losses, the difference in magnitude of the losses arose because the amplitude of the inverter's fundemental voltage is smaller than

the amplitude of the sinusoidal voltage. The iron loss calculation differs the most because FEM considered the losses by harmonics from PWM. These losses increased with load, while the measured losses decreased with load as the voltage drop increased due to the larger resistive load. The rotor losses calculated from the measured values were lower because they did not consider harmonic losses arising from air gap. In summary, it is not possible to compare modulation methods based on this one study alone because of the complicated switching frequency settings.

1.1.5 Loss characteristics of inverter-fed induction machine

The publication [25] defines the loss characteristics of an induction motor fed from a frequency converter. The motors tested are in the power range 5.5 to 55 kW and the losses with sinusoidal supply and inverter supply are compared. The segregation of losses method is used to determine the motor losses, which is one of the main methods of determining motor losses. The publication also explains the problems with this method that arise due to the PWM supply to the motor. The standard defining the segregation of losses test method defines a DC resistor for calculating Joule losses in the stator, which means that additional losses due to skin effect and proximity effect are considered in the stray-load losses section. These additional losses are increased especially when the power is supplied from PWM, meaning that it would be more appropriate to use an AC resistor that considers these losses in the calculation. For the Joule rotor losses, a problem arises in the no-load condition because the no-load iron loss is tightly coupled to the Joule rotor losses and cannot be measured directly. Using FEM, it is possible to calculate the value of no-load iron losses because it considers the skin effect and then subtract the losses to obtain the value of Joule losses in the rotor. In the study, experimental measurements are then performed, where no-load and full-load test are performed and the different components of losses for a 30 kW motor are described. The stator Joule losses were slightly higher at higher load with PWM supply compared to sinusoidal supply, but at very low load the losses with PWM supply increased very much compared to sinusoidal waveforms up to 54.4 %. The same is the case for the Joule losses in the rotor, where similar results as in the stator are shown. For the iron core losses, a significant increase in losses is seen by using PWM power supply. The difference is around 15%, but this kind of losses is little dependent on the load magnitude.

In the last part of the paper, stray-load losses are described, where it can be seen that the losses increase by a significant fraction with the PWM power supply and do not depend on the motor load.

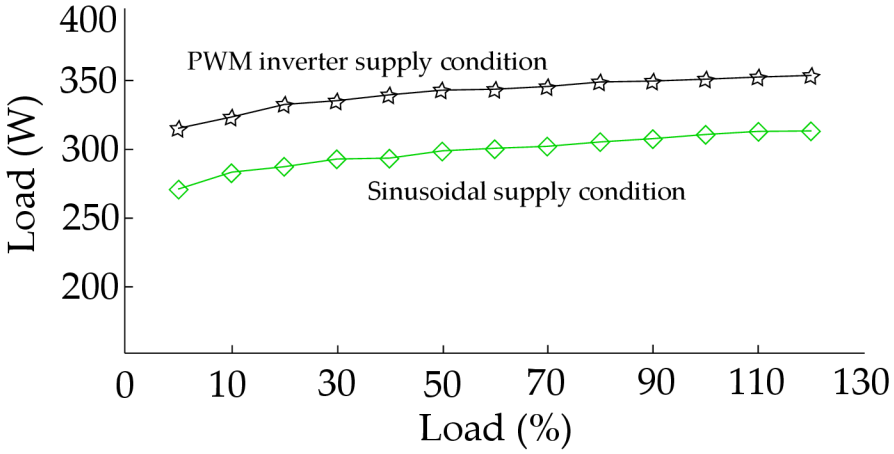

Figure 1.5: Example figure of core loss for the 30 kW motor, redrawn from [25].

1.2 Motor development for inverter-fed machine

Study materials [17] define that the speed of an induction machine depends on the stator frequency, where the rotor rotates at a speed equal to the value of this frequency reduced by a percentage of the slip value. Using a frequency converter, it is possible to supply the machine with a three-phase voltage of a different stator frequency and thus change its speed. The publication [24] defines that induction motors designed for inverter supply do not need to consider the problems that arise with high starting currents in their design. This means that the rotor resistance does not need to be as high and a single cage is sufficient compared to a double cage. The material [17] further explains that voltage source inverters with a DC voltage link are preferred for most motor applications. Pulse width modulation creates a new voltage with varying frequency, where the magnitude of the line-to-line voltage is determined by the size of the pulses. The magnitude of the stator voltage is proportional to the magnitude of the frequency, so to maintain the constant flux linkage, the voltage also changes when the frequency is changed. After obtaining the maximum output voltage, when the frequency is increased, the operation reaches the part where the magnetizing current decreases, and with it the magnetic flux. This also weakens the machine torque, but as the speed increases, the output remains constant. The power mode of the state is limited by the frequency when the breaking torque drops to the load torque requirement.

1.2.1 Inverter technology

The materials [17] also outline drive technology, which consists of different types of inverter switches that are used for the desired inverter characteristics. Turn off gate thyristors (GTO) are chosen for higher voltage limits, and auxiliary circuit thyristors are chosen for frequencies below 500 hz. For lower voltages, metal oxide semiconductor

field effect transistors (MOSFET) are used, and insulated gate bipolar transistors (IGBTx) with a range of 200 to 6000 V are most commonly used. A speed sensor is not needed to control an induction motor with a frequency converter. When the load changes, the slip of the motor will also change, the speed is not constant, and speed oscillations may occur. These oscillations occur at low frequencies when the rotor flux change constant is less than the voltage period. By using a speed sensor and speed control it is possible to reduce oscillations at low rotor speed.

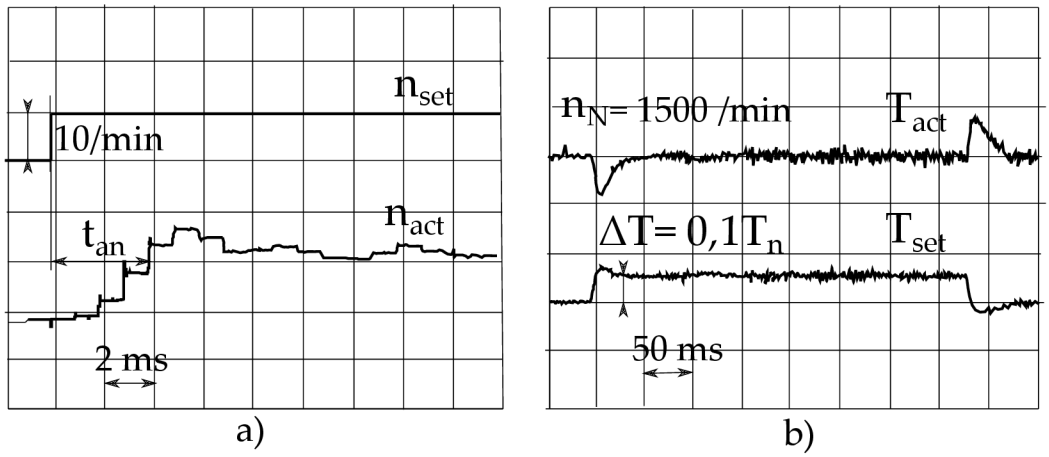

Figure 1.6: Digital speed control of inverter-fed induction machine, redrawn from [17]. Step-up of set-point speed speed response a), step-up and step-down in load torque speed response b)

1.2.2 Features of a high-performance converter-fed induction motors

Some machines will require external cooling due to the demanding duty cycle where full machine torque is constantly needed. This case is explained by [17], the temperature can be controlled by a temperature sensor that is placed on the winding and serves as overheating protection using an auxiliary external fan that is independent. For a very efficient use of the machine volume, which means to design a motor with a dense power volume, the cooling needs to be improved by using, for example, water cooling, which is more efficient. Such motors are often found in transport applications or tools. Changing the cooling from air to water can increase the transfer coefficient by up to three times and thus increase the power output by up to 40%.

Important features include high dynamic performance which is made up of low inertia along with overload capability. With a low ratio of internal stator diameter to stack length, low motor inertia can be achieved, but care must be taken to ensure that the rotor is not too thin for low natural bending frequencies. Another feature of high-performance IM fed by converters tends to be the speed sensor, which allows proper control over a

wide speed range with constant power output. This feature is especially important for various tools where speed is important for the performance of the work, for example cutting.

There are also big differences in the design of induction machine that works directly from the grid or is powered by a frequency converter. An IM working from the line supply operates with a fixed line frequency and a slip ranging from 0 to 1, while an IM fed from an inverter has a variable frequency and operates with a nominal slip or zero slip. There are always some trade-offs to optimizing these power supply methods. For example, for a line-operated IM there is a trade-off in leakage inductance, where a small value of leakage inductance is needed for a large breakdown torque, but a high value is needed for a small starting current, but again a small value is needed for a large starting torque. For inverter-operated IM, a trade-off arises mainly in terms of additional losses, where a larger air gap and at the same time leakage inductance is needed, but a smaller air gap is needed for a small magnetizing current.

1.2.3 Pole count

Next, the text [17] describes the appropriate choice of pole count. With a high rotor speed it is important to have a low pole count for lower stator frequency, which has a direct effect on iron losses, current displacement in winding and limiting switching frequency. The most commonly used IM design for inverter power supply is the four pole machine because the two pole machine has some advantages. In comparison, the two pole machine will be larger, so a larger rotor yoke is needed for magnetic flux. Further, also larger coil span which causes large winding overhangs which further increases copper losses and takes up space. When comparing rotor dynamics, a four pole machine is preferable because in a two pole machine there is a worse effect of elastic bending of the rotor formed by unbalanced magnetic pull due to a smaller air gap on one side. This effect then worsens the flux density characteristics in the air gap, and it forms a pulsating force of twice the frequency at the locations of the smaller air gap. For four pole machines and more, these pulses occur at a higher frequency and are thus able to operate over a larger range.

1.2.4 Harmonics

The output voltage from the frequency converter is made up of rectangular pulses of a certain size to form a sinusoidal waveform. Lecture text [17] explains that switching for asynchronous switching, the switching frequency of the transistors is fixed and independent of the fundamental frequency. Synchronous switching uses the ratio of the transistor switching frequency to the stator frequency as a fixed value and an integer odd number, this method is more suitable for more powerful machines. As far as winding

connection is concerned, it is better to use star connection because its time dependent function fits better in sinusoidal time function compared to delta.

The book [15] explains how a PWM inverter can increase losses in an induction machine. High frequency current components cause a skin effect in the windings. This is especially true for large machines where the windings are made up of a large piece of wire. These components further cause additional high frequency components in the air gap and affect the flux density waveforms, increasing losses in the iron. These losses are reduced by the leakage inductance effect. In particular, the rotor surface can form losses due to the PWM power supply. A part of the time harmonics passes through the magnetizing inductance, forming additional harmonic losses in the air gap, the magnitude of this part corresponds to the ratio of magnetic flux leakage and magnetizing inductance. The eddy current losses arising in the rotor bars and in the iron reduce the magnitude of the harmonic losses, therefore these losses are most at the surface. To reduce these surface losses it is advisable to have a rotor with open slots. The [15] book also mentions a popular type of slot that is designed to reduce losses.

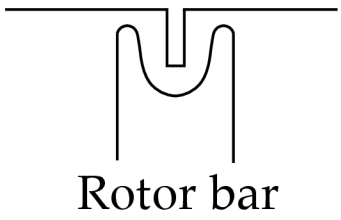

Figure 1.7: Example of slot opening typical for inventer motors, redrawn from [15].

Additional losses are also increased as a result of current displacement, which occurs at high frequency mostly in the rotor conductors and increases the AC resistance of the bars. The special shape of the bars in the rotor allows one to reduce the losses for IM fed by the frequency converter. As for current displacement, round shape bars are the most resistant to such phenomenon. This shape is disadvantageous for high iron saturation for narrow rotor teeth. For a compromise, oval-shaped slots are recommended where all rotor teeth have the same width between the slots. The properties of oval-shaped slots can be further enhanced.

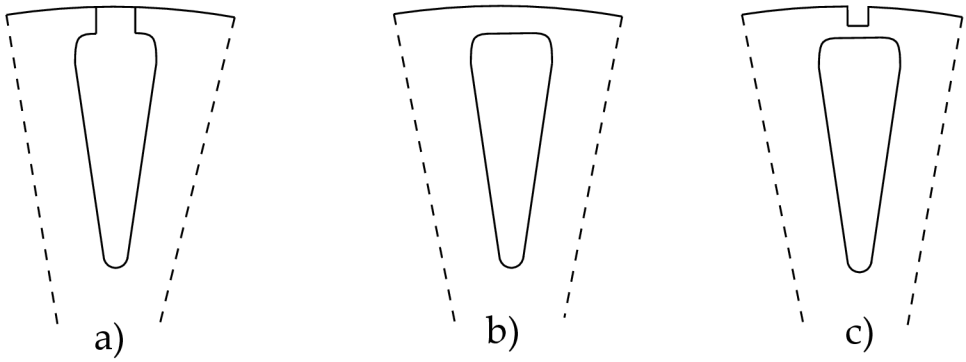

Figure 1.8: Rotor oval slots, redrawn from [17].

Drawn rotor slots are outlined by [17], Type B and C have bridges between the slot and the edge of the rotor yoke. This causes more leakage flux to flow through these areas than in Type A where the reluctance is greater. The lower reluctance of type B and C allows more current harmonics to be reduced. The first type A semi-closed has the lowest leakage inductance of the three types. At the edge of the open slot of the bar, eddy-currents will be induced due to the field change in the air gap, while this effect cannot take place in the closed slots. Slot B will be slightly easier to manufacture than Slot C, during manufacture errors may occur on the surface of the laminates and this may increase additional losses. The main difference of C over B is the added extra slot which causes a by-pass for rotor stray flux, this increases leakage inductance and reduces current harmonics. For a trade-off of reduced losses but higher breakdown torque, slot B is used. Utilizing slot A could increase losses in such a way that the stator winding temperature would increase by up to five Kelvin, which can be a very significant difference for the operating temperature of the motor. Another way to reduce current harmonics is to increase the switching frequency. Increasing the switching frequency will change the ratio and thus reduce the voltage harmonics and also reduce the current harmonics, which will reduce the losses in the rotor bars. However, increasing the switching frequency will increase the switching losses of the transistor, these increase linearly with frequency so it is advisable to find the optimum value.

Powering the machine with a frequency converter also creates a torque ripple. Torque ripple is created by additional harmonics that are generated by the magnetic field in the air gap. This magnetic field is a product of the harmonic currents in the stator and with the interaction with the harmonic currents in the rotor, a tangential force and thus an additional torque is generated. The added moment arises when the rotor harmonics are of a different order in the case of old harmonics, because the fundamental current is a first order harmonic. A pulsating additional torque also arises if the ordinal number of the harmonic is the same for both rotor and stator, but its magnitude is negligible.

1.2.5 Noise

Problems associated with the frequency converter include acoustic noise. Study text [17] describes how is noise created, noise arises from harmonics in the slot, but also from the previously mentioned current harmonics arising in the air gap. Acoustic noise arises magnetically with its tonal frequency, which is usually about the size of the pulsing frequency from the transistor (twice the switching frequency). For Acoustic noise generation, the fundamental harmonic is the most dominant. The harmonic function can be written as a radial force density wave using the trigonometric formula. The radial force density wave forms an oscillating pull on the iron stack. The largest vibrations which then cause the loudest sound occur at medium modulation degree with frequencies. Acoustic noise also arises when the motor is idling because its magnitude depends on the main magnetic flux and stator current harmonics. These quantities have their full effect on the machine even without load. The noise generated can be reduced by increasing the switching frequency of the inverter. With higher frequency, the magnitude of current harmonics is reduced, furthermore, the sensitivity of human ear to sound is reduced and the vibration amplitude of mechanical part is also reduced. The noise can also be affected by the speed range in the operating mode.

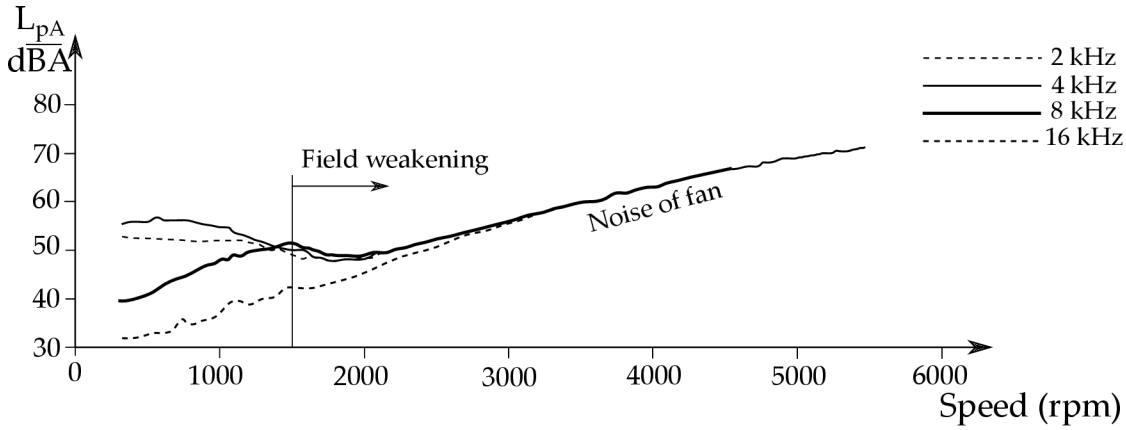

Figure 1.9: Noise for different switching frequencies [17].

For the torque-constant mode, the magnetically excited noise is the largest because the magnetic flux does not change and is constant. For the constant torque mode, the magnetic flux is attenuated and thus the noise is reduced. Other noise generating parts include the fan, this tends to be on standard IMs and can be very loud at higher speeds. For the fan, a fan blade frequency is defined which depends on the rotor speed and the number of fan blades. The noise problem arises with large motors where increasing the switching frequency leads to high switching losses because more power needs to be switched. Larger transistors would be needed to reduce these losses, but these also tend to be much more expensive. Manufacturers of large motors get around this problem with

a special strategy called wobbling of switching frequency. The range of the switching frequency oscillates between two values periodically as a sinusoidal function. This also changes the tonal frequency. The difference arises in the magnetically excited sound so that at one frequency the sound tends to be very unpleasant to the human ear and at the changing frequency the noise changes and mixes, resulting in a much more pleasant sound.

IM fed by frequency converters usually operate in the range of slip at full load to zero slip, in this way they theoretically avoid asynchronous and synchronous torque harmonics arising from slotting at very high slip. However, at low speed, slip at full load approaches unity and thus torque harmonics in the motor will occur. However, the parasitic torque from these harmonics does not show up much because the motor current is within the rated current range due to the gradual ramp up due to the converter. For a line-start motor, the starting current would be many times the rated current.

2 Losses of an asynchronous motor fed by a frequency converter

2.1 Induction machine losses

The losses of an electric motor can be defined as the energy lost that does not contribute to the operation of the motor. The lost energy is converted to thermal energy and heats the motor [14]. Publication [18] describes that the losses of an induction motor depend on several different factors such as the load, frequency of the voltage source, and the size of the motor. The electrical waveforms of the supply voltage have a large effect on the motor losses. If the induction motor is supplied with sinusoidal voltage, the losses are as low as possible. Nowadays, it is very popular to power induction motors with a frequency converter, making it possible to reduce power consumption in variable load applications despite the modulated voltage waveform of the converter being very far from the ideal sinusoidal waveform. Next, [18] shows how induction motor losses can be categorized according to where they occur or their electromagnetic origin. Depending on the location, losses occur in the winding, iron, and friction and ventilation losses. According to the electromagnetic origin, losses in the winding and in the iron can be further classified into fundamental, space harmonic, and time harmonic losses. However, the most common classification is based on both the space and electromagnetism origins. Losses in windings and losses in iron consider all fundamental electromagnetic losses, friction and ventilation losses include all mechanical losses, and all harmonic losses are combined and called additive losses. For induction motor losses, a simple diagram applies.

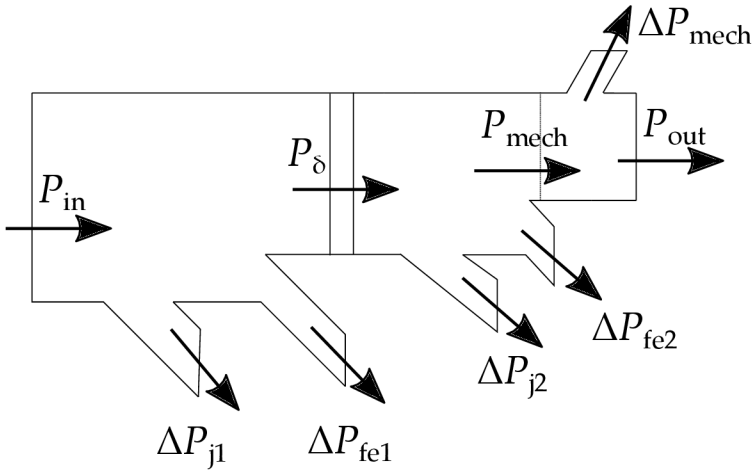

Figure 2.1: Induction motor loss diagram.

The motor input power P_{in} is first reduced by the losses in the stator. These losses are

divided into Joule losses in the stator winding and losses in the stator laminations, which are further divided into losses due to eddy currents and hysteresis. The power is then transferred through the air gap, and in the rotor it is again reduced by Joule losses and losses in the iron. Furthermore, there are mechanical losses due to bearing friction and ventilation losses on the shaft. After these losses, the output power of the machine P_{out} is obtained.

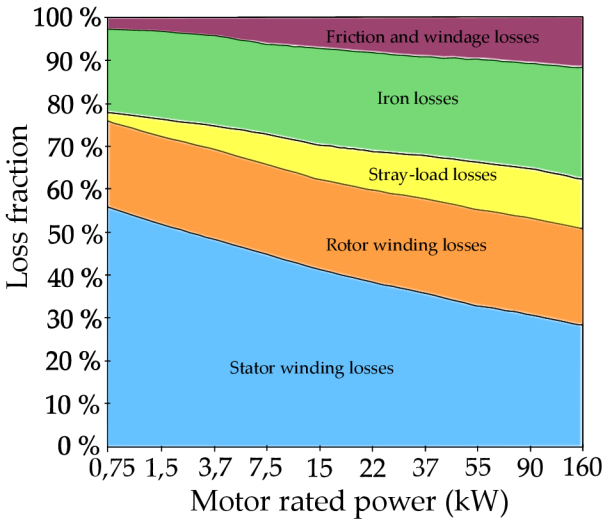

Figure 2.2: Typical distribution of losses of four-pole induction motors, redrawn from [18].

2.1.1 Winding losses

The publication [14] explains that slots filled with copper wires form the winding. In induction machines, a squirell cage rotor design, usually made with aluminum or copper bars, is commonly used. The thesis [18] explains how losses in the winding constitute a significant portion of the total machine losses, especially under load. These losses correspond to:

$$\Delta P_{\text{j}} = R \cdot I^2. \tag{2.1}$$

In the stator, the current that contributes to these losses is made up of the magnetizing current and the torque-dependent component of the stator current. In the rotor, the joule losses are due to the current induced in the squirell cage depending on the slip and the rotor load. The losses in the winding are also dependent on the temperature characteristic of the resistance of the conductor. As the temperature increases, the resistance of the conductor increases according to its coefficient. If the load is constant, and hence the current in the stator does not change, then the losses increase with increasing motor temperature.

2.1.2 Iron core losses

As mentioned earlier, iron losses can be divided into two different sources of origin. The master's thesis [18] describes that iron losses are more intense in the stator laminations than in the rotor laminations because of the higher frequency, as the rotor frequency depends on slip. Iron losses are minimally dependent on load because of the rotor slip, which is load dependent. The dependence of iron losses can be described by the following equations.

$$\Delta P_{\mathrm{fe}} = p_{\mathrm{h}} + p_{\mathrm{ed}} = k_{\mathrm{h}} \cdot f \cdot B_{\mathrm{m}}^2 + k_{\mathrm{ed}} \cdot f^2 \cdot B_{\mathrm{m}}^2. \tag{2.2}$$

Eddy current losses occur from movement and changes in the magnetic field within conductive materials. In a magnetic sheet stack, the alternating current creates a rotating magnetic field, inducing eddy currents. Several methods are used to reduce these losses. In the case of an induction machine, both the stator and the rotor are made of very thin laminations, reducing the surface area for induction of the eddy current. To further decrease eddy current losses, specially magnetically oriented sheets with silicon additives can be employed, particularly in transformers. In the rotor, the losses caused by eddy currents are relatively smaller compared to the stator.

Hysteresis losses depend on the magnetic properties of the metal sheets. When a magnetic field is applied to a ferromagnetic material, the magnetic dipoles align with the direction of the magnetic field. The sheets maintain this alignment even after the magnetic field is removed. When a magnetic field with the opposite direction is applied, energy is needed to change the orientation of the sheets. This energy is then released as heat and behaves as a loss. The magnetic field of the stator changes with the frequency of the source, and the magnetic field of the rotor changes with a reduced frequency of the source due to slip.

Publication [14] explains the hysteresis losses of the first harmonic on the static B-H curve during one cycle. Proper material selection is crucial for high-frequency applications. Thesis [14] described that the perfection of the crystalline structure determines the size of the hysteresis. Various impurities and contaminants present in the ferromagnetic material, causing distortions in the crystal structure. Furthermore, the hysteresis losses considered in this section apply only to hysteresis losses due to the first harmonic. Residual magnetic flux density defines how much residual magnetization remains in the magnetic sheet after the source of magnetization or external magnetic field is disconnected. In induction machines, sheets of magnetically soft materials with smaller hysteresis loops are used to limit hysteresis losses. Coercive magnetic field strength H_{c} defines hard and soft magnetic materials. Its value describes how easily a material can be demagnetized, which means that the material loses its magnetic properties. The paper [26] describes an iron loss model with optimized calculation. The basic form of the

equation to describe the losses in iron is shown above. From this mathematical model it is possible to express a relation describing a linear line, where the coefficients k define its properties. To increase the accuracy of the model, it is necessary to consider the dependence of the coefficients on the magnetic field properties and temperature. At low switching frequency, a worse sinusoidal current waveform is produced, which affects the shape of the flux density. This results in small hysteresis loops, which cause hysteresis losses and also additional eddy current losses. To better describe hysteresis loops, the paper [26] introduces a coefficient describing the ratio of hysteresis losses with and without loops.

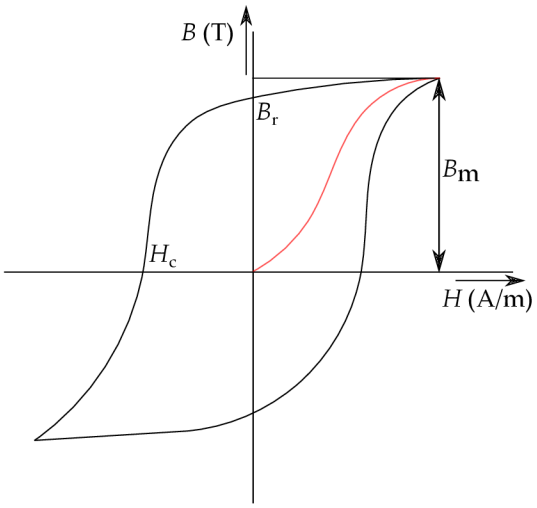

Figure 2.3: Static B-H curve.

2.1.3 Mechanical losses

The work [18] further explains that mechanical losses are made of friction and windage losses. Mechanical losses can be difficult to determine because of the complicated aerodynamic friction phenomena. Publication [23] describes that they depend on rotational speed, lubrication, bearing type, and temperature. Windage losses occur due to the operation of a cooling fan and air resistance in the machine, while friction losses arise in the bearings and places where the parts are sealed together. Mechanical losses are not load dependent but are proportional to the machine's speed. Induction motor slip reduces mechanical losses because rotor speed is dependent on slip and slip increases with increasing load. To reduce friction losses, it is important to choose high-quality bearings. For high-speed machines, air or magnetic bearings are recommended. Windage losses can be effectively reduced directly through the proper design of the fan and motor casing. Indirectly, with higher motor efficiency, the cooling demand decreases as the machine does not heat up as much.

2.1.4 Stray-load losses

Stray-load losses can also be called additional losses, the next part of the thesis [18] explains that stray-load losses specifically express losses due to harmonics that are not considered in winding losses, iron core losses and mechanical losses. These harmonic losses include spatial harmonic losses occurring in the air gap and time harmonic losses of the supply voltage. Additional losses depend on the load and are proportional to the torque power. Ideally, we would like to have a sinusoidal shape of magnetic induction in the air gap. However, this is not possible, and the shape of the flux density characteristic is more saw-like, because the magnetic flux flowing through the air gap must find its way through the stator tooth and not the slot. This shape can be influenced by the arrangement of the winding in the stator slots. Spatial harmonic losses occur precisely because of this problem, creating additional undesired spatial harmonics that induce currents into the rotor. These currents can then create losses due to eddy currents and joule heating in both the stator and the rotor. Furthermore, spatial harmonics cause vibrations, torque fluctuations, and noise. Proper design of the stator winding can reduce spatial harmonics. Certain combinations of stator and rotor slots can increase or decrease these losses. Time harmonics occur at higher frequencies, especially when a frequency converter is used. Time harmonics have a similar impact on machine losses as spatial harmonics. Time harmonics are reduced by the inductance of the stator, but can be significant in the rotor.

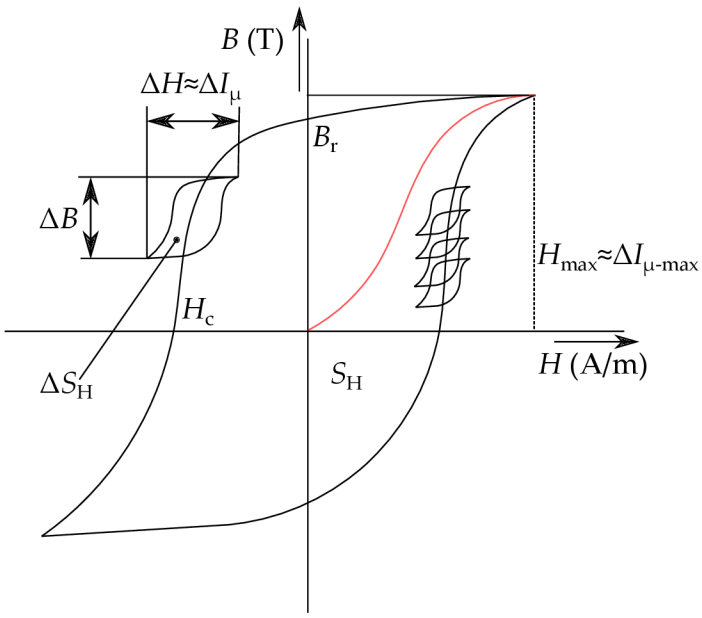

Figure 2.4: Additional time hysteresis losses.

The thesis [14] describes that assuming that the amplitude of the first harmonic of the magnetizing current is directly proportional to the maximum value of the magnetic

field strength, it is possible to express the relationship between current fluctuation and the change in magnetic field strength. The high-frequency component, which causes the magnetizing current to oscillate and thus fluctuations in magnetic intensity, is applied to the main loop because the first harmonic is superimposed on the miniature loops. The sizes of the superimposed loops will depend on the size of the higher harmonics in the signal.

3 Methods of measuring and evaluating losses in an asynchronous machine

3.1 Approaches to measuring additional losses

Master thesis [14] offers two methods to verify the losses caused from the power supply of a frequency converter. The first method is to compare the losses at the same magnitude as the first harmonic voltage. An induction motor powered by a sinusoidal voltage with a frequency of 50 Hz is used as a reference for the losses. Only the fundamental harmonic is considered for the calculation. For subsequent measurements with a frequency converter, the PWM modulation is set to 400 V. The losses incurred with this power supply already consider the whole spectrum of higher harmonics. For such measurements, a measurement system capable of measuring the high-frequency voltage and then converting the signal into a tracking spectrum and tuning the first harmonic to the same value as if the machine were supplied with a sinusoidal voltage is required so that the contribution of the higher harmonics to the total voltage value is detected. For accurate measurement, the upper cutoff frequency of the measuring instrument must be in units of MHz and above, and the sampling frequency must exceed this value. The measurement results are determined at steady-state machine temperature.

The second method defined in the thesis [14] is the determination of losses using a DC intermediate circuit, where the active power of the inverter is determined and then the losses on the components of the inverter are subtracted. Several assumptions apply to this calculation. First, a capacitance large enough to minimize the ripple in the waveform to keep the voltage constant. High inductance in the intermediate circuit to keep ripple minimal for constant current. With such simplifications, it is possible to measure the voltage and current with a multi-meter and calculate the power of the inverter in the inter-circuit. Then the losses of the switching components need to be calculated using analytical formulas. Assuming a actual power at the motor shaft with the same value under PWM power supply and under sinusoidal power supply, the calculated power input versus the power input of sinusoidal power supply will make up the difference in the form of added harmonic losses.

3.2 Measurement of negative effects of converter supply

Induction machines have a long history and, therefore, there are several different methods of measurement and diagnosis to detect certain motor defects. The [16] thesis defines several diagnostic methods that are able to detect certain motor conditions. The author describes his personal experience of investigating the negative effects of a frequency converter using the methods mentioned below. These operating and testing

diagnostics can provide information about the current state of the machine, but at the same time, diagnostics after a machine failure can reveal a fault that has occurred and can be prevented next time.

Table 3.1: Methods of measuring negative effects of converter supply according to [16].

Measuring method
Measurement of insulation status
Shock wave or double shock wave winding test
Partial discharge measurement
Vibration measurement
Shaft tension measurement
Bearing stress measurement
Measurement of bearing current and auxiliary conductor current through the bearing
Measurement of voltages in machine components (frame, rack, machine)
Measurement and analysis of the machine supply current
Measurement of electromagnetic field leakage.

The [16] thesis further specifies the following methods of diagnosis and measurement according to appropriate standards. When choosing a diagnostic method, it is important to limit the influence of a change in the power supply on the diagnosed variable. However, for most of these methods, the output waveforms from the frequency converter present a serious problem where time harmonics affect the shape of the output waveform and voltage. One option is to use a filter that can use mathematical functions to filter out the waveform shape, but such a filter can reduce the credibility of the frequency spectrum analysis. Filters are useful when measuring the RMS value of a variable.

3.3 International standards of measuring and evaluating losses according to IEC 60034-2-1

International standards define methods and procedures for determining losses in electrical machines. In the IEC 60034-2-1 standard from 2015, measurement methods for basic types of machines, namely DC machines, induction machines, and synchronous machines, are described. For the evaluation of induction motor losses, the standard defines three preferred methods. The methods are categorized by the power of the measured machine, so one method is always applied for the selected power range. Table 3.2 describes the basic characteristics of these methods. Publication [18] explains that these methods are applicable for practical and routine testing. For our case of an induction motor powered by a frequency converter, the IEC 60034-2-3 standard specifies

the measurement methods. These methods closely resemble those in the IEC 60034-2-1 standard, where machines are powered by a conventional sinusoidal source. However, the IEC 60034-2-3 standard refines the measurement of harmonic losses arising from the use of a frequency converter.

Table 3.2: Preferred methods of measuring induction machine losses according to IEC 60034-2-1 (2014) from [27].

Label	Method	Description	Application
2-1-1A	Direct measurement: input-output	Torque measurement	All single-phase machines
2-1-1B	Summation of losses: Residual losses	Stray-load losses from residual loss	Three-phase machines with rated output up to 2 MW.
2-1-1C	Summation of losses: Assigned value	Stray-load losses from assigned allowance	Three-phase machines with rated output greater than 2 MW

3.3.1 Direct measurement: input-output

Testing method in which the mechanical power of the machine is determined by values of the torque on the shaft and by measuring the rotation speed. The input power of the machine is also measured. Most commonly, the tested machine is coupled with a dynamometer, which serves as a loading machine and simultaneously indicates the applied torque. Alternatively, the tested machine can be coupled with another machine. In the case of a loading machine, it is necessary to measure the torque, for example, using a torque measuring shaft. The tested machine is allowed to thermally stabilize at the operating temperature, and the required values of quantities are recorded. The difference between input power and output power then equals the losses of the machine. Publication [18] describes that such a type of measurement can be very imprecise. Single-phase machines achieve lower efficiency, so it may not seem like a significant problem, but the entire precision of the measurement relies on the accuracy of measuring torque, speed, and input power. Especially when measuring torque, higher uncertainty can arise, as measuring shafts may not be sufficiently precise, and a 1% error in measuring torque can result in up to a 10% error in determined losses. The measured losses cannot be divided into components, and only the efficiency value is known. This method is very fast, and the longest part is waiting for the machine to heat up to its operating temperature.

3.3.2 Summation of losses: residual losses

A test method for which the efficiency is determined by the sum of the measured losses. The standard describes a flow chart for determining the effectiveness of using this method. Iron losses and windage and friction losses are determined in a no-load test, which is in the voltage range from 30 % to 110 %. The lower half of the voltage range is for determining windage and friction losses and the upper half is for determining iron losses. Joule losses in the stator and rotor are determined at full load when the machine has thermally stabilized, it is also important to measure the value of the resistances at ambient temperature. Stray-load losses are measured by loading the motor with a load curve that is in six operating points ranging from 25% to 125%. This test is also performed immediately after the rated load test to maintain the operating temperature and temperature changes should be as small as possible. As defined, this method is used for most three-phase machines on the market up to 2 MW. This method offers a breakdown of motor losses compared to the first method where only efficiency was determined.

3.3.3 Summation of losses: additional losses under load from assigned tolerance

This method is very similar to the previous one and the efficiency is determined by the sum of the measured losses. The method is adapted for power above 2 MW, as it is difficult to achieve the nominal values in tests for such power. In the load test, the voltage is reduced and a value is assigned for the additional load losses. Full load and load curve tests are not required. In the load test, the machine is operated as a motor with reduced voltage with the maximum available load so that the speed is maintained at rated speed. The current decreases with voltage, the machine power then decreases with the square of the voltage. Using a no-load test with full voltage, the current is then measured. From this current value, the magnitude of the current for the loaded machine can be determined. Stray-load losses are determined by the standard according to the rated power of the machine, which may not be a completely accurate estimate.

3.3.4 Testing methods for field or routine-testing

Standard [27] explains that other methods or test methods are used for other cases such as operational testing, customer acceptance testing and routine-testing. The publication [18] describes that these tests are less accurate than the main three preferred ones.

Table 3.3: Additional methods of measuring induction machine losses according to IEC 60034-2-1 (2014) from [27].

Label	Method	Description	Required equipment
2-1-1D	Dual supply back-to-back	Dual supply back-to-back	Machine designed for full load; two identical units
2-1-1E	Single supply back-to-back	Single supply back-to-back	Two identical units (wound rotor)
2-1-1F	Reverse rotation	Stray-load losses from removed rotor and reverse rotation test	Auxiliary motor with rated power up to 5 times the total losses
2-1-1G	Eh-star	Stray-load losses from Eh-star test	The windings must be connected in a star
2-1-1H	Equivalent circuit	Currents, powers and slip from the equivalent circuit method, stray-load losses from assigned value	If test equipment for other tests is not available (no nominal load application, no duplicate machine)

The [27] standard briefly describes the working procedures for the evaluation of these test procedures. For the 2-1-1D test, two identical machines are mechanically coupled together and only the power supplies are swapped during the measurement. One machine is supplied with nominal voltage and frequency values and the other machine is supplied with either a lower or higher frequency value depending on the machine mode of the generator or motor. The voltage of the second machine is balanced in proportion to its frequency. The 2-1-1E method uses a similar principle, but is only applicable to IM with a wound rotor. Both machines operate at rated values, one as a generator and the other as a motor. It is important to short-circuit the motor rotor windings and connect the generator rotor windings to a suitable power supply. The 2-1-1F method uses the same principle for determining efficiency as the 2-1-1B method. The added losses are obtained by two measurements namely, a machine with the rotor removed and a machine rotating with the reversing speed. Method 2-1-1G again uses a similar principle, but the additional losses are determined by the Eh-star test. Eh-star wiring requires the motor to operate with a dissimilar voltage supply without coupling to another motor. A

resistor is used to connect the machine to the power supply. The last method, 2-1-1H, is suitable when a load test cannot be performed. It uses a T-model of the IM circuit phase, where the substitution resistance represents the equivalent of the losses in the iron. A no-load test, a reduced frequency test, or a nominal frequency test is performed. With the measured values of reactance and resistance, the values of the replacement scheme can be calculated.

3.4 Specific methods for converter-fed machines according to IEC 60034-2-3

In 2020, an IEC standard was published that modified the definition of test methods for measuring machines powered by a frequency converter. The standard [28] describes that these measurement methods should be used to determine the total losses, including the additional high frequency losses of motors, and the efficiency of inverter powered motors. The following table 3.4 shows the methods recommended by the standard. The [28] standard is based on the fact that drive systems consisting of a motor and an inverter often come from different manufacturers, which can change the basic characteristics of the inverter such as the switching frequency. These different characteristics affect the efficiency of the system. For practicality, the standard defines a limited number of approaches depending on the voltage level and nominal parameters of the machine under test. This means that the losses determined by the standard do not represent the losses in the final application, but serve as an objective basis for comparison of motors with other designs.

Table 3.4: Preferred methods of measuring frequency converter driven machines losses according to IEC 60034-2-3 (2020) from [28].

Label	**Method**	**Description**
2-3A	Direct measurement: input-output	Torque measurement
Other testing methods		
2-3B	Summation of losses	Determination of additional high-frequency losses with inverter for final application
2-3C	Alternative method of determining efficiency	Calculation using a qualified analytical model
2-3D	Determination of efficiency by calculation	Calculation method for engines with rated power greater than 2 MW

The 2-3A direct measurement method is similar to the previous IEC 60034-2-1 standard. The 2-3-B method describes that the high-frequency additional losses due to added harmonics from the frequency converter are independent of the load. This allows the use of no-load measurements with a line frequency supply and a frequency converter supply. The results of these measurements are compared and the additional harmonic losses are reflected in the calculation. The 2-3-C method uses an analytical model to calculate the efficiency, which consists of several steps. The analytical model is qualified by the manufacturer according to the manufacturing procedures. The last method 2-3-D, where the efficiency is determined by calculation, is applied to motors with a power rating higher than 2 MW. For machine characteristics beyond testing capabilities, calculation of harmonic losses due to the inverter may be an alternative method. The calculation is based on the actual inverter pulse shape, the frequency dependent surrogate parameters and the motor models used involving higher frequencies.

3.5 Computational analysis

Dissertation [29] describes the importance of the time step and analyses the comparison between the speed of the calculation and its accuracy. Reduction of computation time can be achieved by high performance hardware. Some of the most important components include the central processing unit (CPU), storage drives, and also the size of the random access memory (RAM). CPU memory can run out during a demanding computational task, so it is important to have a good solid-state drive (SSD) or hard disk drive (HDD). An SSD is much faster at writing data, so fast storage is used, while an HDD is used purely for backup and storage, where it can be more durable but much slower than an SSD. The performance of a CPU is specified by its Clock speed usually given in GHz, the number of CPU cores and the size of the CPU cache. Higher Clock speed allows all operations to be sped up, most CPUs will take advantage of the temporary speed increase at the cost of its lifetime. The number of CPU cores allows an application using FEM to work on multiple tasks at the same time, this feature is referred to as the parallelization technique or to use multiple cores per task, which increases the computation speed several times. The CPU cache size represents temporary memory for frequently used data, allowing easier access, thus speeding up processes. It has several levels ranging from L3 to L1. A CPU with a higher cache memory that is large enough to compute the selected task allows the task to be sped up, thus reducing computation time. The CPU also has so-called memory channels, which allows access to RAM. The number of memory channels affects its bandwithd, again a higher number of memory channels is better for reducing simulation time.

Several types of analysis are used in electrical machine modelling. These analyses examine the basic properties of the machine such as temperature, electromagnetic properties and mechanical properties. They work closely together and modify each other, iterating the best possible solution according to the specified requirements. For example, the resulting losses from the electromagnetic model are fed into the thermal model for the correct choice of cooling and operating temperature. Thesis [30] calls this principle as multidisciplinary modelling. The doctoral thesis [31] explains the possibilities of modelling PWM using an externally connected circuit modelled in software such as SIMULINK.

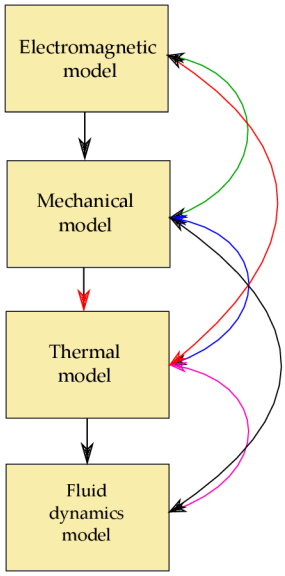

Figure 3.1: Hierarchy of mathematical models in calculation, modified from [30].

Furthermore, the dissertation describes the importance of finite element analysis (FEA), where the use of these software interfaces enables a great acceleration of optimization and modeling of electrical machines. The computational complexity of the analysis is highly dependent on the complexity of the model and this determines the time required, which can be in the range of days. There are several methods to reduce this time including parallel and distributed partitioning analysis, as well as time decomposition methods. These methods use software programs for calculation. The widely used solvers include transient magnetic (TM), time harmonic (TH) and magnetostatic (MS). Each solver has its advantages and disadvantages, where in the analysis of electrical machines the transient magnetic solver is most commonly used. Its disadvantage is the long computation time, which is good to reduce by the methods mentioned earlier. The remaining solvers TH and MS are relatively fast but bring some disadvantages, so they may not be suitable for all tasks. TH linearizes the materials, so its computation produces computation error with higher harmonics. MS does not allow

the calculation of eddy currents losses, which for example for an induction motor is an important parameter.

The dissertation then discusses the importance of the time step, where in the actual measurements the values were recorded with a step of one micro second, while using such a step in a calculation with a very dense mesh FEA would be very time consuming and a lot of computational power would be needed. So, in this work, the sampling time was increased up to one hundred micro seconds. With lower sampling time, the high frequency was reduced in any case. With higher sampling rate the pulses lost their shape due to harmonics and the harmonic content also changed. Data with a higher time step had reduced performance due to harmonic current losses. With a smaller time step, the waveforms are smoother and there are fewer errors due to signal distortion. The reduced power due to higher losses in the iron was compared to the measured results, which were larger when compared. The author of the paper described that this is due to incomplete consideration of additional losses and mechanical losses in the finite element method calculation.

3.5.1 Finite element method

The book [32] describes a brief history of design, where a large number of authors are involved in the design of electrical machines to make the electrical and magnetic properties of the machine as efficient as possible for a variety of applications. For such design, analytical methods were and are popular, using empirical formulas validated by experience and long practice. The finite element method (FEM) is not a new method of calculation, but the modernization of computational units has allowed better use of computational power, making FEM a good alternative. FEM is based on dividing the electromagnetic model into small parts which are calculated and the user determines the density of the network. Book [32] states that nowadays FEM is very popular and is also used in other sectors such as medicine. For electrical machines, 2D and 3D models are used, which are computed using Maxwell's equations. The 2D model of the electrical machine section is usually sufficient for computation because its cylindrical shape is defined by the depth of the machine. FEM calculation of an electrical machine can be very accurate, the book describes a deviation of about 1% for reluctance machines and 10-20% for induction machines. There are several software using FEM, this work will use the Ansys Maxwell interface. The great advantage of FEM is the simplicity of the machine design, which is not yet fully defined. Several designs are calculated and then the best geometry for the chosen application is selected, the parameters can always be adjusted to get perhaps the best optimized machine. The parameters of an electrical machine obtained by FEM should be more accurate than those obtained from an analytical calculation, because FEM considers the electromagnetic field distribution as the basis

for its calculations, which affects material saturation, flux density waveforms, slotting, and more, compared to the analytical calculation of an electrical machine, which obtains the parameters using dimensions and material properties and also simplifies the magnetic field distribution. The book [32] further describes the basis of FEM calculations. It uses Maxwell's equations to solve FEM. To calculate an electrical machine, it is usually sufficient to use magnetostatic analysis, which uses only some of Maxwell's equations, because it is a low frequency problem. It is also possible to use the time-harmonic problem, where FEM models the materials of the machine's thin sheet with consideration of hysteresis in ferromagnetic materials.

To calculate the force and torque, which is one of the most important parts of this method according to the book, FEM uses Maxwell's stress tensor, the coenergy method and the Lorentz force equation. Maxwell's stress tensor uses a flux density distribution on the dimension of the curve or line that can be chosen. For electrical machines, the curve is defined in the air gap. The coenergy method uses the conversion of energy to mechanical energy for a system where the air gap and ferromagnetic core change, for example for a switched reluctance machine. The Lorentz force is defined as a function of the phase values of the induced voltage and the phase values of the current for a three-phase system. For linear systems, the inductance is calculated from the magnetic field energy, where in the case of electric machines this is valid if the machine is operating in the linear B-H part of the magnetization characteristic and for nonlinear systems from the flux linkage when the machine enters the knee of the magnetization characteristic and the over-saturation state.

The publication [5] explains that finite element method is particularly suitable for modelling and calculating an electrical machine compared to other methods. The use of a transient solution is appropriate for most induction motors, but such an analysis can take a very long time.

3.5.2 General procedure for calculating FEM

The process of FEM calculation, according to the book [32], can be divided into three basic parts. The first part is the pre-processing, where the model is prepared and processed. The next part is the solver, where the system of differential equations is assembled and subsequently solved. The last part includes post-processing, where the results are analyzed, and additional quantities are computed.

The preparation of the model in pre-processing involves creating the geometry of the model by defining units, choosing 2D or 3D interfaces, and selecting a coordinate system. Then, the model can be drawn or imported from CAD programs. In the drawn geometry, it is necessary to define materials for corresponding parts, excitations in electrical machines, usually in windings, and boundary conditions. At the end of pre-processing, it is

also necessary to create a computational network called mesh. Mesh is the main principle of FEM, where finite elements divide the modeled machine into small parts, usually triangles, but other shapes can also be used. The user changes the number of finite elements, thereby increasing accuracy, but a higher number of finite elements lengthens the calculation. However, it is not always true that if we want the highest accuracy, we must add as many elements as possible. For such a calculation, it is necessary to find an optimum, for some parts, accuracy with a small number of elements is sufficient, and adding more elements is unnecessary and only adds to the calculation time. Meanwhile, for highly saturated areas in an electrical machine, it is advisable to expand the mesh.

In the solver part, partial differential equations are assembled in each finite element, represented by the vertices of triangles. Vector magnetic potential is computed for these vertices. The software then calculates the differential equations using defined iterative methods, and there are two possible outcomes. Either the solution will be convergent, meaning the expected solution is obtained, or it will be divergent, indicating that the results could not be successfully computed. It is then necessary to check the model and reapply the solution.

The final part, post-processing, involves result analysis. Software provides displays of results through profiles and can be visualized in the geometry as well as the distribution of magnetic flux or magnetic induction. From these distributions, values such as torque can be calculated using curves and similar methods.

3.5.3 Accuracy of analytical model

The publication [24] explains that the first steps of IM design include an analytical calculation process, which is later used for optimization through various objectives such as cost of materials, energy efficiency and so on. The output power of the designed machine is defined using the machine dimensions. The range that can be used to choose the dimensions is limited by the temperature rise. Temperature rise corresponds to the losses generated by the machine. Using material properties and geometry, the losses can be determined. To facilitate this, the very popular finite element method (FEM) can be used. However, in some respects the FEM is inadequate for an induction motor. Most often the model is created in 2D, because in 3D it would be too complex and the calculation time would be too long. The model in FEM is a circuit model that is used with an external model to model the 3D effects. When modeling IM with FEM, end-winding resistance and end-winding leakage inductance are written into the stator model. In the rotor model, the resistance and short-circuit ring inductance are written into the rotor model. These parameters can be very challenging to determine accurately compared to the conventional stator winding resistance and rotor bar resistance, which can be determined using temperature and neglecting AC-induced losses. Inaccuracy in the

calculation of iron losses arises when using the Bertotti model, where the calculation equation is modified by empirical coefficients that are set to match the specific properties of the iron core used for the calculation. Another uncertainty for modelling an induction machine is the fixed slip. This varies with rotor losses and rotor resistance. This publication presents an alternative analytical model to the FEM model. The analytical model is built with the same parameters as the FEM model, but compared to the FEM the calculation is much faster and in seconds. Another advantage is the possibility to investigate the influence of other parameters. This paper compares the analytical model of a 5 kW induction motor with the measured values using IEC segregation method. The paper [24] also describes the calculation of the design of the analytical model using the book by Juha Pyrhönen, Valeria Hrabovcova and Tapani Jokinen: Design of Rotating Electrical Machines. The calculation is adapted to the geometry and size of the machine, for example, DC resistance is considered for the calculation of Joule losses. Empirical coefficients for iron losses are defined and mechanical losses are defined from friction only, since the motor rotational speed is small and the motor does not have a fan on the shaft. The additional losses are defined as 1.2 %. As a result, the measured losses are compared with the analytical ones. The author describes the inaccuracies that arise, where for example the inaccuracy in the stator calculation may be due to a poor estimation of the end-winding resistance, as well as copper impurity and the effect of load losses, where additional losses from harmonics arise. In small machines these load losses are insignificant, but in large machines they can cause quite large losses, this is due to the skin-effect which changes the AC-resistance. The publication outlines that the analytical model can be suitable as a precomputation with its mediocore accuracy and then the model can be optimized by other methods.

3.5.4 Finite element method disadvantages

The work [29] further explains that several computational inefficiencies need to be considered when using the FEM method. Constantly changing material properties can be challenging for the calculation to determine. The magnetic properties of the material are considered in the calculation, but the constantly changing magnetic field in the iron core can be complex to properly model the magnetic flux in electrical machines. For core losess the previously mentioned eddy-current distribution and hysteresis losses apply, these losses usually have to be calculated using various post-processing methods by which real results can be achieved but with certain boundaries and limits. Several factors are responsible for inaccurate core loss calculations using the FEM method, but one of the most notable is the shape of the B-H curve. The shape of pure sine waveforms that are affected by the loop of the B-H curve are corrupted by the additional harmonics, causing additional losses. Today's FEMs can effectively calculate the behaviour of a

rotating machine if the machine losses and heat transfer are calculated. Time scaling is needed to calculate temperatures in different parts of the machine. The thermal eqilibrium of an electric machine sometimes takes several hours to settle. The FEM calculation has to consider this fact and therefore a large number of time steps are needed. It is also important to model the airflow correctly, where turbulent flow can occur in the air gap, which is challenging to simulate.

Nowadays, high efficiency of electric machine is one of the main goals in electric machine design. FEM calculation results can tell us what losses the machine will have, but the additional losses and mechanical losses will always need to be analytically calculated or measured on a prototype machine. In a 2D model of the machine, additional losses can be included by some factor, but these losses are only considered in the air gap. Additional losses also occur in the machine frame and in other parts of the machine that are not modelled. Experience from previous designs and laboratory measurements are needed to estimate these losses correctly. Different machine geometries, motor fan settings, etc. are variables that can change the resulting calculated losses. The thesis [29] describes three methods for determining these problematic losses using a segregation method.

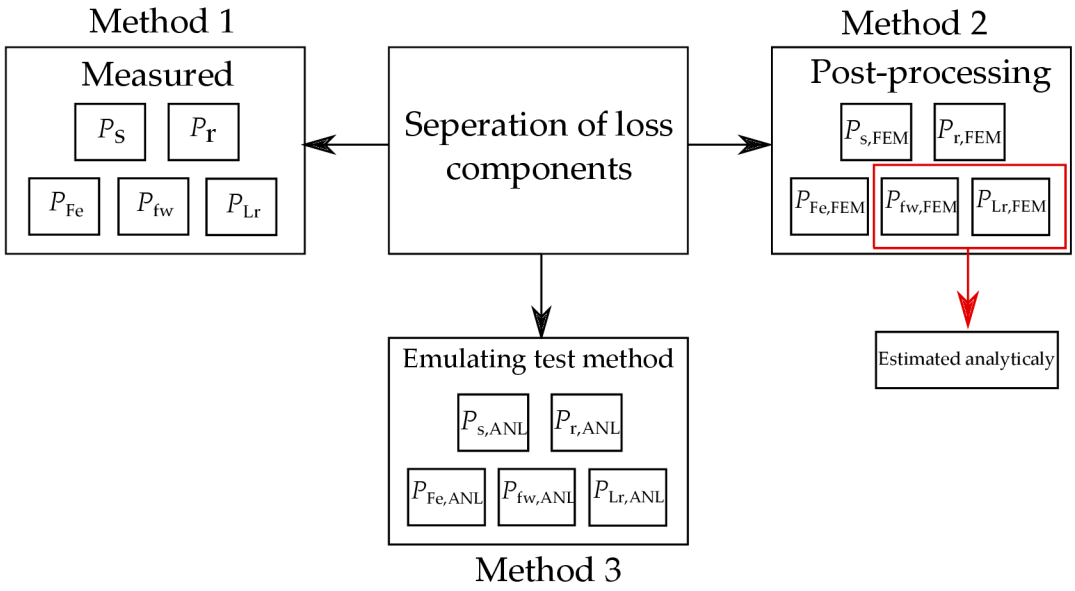

Figure 3.2: Separation of loss components, redrawn from [29].

3.6 Segregation of losses

The article [23] defined that popular methods for determining the losses of an electrical machine include the loss segregation method, which consists of three measurements, namely no-load, rated load and load curve test. This method is particularly suitable for high-efficiency machines because it uses indirect measurements. As explained in the

previous chapter, induction motor losses can be divided into five parts. Stator and rotor winding losses, iron losses and mechanical losses can be analytically calculated. Stray-load losses or additional losses cannot be modeled. Based on the publication [23] to determine winding losses, the value of winding resistance must be measured. There are several ways to measure the required resistance, but the IEC standard specifies a test in which the DC resistance is measured after the motor has warmed to thermal equilibrium. The IEC standard then assumes that the skin effect and proximity effect is attributed to the additional losses. For motors powered by a frequency converter, the AC resistance value would be more important.

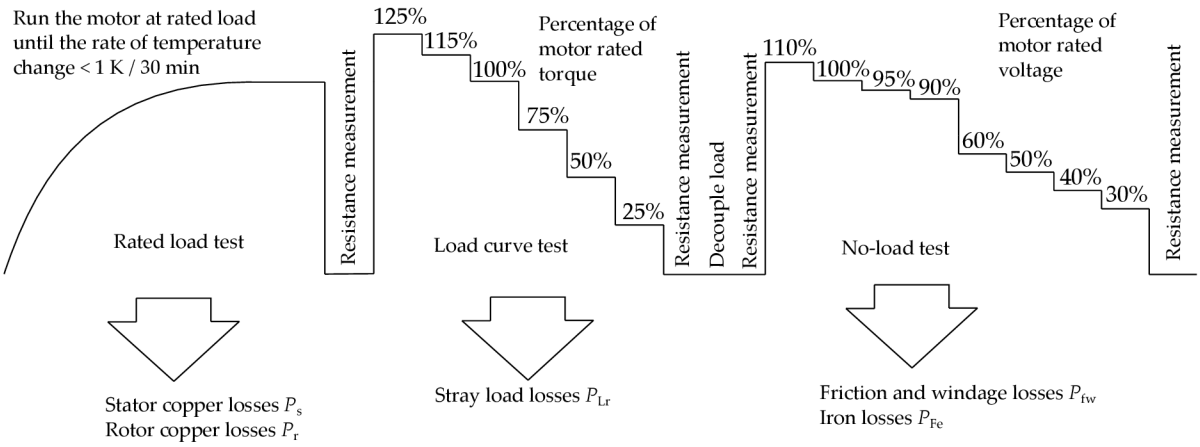

Figure 3.3: Segregation method according to IEC, redrawn from [29].

In the first part, the load rating is first measured until the temperature rise is stabilized. After the first measurement, it is necessary to ensure that the ambient temperature does not change and after stopping, the stator resistance is immediately measured at the operating temperature. The next part of the measurement involves gradually loading the motor with a percentage of the rated torque. The warmed up motor is loaded with 125% load and gradually reduced to 25% of the rated torque. Reducing the torque will also reduce its operating temperature, so subsequent stator resistance measurements must be made quickly. The last part involves the motor itself at no load, where certain magnitudes of voltage are supplied, and again the winding resistance is measured. The determination of iron losses is made using the measured no-load voltage using operating points from 90% to 110% of the rated voltage. The result is the final loss equation for the motor being measured.

$$P_{\text{loss}} = P_{\text{s}} + P_{\text{r}} + P_{\text{Fe}} + P_{\text{fw}} + P_{\text{Lr}} \tag{3.1}$$

Calculation of additional losses and mechanical losses using FEM is possible. As mentioned above, these losses are usually determined as a percentage of the total power

input. These percentages have been the subject of several articles in which they have been verified with an actual machine, but the IEC standard defines an exact value of the motor input power. For the FEM to be able to calculate the additional losses and mechanical losses, a 3D model is needed. This can prove to be a very challenging task because the whole machine with bearings, housing, end windings (rings), etc. needs to be modeled. However, even for 3D it is challenging to model the eddy current losses occurring in the bearings, housing, and in the end rings. In the next section of the work [29], the FEM with a PWM voltage source is explained. The motor speed can be effectively varied depending on the load, which allows us to increase the efficiency of the system when using a converter. As explained, such a high frequency voltage converter can further lose harmonics, which increases the temperature of the machine, and this again increases further losses. This paper presents a loss distribution model for a motor controlled with a frequency converter.

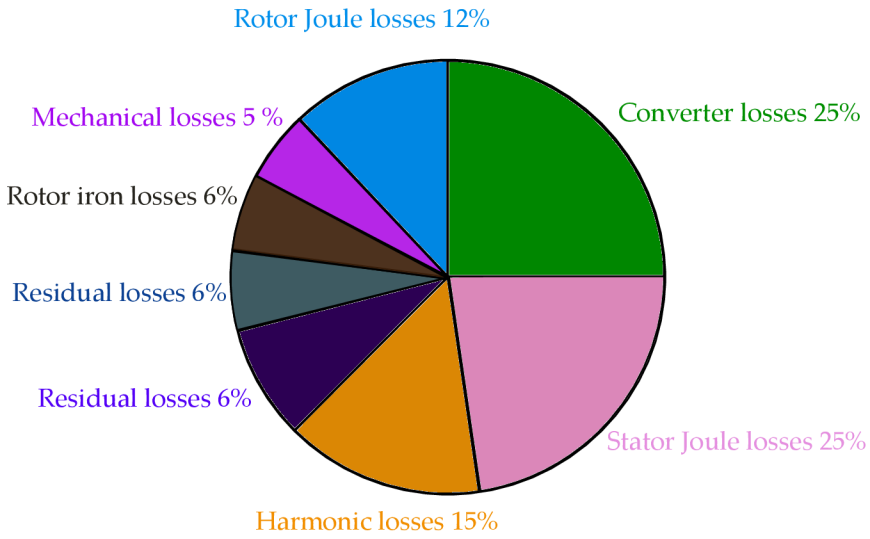

Figure 3.4: Typical loss distribution for converter-fed induction machine, redrawn from [29].

For machines powered by frequency converters, there are special IEC standards that specify how losses can vary when powered by a frequency converter at a certain power output. The losses generated in the frequency converter in the semiconductor components are proportional to the harmonic losses in the motor.

Dissertation [29] explains that when calculating with PWM power supply, several methods can be introduced to get the correct result. The first method includes setting the PWM into the model according to a pre-measured current waveform. This is useful if the load is resistive in nature, but with loads such as electrical machines, the current waveform may be altered due to inductance, as high inductance will resist the change in current. Another option is to use a recorded PWM waveform in the model. This

method much better for electric motors because the current source is fixed. This method can be very time consuming and computationally intensive as it requires a very small calculation step and a very good mesh size to calculate the high harmonics in the PWM waveforms. In addition, the embedded PWM waveforms are only valid for one operating point, where the motor temperature can increase the rotor resistance during actual motor operation, which can further increase the losses. This drawback can be circumvented by adding the actual measured machine values to obtain the slip value. Another disadvantage is that there is no damping phenomenon in the machine model, which makes setting the time step and balancing it a problem. If the set PWM waveform will have fluctuation of the waveform oscillations will arise in the calculation. This guarantees the time-stepping FEA that is needed for the calculation of harmonics. In the third case, linking the converter hardware to the model, which may seem like a very complex task, but some commercial software offers this as an added feature.

3.7 Uncertainty in motor efficiency measurements

To begin with, it is necessary to briefly describe today's methods of determining efficiency and losses. The lecture presentation [33] state that the methods of determining efficiency can be divided into two methods of measurement, namely the direct and the indirect method. The direct method of determining the efficiency of electrical equipment is defined by the ratio of output power to input power or input power. The indirect method incorporates known losses that are either subtracted from the input power or added to the output power. For the direct method:

$$\eta = \frac{P_{\text{out}}}{P_{\text{in}}}. \tag{3.2}$$

For the indirect method:

$$\eta = \frac{P_{\text{out}}}{P_{\text{out}} + P_{\text{loss}}} = \frac{P_{\text{in}} - P_{\text{loss}}}{P_{\text{in}}}. \tag{3.3}$$

Furthermore, the publication [33] mentions the methods used to determine losses. Again, these can be divided into two different methods, namely input-output or calorimetric. These two methods can be applied to all electrical machines and converters and are independent of each other, so both can be used for the same result. The input-output method is straightforward:

$$P_{\text{loss}} = P_{\text{in}} - P_{\text{out}}. \tag{3.4}$$

For the calorimetric method:

$$P_{\text{loss}} = q_{\text{m}} \cdot C \cdot \Delta T. \tag{3.5}$$

The [33] teaching materials show some differences in these methods. The input-output method is based on the measurement of input and output power, while the calori-

metric method uses direct measurement of the generated heat. Naturally, the calorimetric measurement is much more time consuming than the input-output method, and for this reason it is also much less common, generally regarded as an inferior option and sometimes not even acknowledged by [33]. The input-output method also has downsides, mainly the uncertainty of measuring losses with higher magnitudes of efficiencies. It also introduces some error because electrical measurements depend on electrical waveforms such as current, voltage and also their harmonic frequencies. For this reason, it has a limited bandwidth that can be considered in the measurement. These errors are dampened by the high frequency parts in the electrical measurement. Such negatives are completely eliminated by the calorimetric method, it is possible to measure losses even with imperfect electrical waveforms because they do not affect the measurement error. For machines with high efficiency, the calorimetric method is the most suitable because the efficiency has no effect on the measurement uncertainty. Furthermore, only heat is measured, so it has unlimited bandwidth, which could be an advantage in high-frequency measurements. Last but not least, it is an advantage to be able to see from the measurement results whether the measured data is trustworthy, for example from the temperatures. Uncertainties will be further explained in the following figure 3.5.

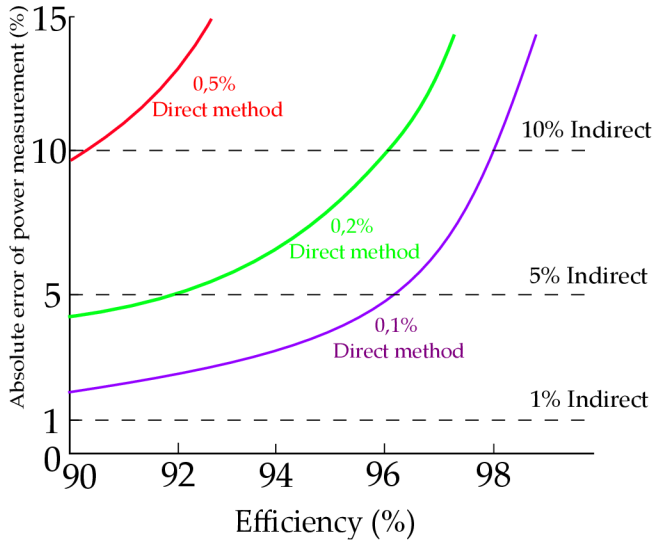

Figure 3.5: Power measurement error dependence on efficiency, redrawn from [33]. The graph shows the power measurement error for the direct and indirect methods.

Figure 3.5 describes how the measurement uncertainty increases for certain efficiency values. The rising colour curves show the direct measurement or efficiency measurement. The percentage values next to the curves show the error in power and power measurements. It is important to note that for direct input-output measurements, the uncertainty of the loss measurement increases as a function of efficiency. Next we need to describe the efficiency measurement error, again explained by the figure below 3.6.

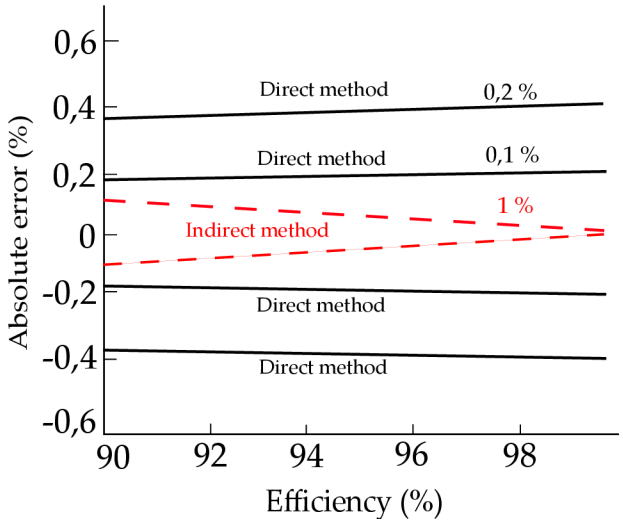

Figure 3.6: Dependence of absolute power measurement error on efficiency, redrawn from [33].

In the figure 3.6 the black lines represent the direct measurement method and the red ones the indirect measurement method. It can be seen from the figure that for the direct method, for a curve of 0.1 %, the uncertainty in the efficiency measurement is less than 0.2 %, while for the indirect method, the error decreases to zero as the efficiency approaches 100 %. This is naturally due to the higher efficiency, which reduces losses and hence uncertainty.

For a better understanding of both principles, the [33] lecture gives examples. For figure 3.5, an example is shown by considering a purple curve where the error in the power measurement corresponded to 0.1 %. Measured power input 1000 W, power output 960 W and efficiency 96 %.

$$|\Delta P_{\text{loss}}| = |\Delta P_{\text{in}}| + |\Delta P_{\text{out}}| = |0,1\% \cdot 1000| + |0,1\% \cdot 960| \approx 2. \tag{3.6}$$

$$P_{\text{loss}} = P_{\text{in}} - P_{\text{out}} = 1000 - 960 = 40\,\text{W} \rightarrow |\Delta P_{\text{z}}| = \frac{2}{40} = 5\,\%. \tag{3.7}$$

For this example, the combined uncertainty of the loss measurement corresponds to 5 %. For the second figure of the efficiency measurement uncertainty **??**, an example case is again given by considering the same measured input and output.

$$\eta_{min} = \frac{P_{\text{out}} - |\Delta P_{\text{out}}|}{P_{\text{in}} + |\Delta P_{\text{in}}|} = \frac{960 - 1}{1000 + 1} = 95,8\,(-). \tag{3.8}$$

$$\eta_{max} = \frac{P_{\text{out}} + |\Delta P_{\text{out}}|}{P_{\text{in}} - |\Delta P_{\text{in}}|} = \frac{960 + 1}{1000 - 1} = 96,2\,(-). \tag{3.9}$$

From these examples, it is important to understand the principle of uncertainty in loss measurement, which approaches infinity when the efficiency approaches 100 %. The

principle can also be understood in reverse, where a more accurate measuring apparatus is needed to measure high efficiency devices to get the same measurement error tolerance.

4 Finite element model

4.1 SEMTEC induction motor model

The fourth chapter shows the modelling of an SEMTEC induction machine with squirrel cage with aluminum bars for two different power supplies of a frequency converter and a generator power supply. The machine geometry was created according to the [34] documentation, all necessary dimensions are given in this document. ANSYS MAXWELL is used to create the geometry. ANSYS uses RMXprt for model generation 4.1.

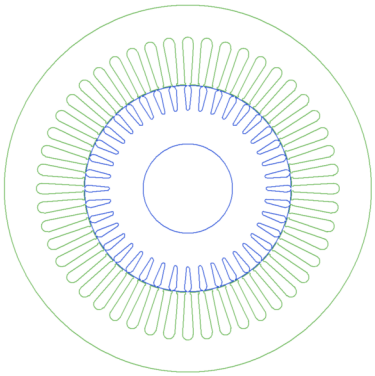

Figure 4.1: RMxprt geometry.

After entering all dimensions and parameters to RMxprt, a 2D model is obtained in MAXWELL 2D, displayed in figure 4.2.

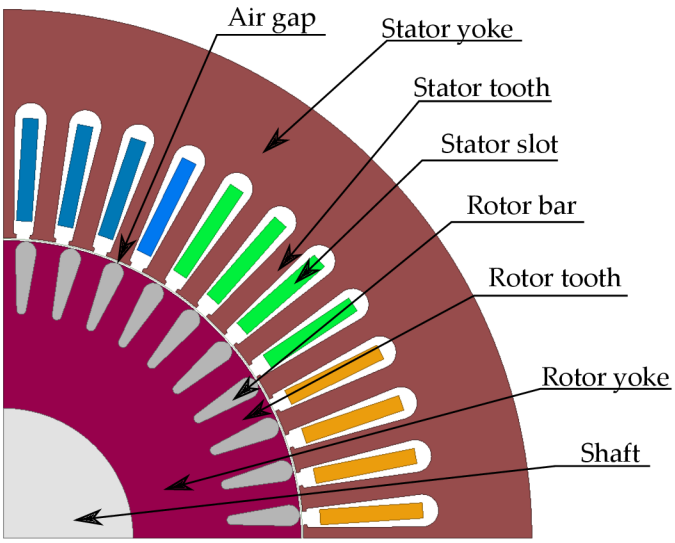

Figure 4.2: Ansys MAXWELL 2D geometry.

The physical parameters of the motor are listed from the 2D model in the table 4.1.

Table 4.1: Physical parameters of the 2D induction model of the motor.

Motor physical parameters	Value
Stack iron length (mm)	160
Stator inner diameter(mm)	125
Stator outer diameter (mm)	220
Rotor outer diameter (mm)	124
Rotor tangential tension (kPa)	8.51
Number of stator slots (-)	48
Number of rotor bars (-)	40
Number of stator parallel branches (-)	2
Stator coil-turns per phase (-)	32
Winding factor (-)	0.96
Number of pole pairs (-)	2
Number of slots per pole and phase (-)	4
Stator core material	M800-65A
Rotor bars material	Al99.5

The nominal operating parameters of the motor are listed in the table 4.2.

Table 4.2: Operating parameters of the motor.

Motor parameters	Value
Rated speed (rpm)	1450
Rated frequency (Hz)	50
Rated line-to-line voltage (V), star connection	400
Rated phase voltage (V), star connection	230
Output power (kW)	5
Rated torque (Nm)	32.9
Current (A)	10.4
Efficiency from losses (-)	0.89
Power factor (-)	0.74
Stator resistance (Ω)	0.94

Operating parameters are obtained from the SEMTEC engine datasheet [35] and available materials.

4.2 Simulation of generator sine supply for loading point P1

The first section firstly shows the modelling of an induction motor fed from a sine wave power supply. This section is an example for load point P1 or 90 % speed and 100% torque. The simulation has been performed in steady state of the motor, with the simulation time set to 700 ms for the sinusoidal source and the calculation time step set to one millisecond. The following table 4.4 shows the analyzed values from the simulation for load point P1.

Table 4.3: Operating parameters of the motor for load point P1 with generator supply.

Motor parameters	Value
Rated speed (rpm)	1302
Fundemental frequency (Hz)	44.599
Rated line-to-line voltage (V), star connection	400
Rated phase voltage (V), star connection	230
Output power (kW)	4502
Rated torque (Nm)	33
Input power (W)	4960
Rated phase current (A)	10.26
Efficiency from losses (-)	0.881
Total loss (W)	605.6
Power factor (-)	0.766
End-winding resistance (μΩ)	0.697
End-winding inductance (nH)	5.5
Torque ripple (%)	5.57

The values are close to the actual values of the SEMTEC engine. Some deviations can be seen in the speed value, where the slip value is not completely accurate due to the material and load settings in the FEM. To get more precise squirrel cage resistance, the conductivity of material was adjusted according to the measured rotor temperatures. The biggest difference arises in the value of losses, the loss model was not completely accurate and requires more adjustments. The power factor was adjusted by increasing the air gap by moving the rotor. This agrees with the real machine, where due to manufacturing the air gap increases by a few millimeters. The current in phase is also higher.

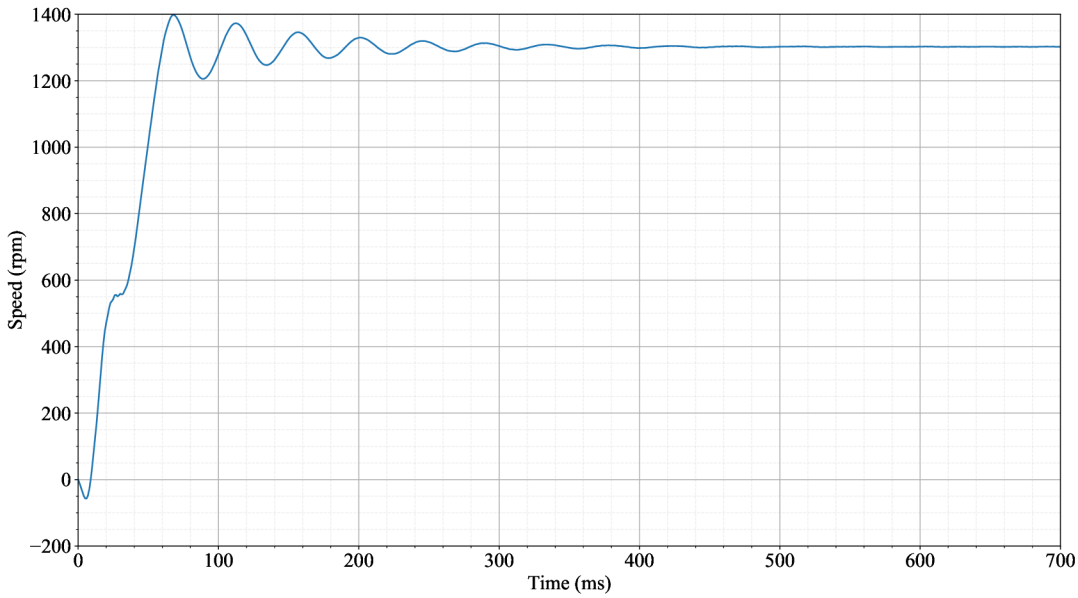

Figure 4.3: Rotational speed.

For operating point P1, the rotor speed corresponding to 1305 rpm is reached after 60 ms and is steady after 400 ms.

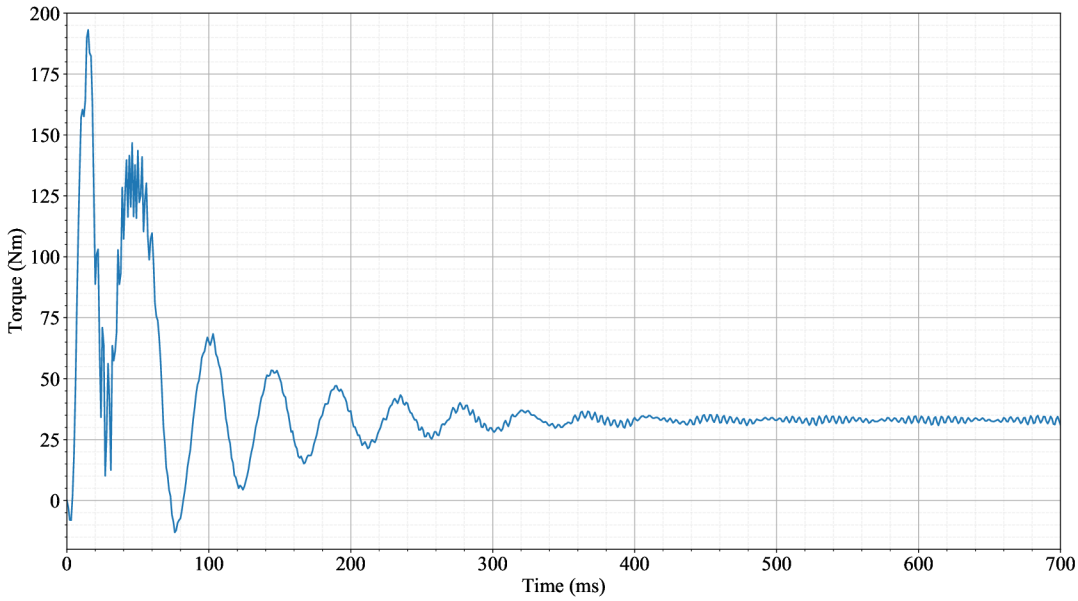

Figure 4.4: Torque during start.

The torque stabilizes in 480 ms at the nominal value of 33.02 Nm.

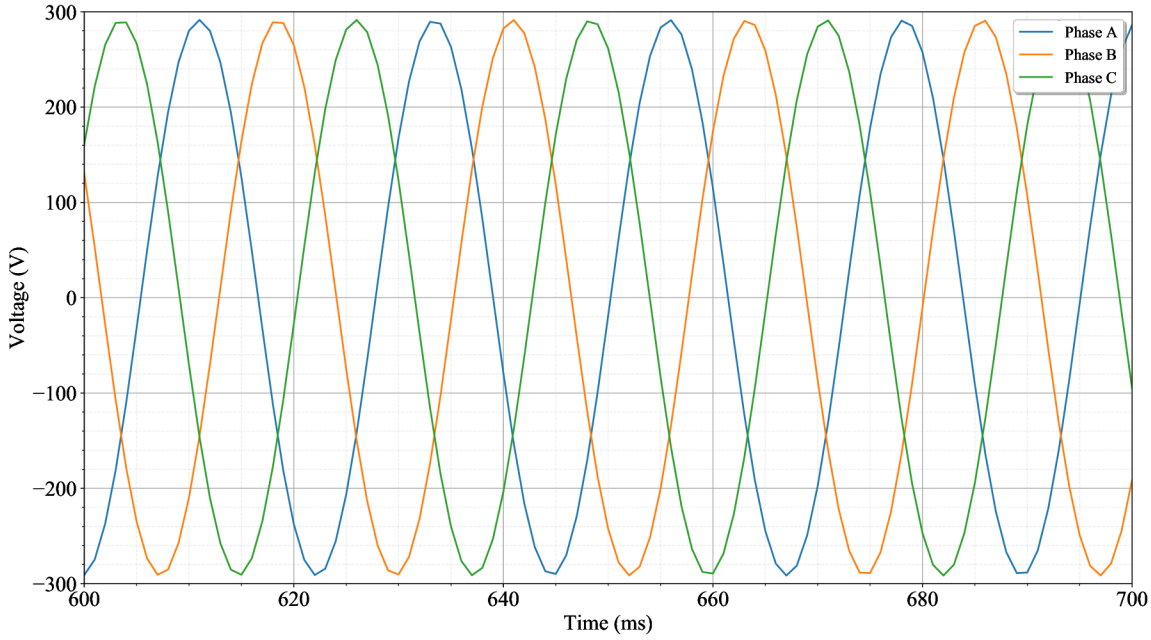

Figure 4.5: Supply sinusoidal voltage.

Later used for comparisons with PWM voltage.

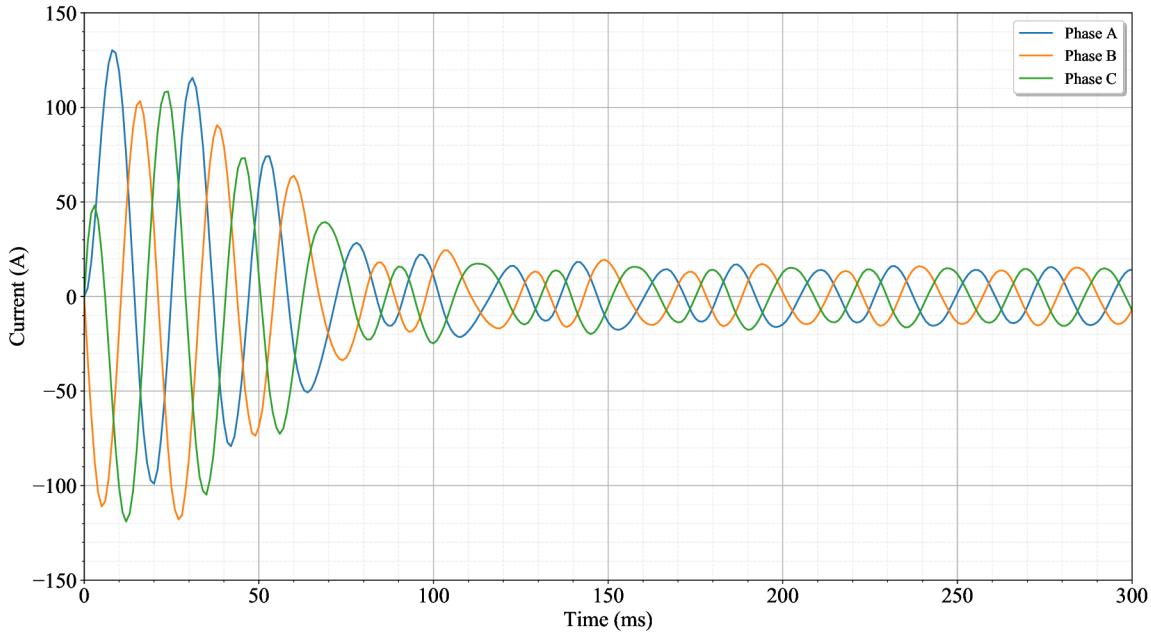

Figure 4.6: Currents during start.

The rated current of the machine after steady state is 10.26 A. The highest value of current at start-up is 130.16 A

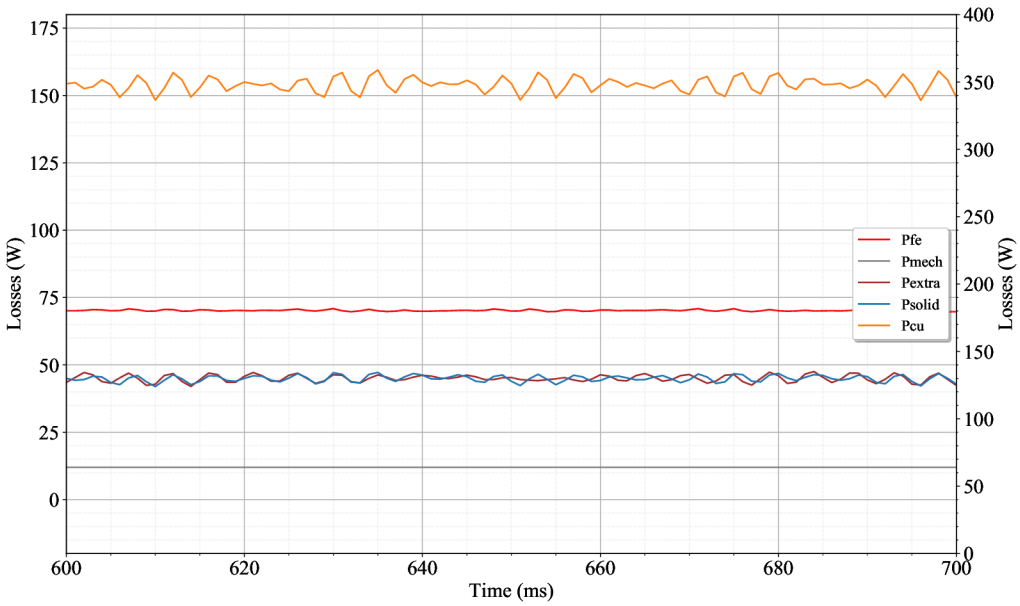

Figure 4.7: Losses in the induction motor at steady state.

For a better view of the distribution of losses, a pie chart is chosen 4.8.

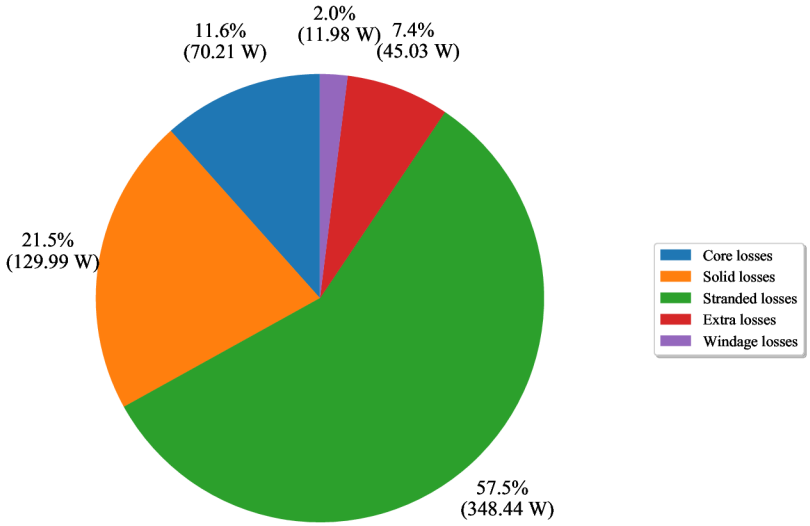

Figure 4.8: Distribution of losses at steady state.

The magnitudes of the losses are not trustworthy compared to the measurements, there is a large deviation. The loss figures are shown here only to compare simulations with sinusoidal power and PWM.

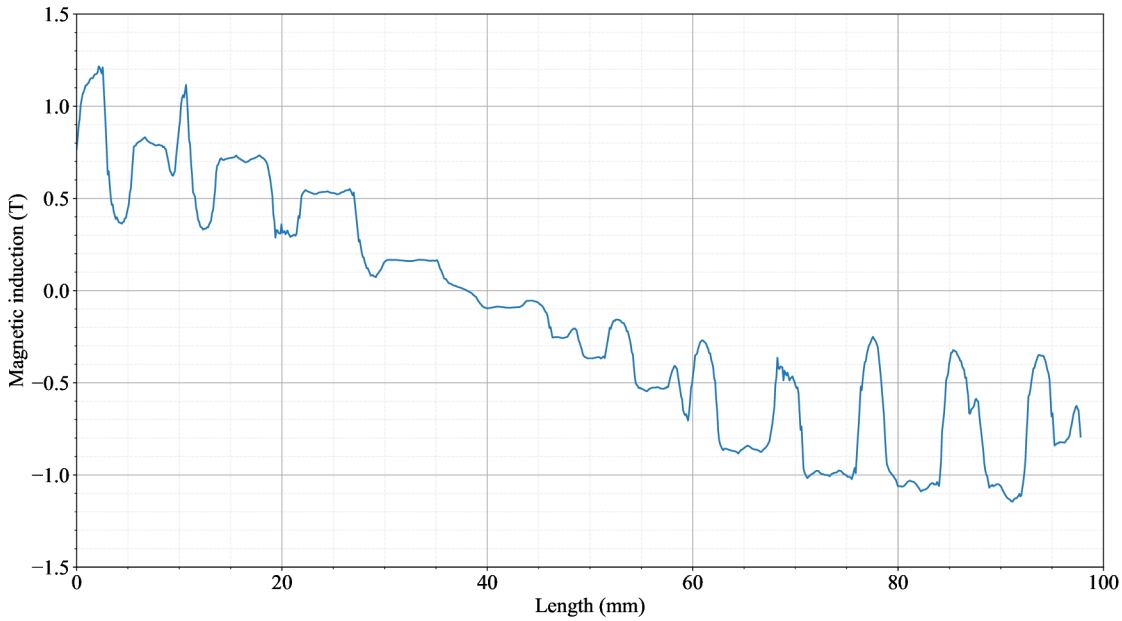

Figure 4.9: Flux density in the air gap.

Flux density in the air gap with the fundamental harmonic is equal to 0.863 T.

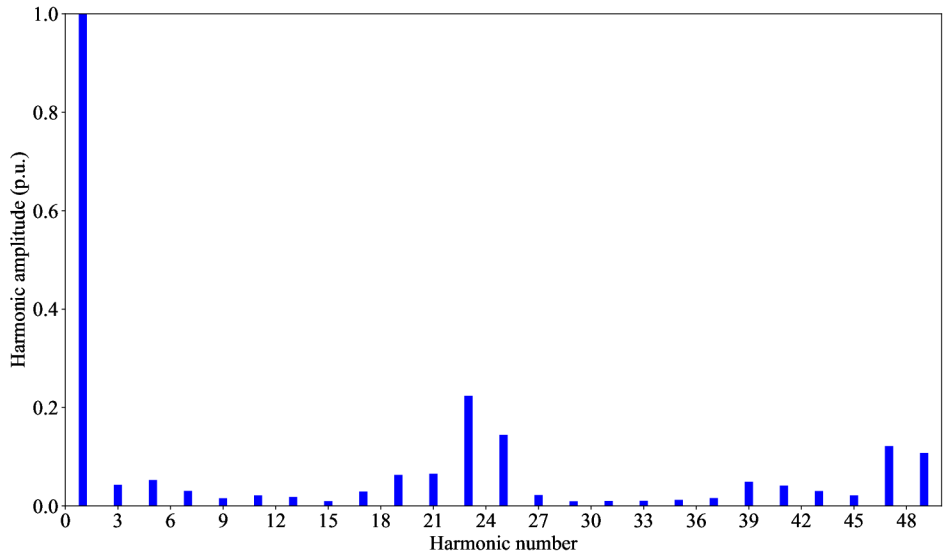

Figure 4.10: Normalized harmonic content of flux density radial component.

The harmonic content of air gap flux density with the highest harmonics are the 1, 21, 23, 25, 47 and 49.

4.3 Simulation of converter PWM supply for loading point P1

This section describes the process of simulating the frequency converter with PWM. During the measurements of the SEMTEC motor with converter supply, the voltage waveforms of the motor were also recorded. To obtain the voltage equations with PWM harmonics, it was necessary to analyze the voltage waveforms using Matlab. The first step was a Fast Furier Transformation of the waveform. In figure 4.11 the FFT analysis of one phase can be seen. The idea behind the PWM simulation is to create voltage equations that will then be used in ANSYS 2D. The equations are made up of harmonics obtained from the FFT of the measured voltage waveform.

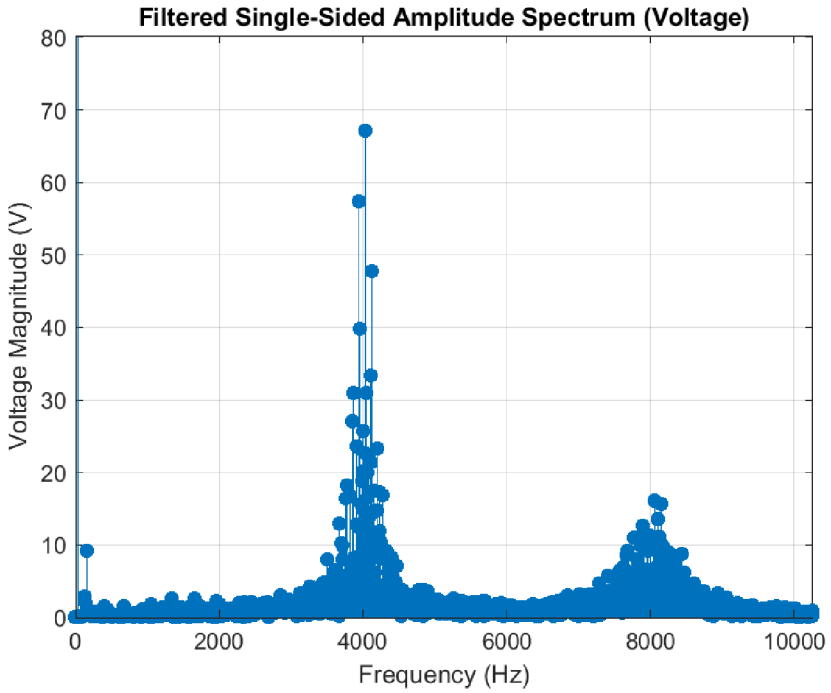

Figure 4.11: FFT of voltage waveform measured with converter measurements.

The value of the first harmonic corresponds to 291 V, the picture is enlarged to better show the other harmonics. Since this is PWM, there are too many harmonics to create an equation. For this reason, it was decided to limit the harmonic spectrum using the per unit value of the first harmonic. The limit was set at 5% p.u. The limit was chosen to include as many harmonics as possible, but still allow the voltage equation to be inserted into the FEM. The creation of the equation was done by a code that generated the equation depending on the number of harmonics. This produced the following FFT 4.12.

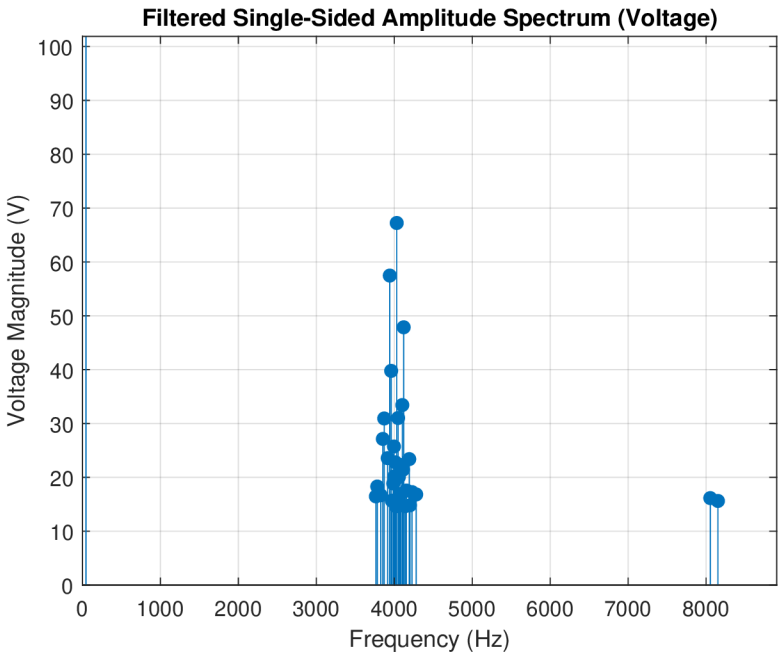

Figure 4.12: FFT of voltage waveform with limited harmonics.

Most of the harmonics are around the switching frequency. Furthermore, for accuracy, it was also necessary to find out the harmonic angles. These are shown in the following figure 4.13.

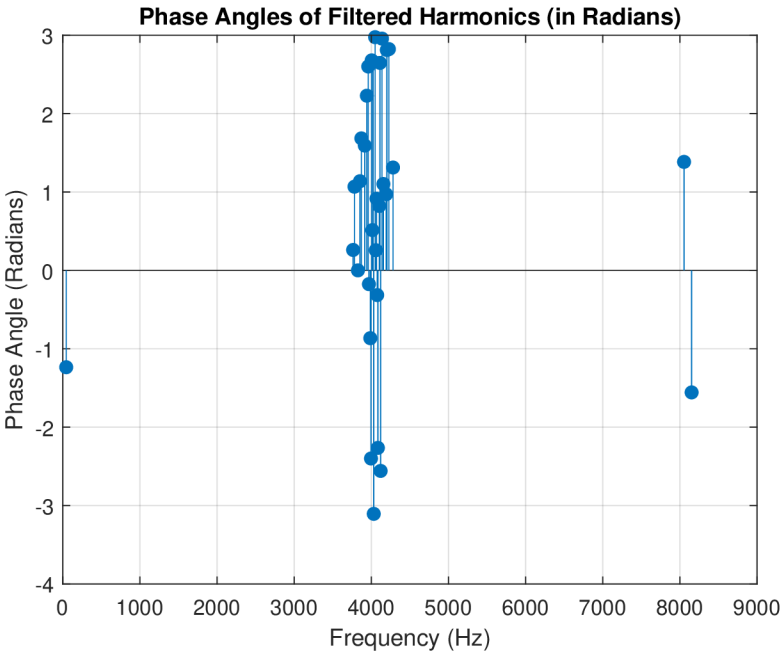

Figure 4.13: Phase angles of filtered harmonics.

The angle, together with the harmonic amplitudes, is written into the equation.

It was also necessary to check the recreated voltage waveform because a frequency filter was applied to the voltage waveform to attenuate the noise from the waveform. The following figure 4.14 shows a comparison of the original measured waveform and the waveform that was filtered by the frequency filter.

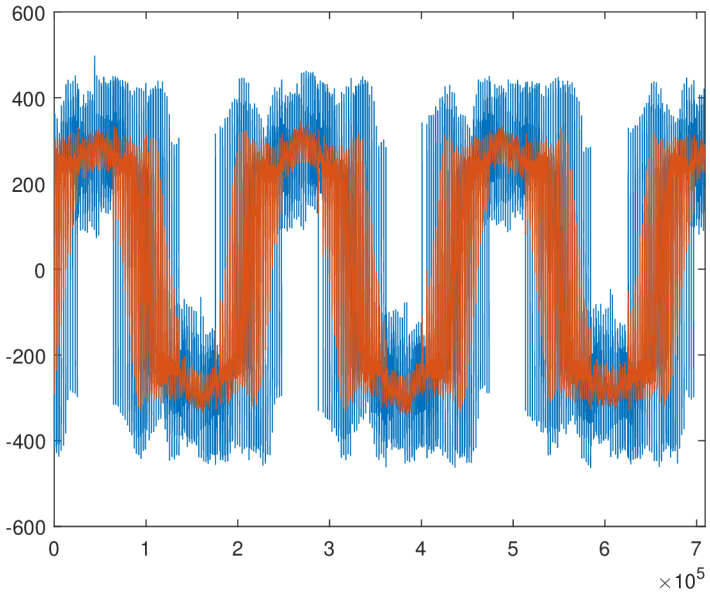

Figure 4.14: Original measured voltage waveform and filtered waveform.

The FFT was again applied to this voltage waveform. A new waveform was created from the harmonic amplitudes, which is compared in the following figure 4.15.

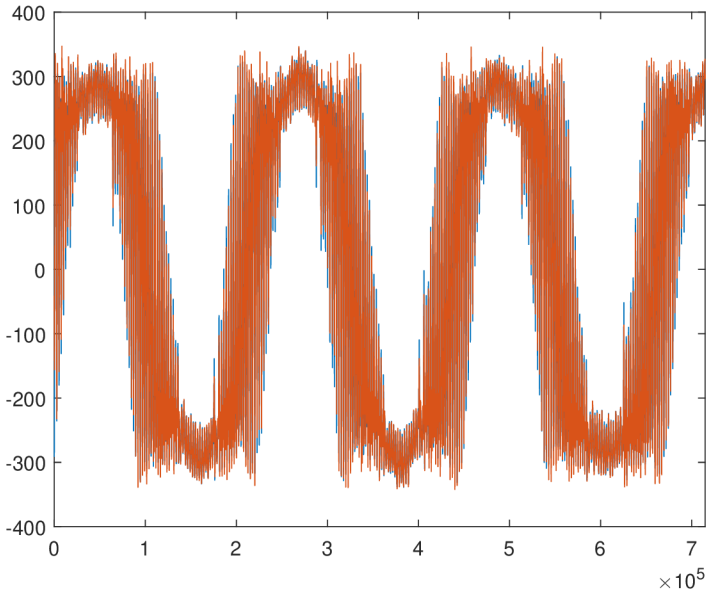

Figure 4.15: Original filtered waveform compared with recreated full one.

The use of per unit threshold produces a filtered voltage waveform seen in the next 4.16.

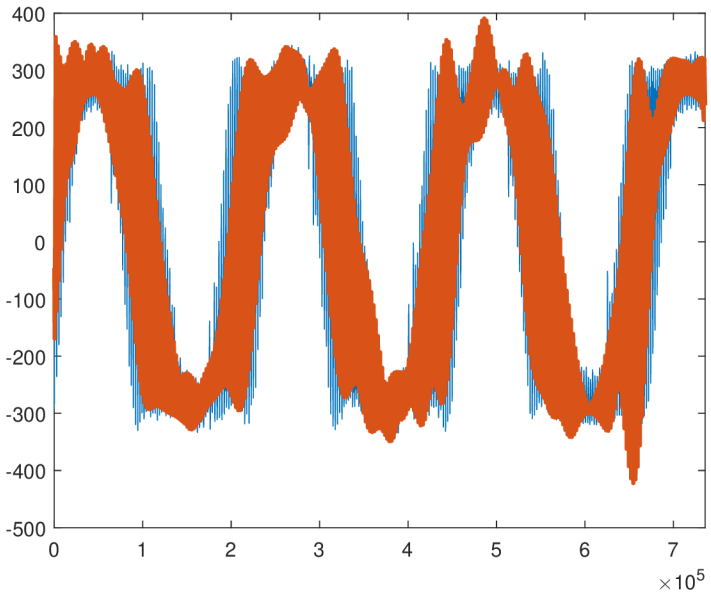

Figure 4.16: Original filtered waveform compared with recreated filtered one.

To check the correctness of the recreated voltage waveform, the current waveform in the following figure 4.17 was also compared.

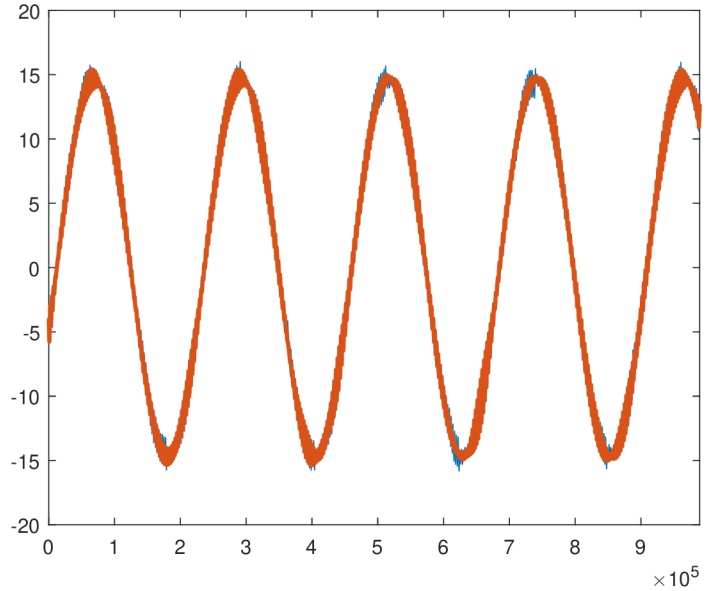

Figure 4.17: Original current waveform compared to the recreated one.

In the last part we check the correctness using cumulative power. The figure 4.18

shows the critical frequencies based on the inverter switching frequency. The comparison allowed for checking how much power is lost by using a filtered waveform.

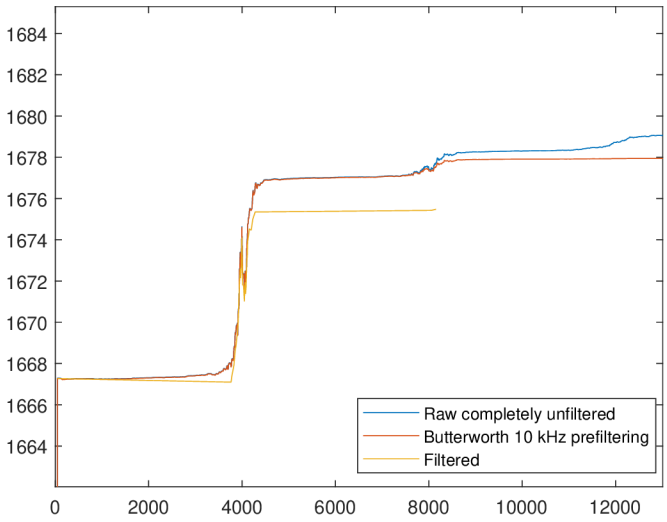

Figure 4.18: Original filtered waveform compared with recreated full ones.

Table 4.4: Operating parameters of the motor for load point P1 with converter supply.

Motor parameters	Value
Rated speed (rpm)	1302
Fundemental frequency (Hz)	44.594
Fundemental voltage (V)	206.1
Output power (kW)	4526
Rated torque (Nm)	33.2
Input power (W)	5140
Rated phase current (A)	10.72
Efficiency from losses (-)	0.87
Total loss (W)	685.936
Power factor (-)	0.66
End-winding resistance (μΩ)	0.697
End-winding inductance (nH)	5.5
Torque ripple (%)	23.07

The difference with the generator was the higher current and higher losses. The power factor is lower and the torque ripple has increased significantly. However, compared to the torque ripple, the operating parameters have not changed that much.

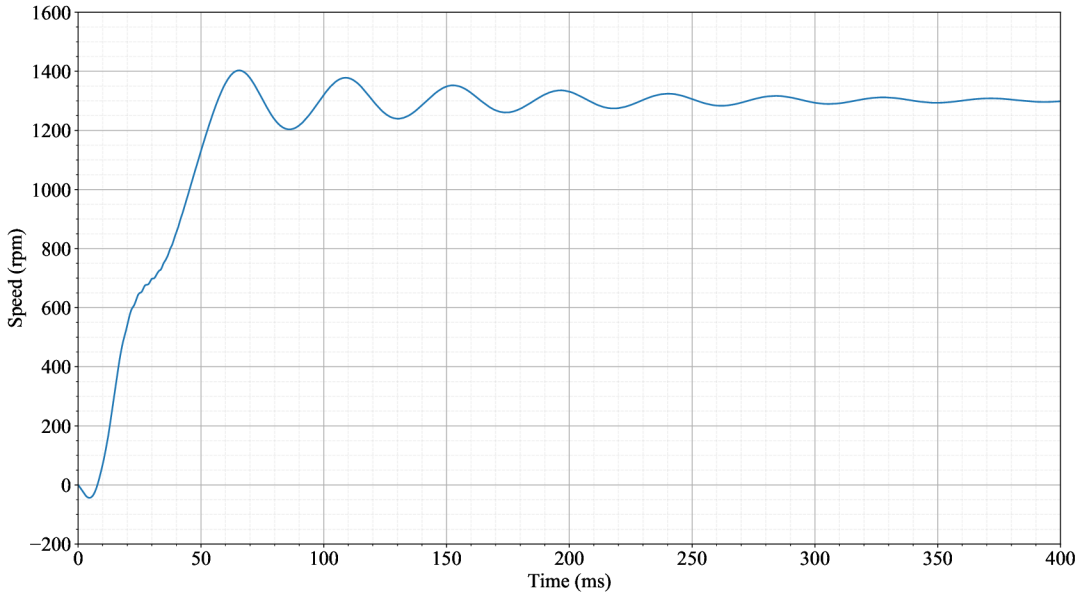

Figure 4.19: Rotational speed.

The motor start-up remained almost the same.

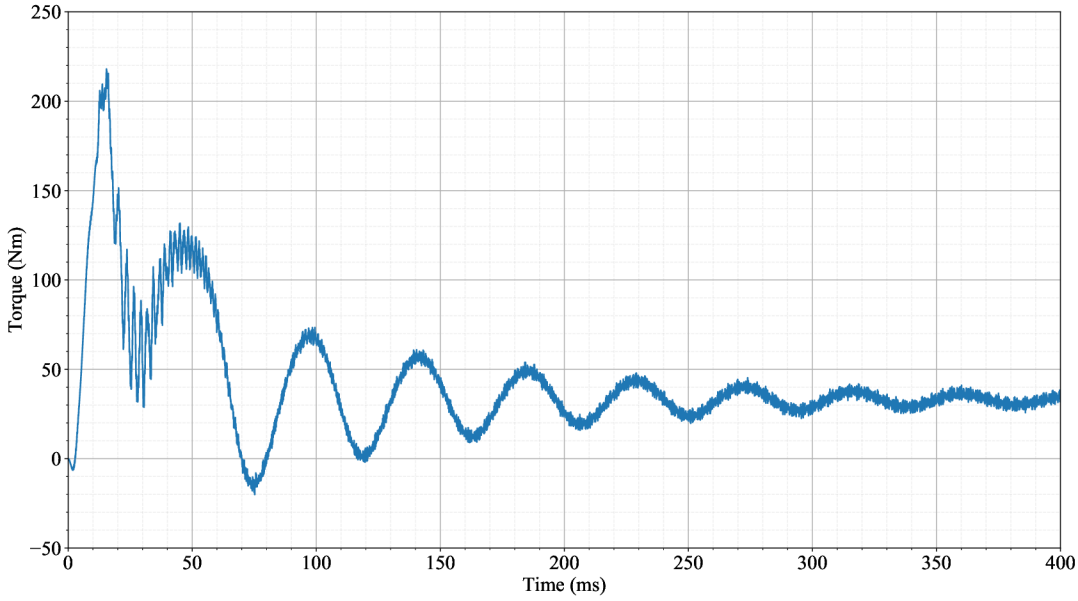

Figure 4.20: Torque during start.

Additional harmonics from PWM supply increased torque ripple from 5.57 % to 23.01 %.

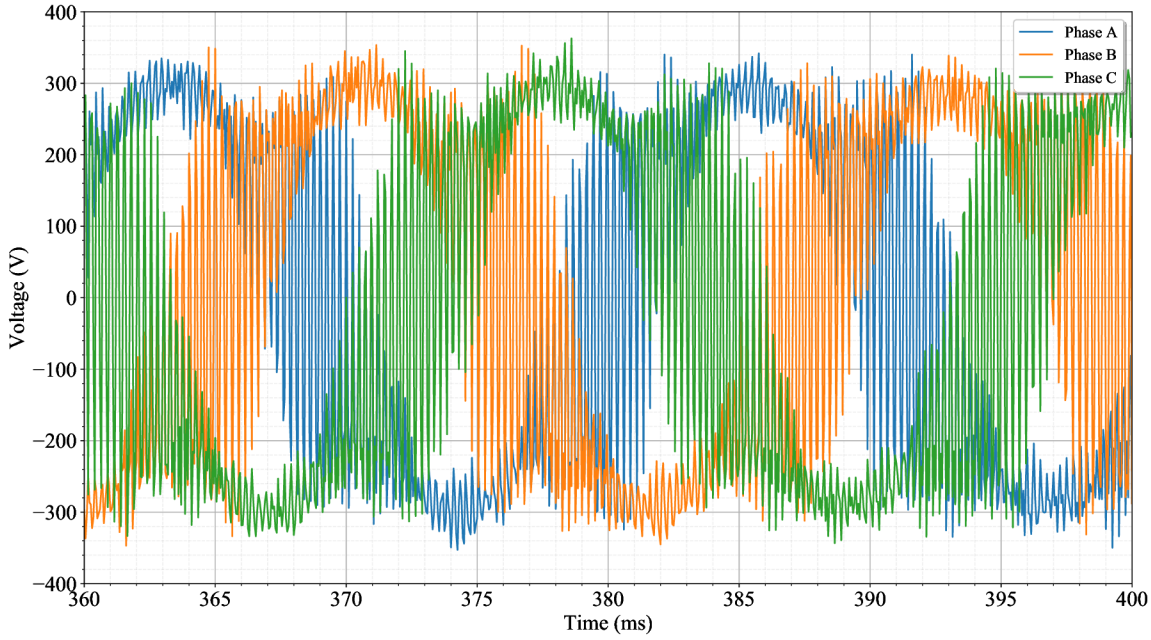

Figure 4.21: Supply sinusoidal voltage.

Detailed look at the input voltage distorted with additional harmonics.

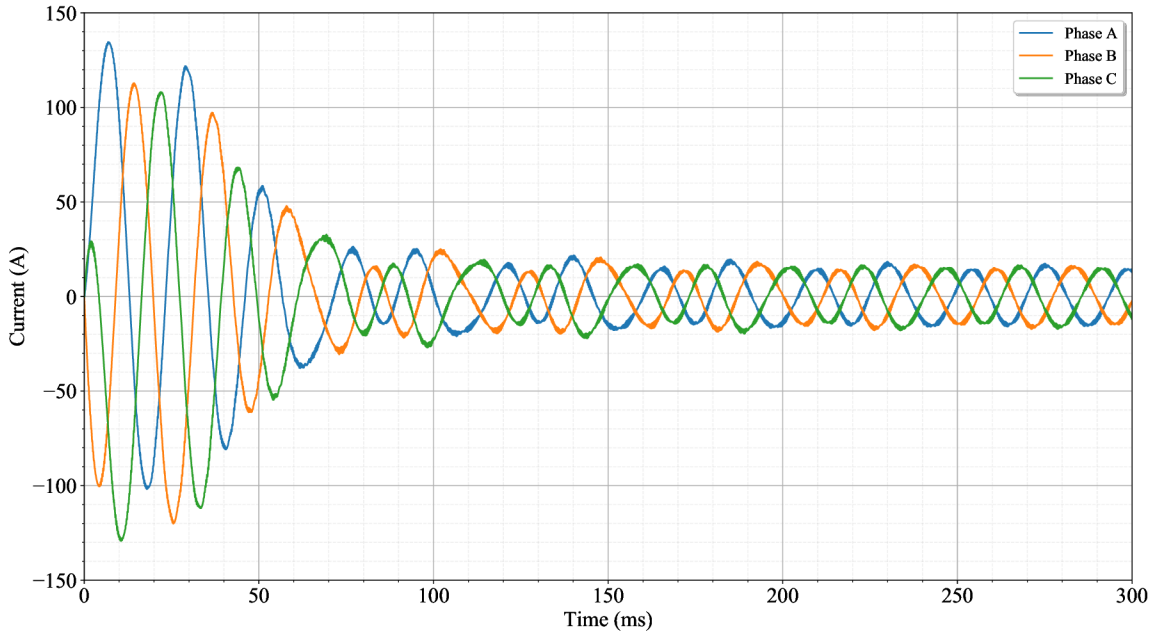

Figure 4.22: Currents during start.

The same is true for the current in the motor. The current waveform is more distorted and the mean value is higher.

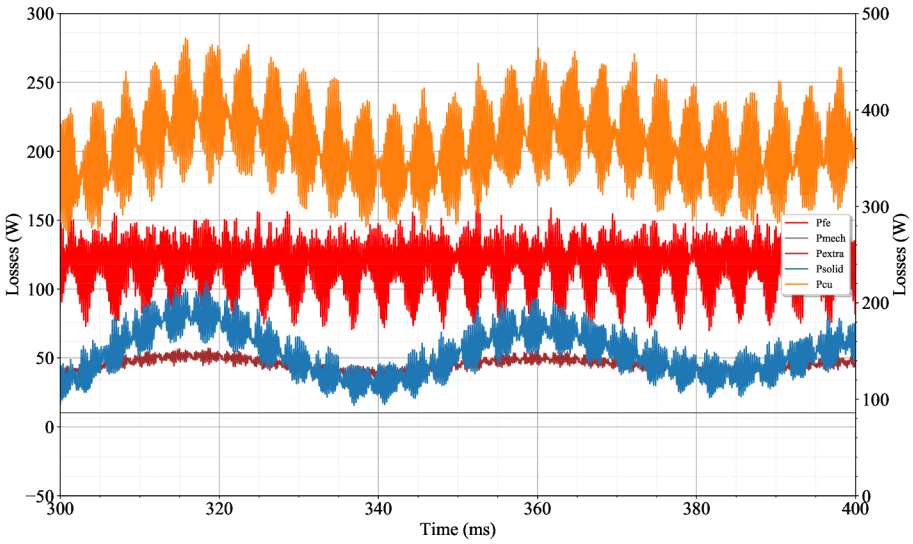

Figure 4.23: Losses in the induction motor at steady state.

Voltage ripple appeared in the loss waveform. For a better view of the distribution of losses, a pie chart is chosen 4.24.

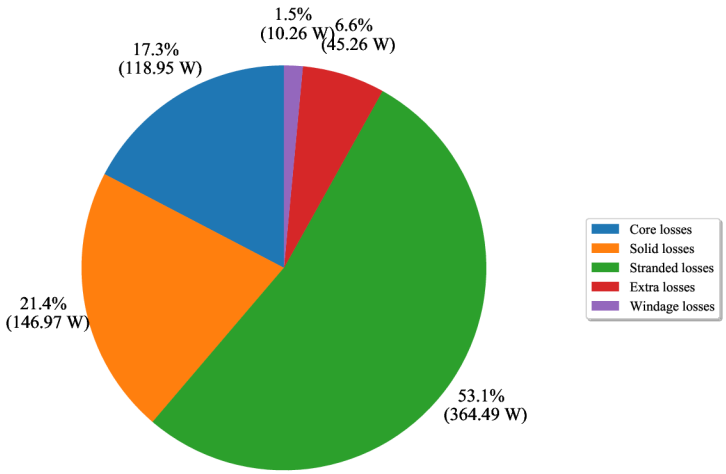

Figure 4.24: Distribution of losses at steady state.

With the comparison of sinusoidal power supply, the losses increased by 80 W. The biggest increase occurred in core losses with an increase of almost 50 W. Solid losses and joule losses increased slightly.

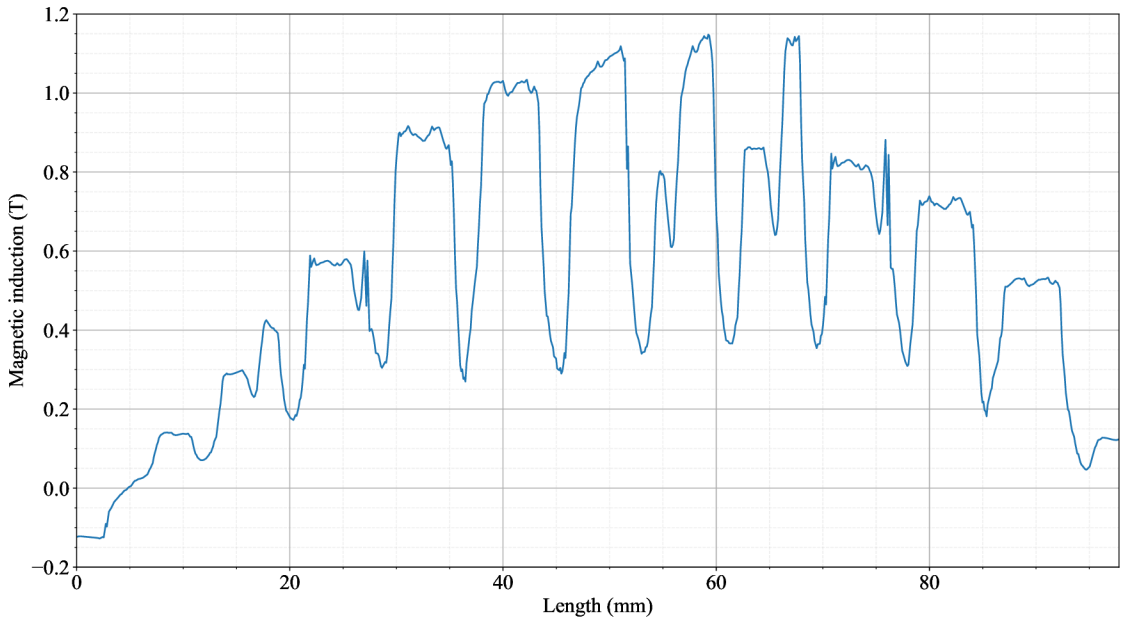

Figure 4.25: Flux density in the air gap.

The fundamental harmonic is almost the same 0.86 T, but the waveform of flux density in the air gap changed significantly with higher peaks.

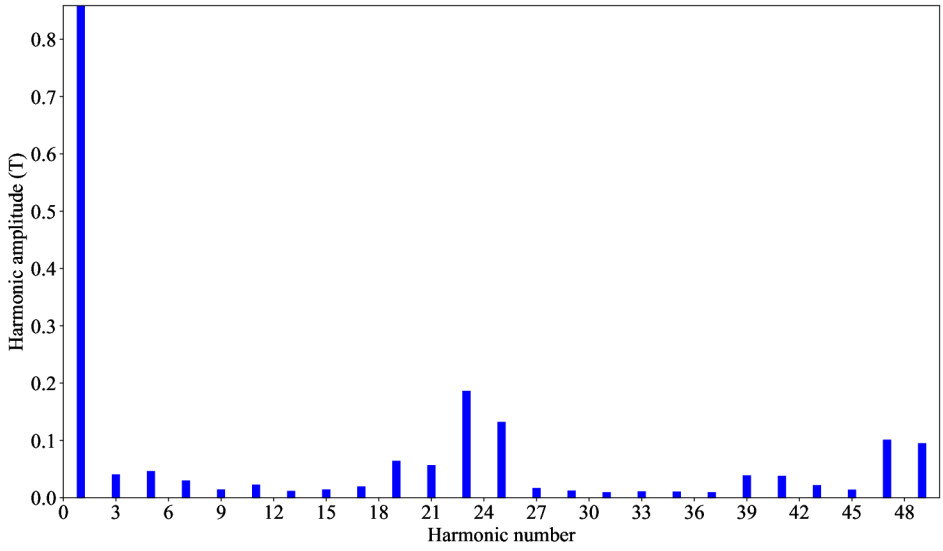

Figure 4.26: Normalized harmonic content of flux density radial component.

The highest harmonics are still the 1, 18, 23, 25, 47 and 49, but have their amplitudes increased.

5 Experimental measurements

5.1 Induction motor

For the experimental measurements, a timetable was established that divided the measurements into several parts. According to the EN IEC 60034-2-3 standard, the load points were chosen and are described in the following table.

Table 5.1: Normalized operating points from [28].

	n	T	P	Comment
$P1$	0.9	1	0.9	Also included in IEC 61800-9-2
$P2$	0.5	1	0.5	Also included in IEC 61800-9-2
$P3$	0.25	1	0.25	
$P4$	0.9	0.5	0.45	Also included in IEC 61800-9-2
$P5$	0.5	0.5	0.25	Also included in IEC 61800-9-2
$P6$	0.5	0.25	0.125	Also included in IEC 61800-9-2
$P7$	0.25	0.25	0.0625	
The numbering of the points is slightly different from the numbering used in IEC 61800-9-2				

For a better view, the load points are shown in the following graph.

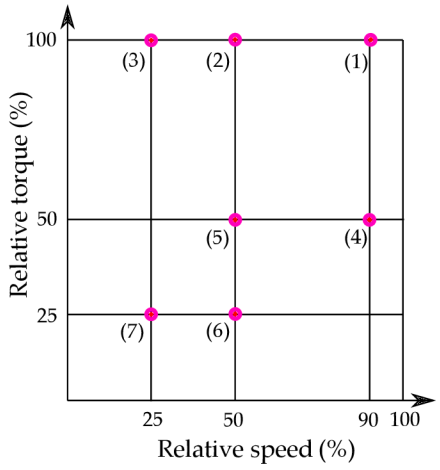

Figure 5.1: Chosen load points from the standard [28].

The SEMTEC test fanless 3-phase induction motor will be loaded with seven standardized operating points with two different power supplies.

As a first test, a retardation test will be performed to determine the mechanical losses, which will have to be performed at high speed. The retardation test will be performed after the no-load heat-run with the converter supply. The retardation curve will range from 3500 1/min and there will be several retardation curves taken while cooling down. In the next measurement, the motor was fed by an ABB frequency converter using four different switching frequencies with the same loading point P2. After this measurement, the next step was to measure the other operating points for which the switching frequency of 4 kHz was determined. The third measurement involved measuring with a standard sinusoidal waveform, which was supplied by a generator. The last measurement covered the measurement of the voltage curve with the generator, which was measured according to the standard.

Table 5.2: Measurement plan

Measurement	Operating ambient temperature is 27 °C for the chamber.			
1. Retardation test	No-load heatrun with converter supply + retardation curve			
2. Converter supply		n	T	P
4kHz	$P1$	0.9	1	0.9
Four switching frequencies	$P2$	0.5	1	0.5
4kHz	$P3$	0.25	1	0.25
4kHz	$P4$	0.9	0.5	0.45
4kHz	$P5$	0.5	0.5	0.25
4kHz	$P6$	0.5	0.25	0.125
4kHz	$P7$	0.25	0.25	0.0625
3. Generator supply		n	T	P
	$P1$	0.9	1	0.9
	$P2$	0.5	1	0.5
	$P3$	0.25	1	0.25
	$P4$	0.9	0.5	0.45
	$P5$	0.5	0.5	0.25
	$P6$	0.5	0.25	0.125
	$P7$	0.25	0.25	0.0625
4. No-load test	No-load heatrun + voltage curve test with generator supply			

A plan was established for the measurements.

5.2 Methology

The measuring station consists of several parts. The block diagram describes the basic measurement methodology.

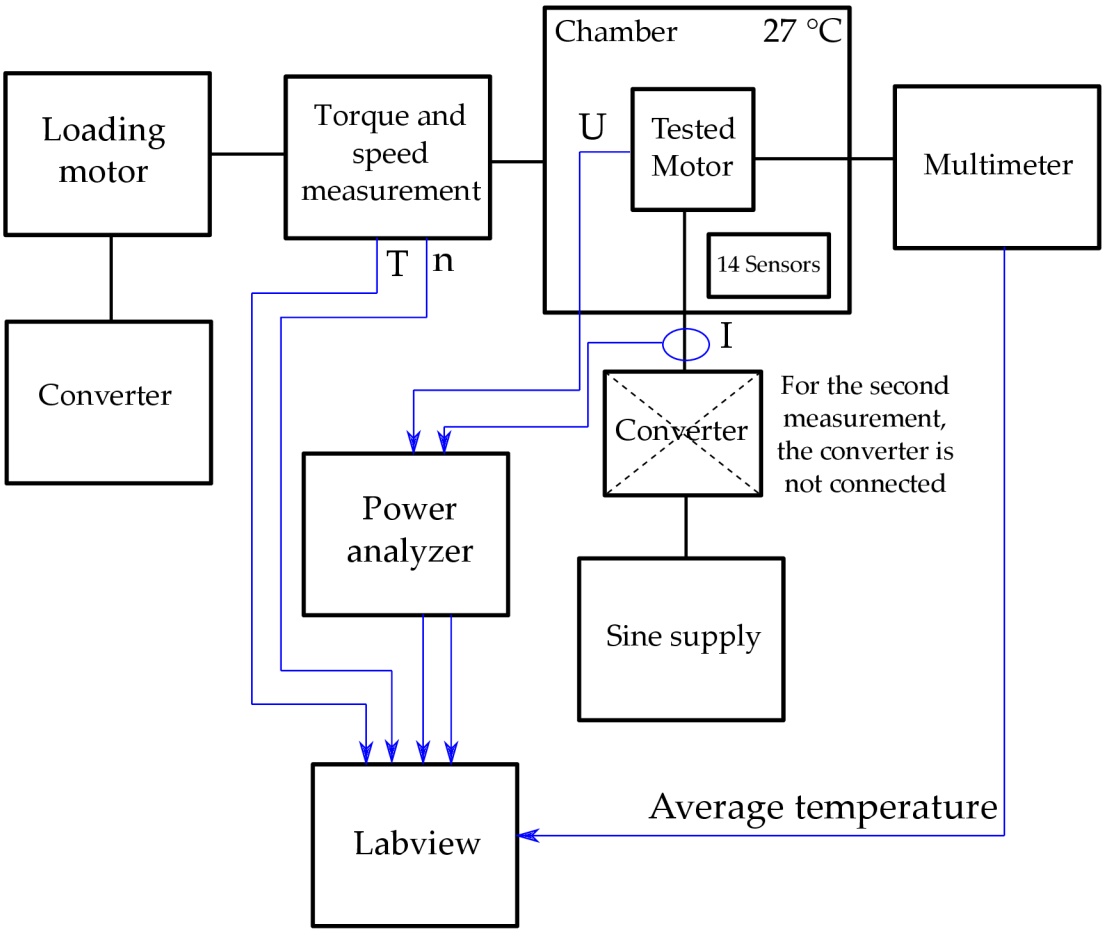

Figure 5.2: Analyzed geometry.

The induction motor under test is located in a chamber that has the function of maintaining constant ambient conditions. The operating temperature of the chamber is 27 °C. The temperature in the chamber is maintained by a heating resistor and is controlled to a predetermined temperature using the LabVIEW interface. To be able to control the temperature, there are several thermal sensors in the chamber that sense the temperature at specific locations in the chamber. PT100 sensors are also installed in the induction motor to sense temperature at specific locations.

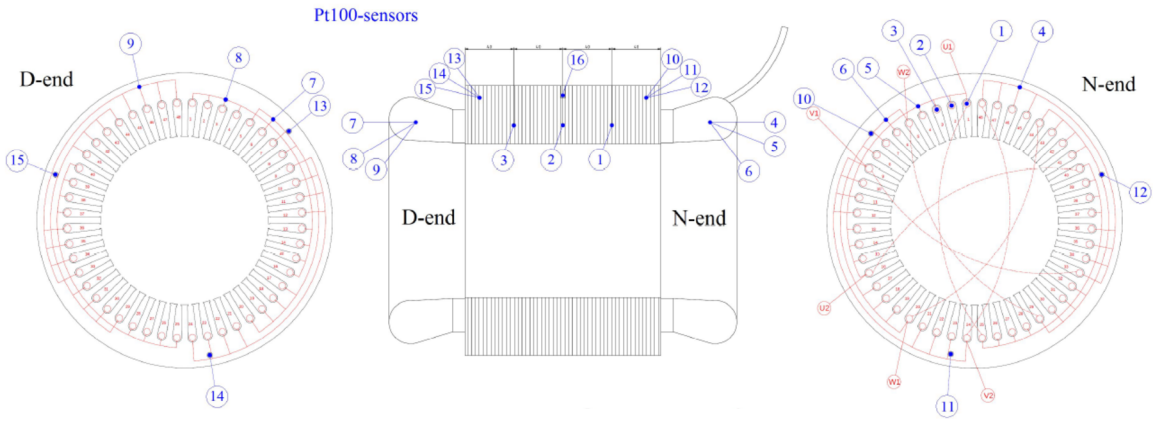

Figure 5.3: Distribution of sensors in the motor from [36].

the sensors in the motor are placed in groups in certain parts. The sensors in the stator slots are evenly spaced throughout the depth of the motor. Sensors are also placed in the drive end a non drive-end in the stator iron and in the end windings. In addition, there are sensors in the rotor of the machine where one is placed in the rotor yoke and the other in the end ring. These sensors work on the basis of transformers and transmit temperature readings. A load in the form of a second electric motor is connected to the tested induction motor. The load is controlled by its own frequency converter. A measuring shaft is connected before the load, which measures the machine speed and torque on the shaft with great accuracy. The power supply for the motor under test was selected according to the type of test. In the block diagram, this is indicated by the two Sine supply and Converter blocks below the chamber block. The last part is the power analyzer, which is used to measure the electrical quantities of the machine. These quantities are then viewed with the LabVIEW interface, where they are sequentially recorded and thus the entire progress of the measurement can be monitored.

Table 5.3: Compensation of torque for measurement values of load.

Calculated load points		**Bearing + zero**	**HBM Torque reading**
	T (Nm)	T (Nm)	T (Nm)
P1	32.93	-0.48	-32,45
P2	32.93	-0.46	-32,47
P3	32.93	-0.37	-32,56
P4	16.46	-0.48	-15,98
P5	16.46	-0.46	-16,00
P6	8.23	-0.46	-7,77
P7	8.23	-0.37	-7,86

Conventional bearings were used to connect the load, the measuring shaft, and the machine under test. Such bearings have their own torque and, therefore, it was necessary to apply a correction to the load prior to measurement.

5.3 Measurement results

5.3.1 Retardation test

In the first part, a retardation test was performed.

Table 5.4: Results from retardation test.

Retardation test	Friction and windage loss (W)	16.63 at 1450 rpm
Inertia used from FEA	Inertia (kgm^2)	0.029
Inertia of bearings	Inertia (kgm^2)	0.00343

In the table 5.4 the measured data are given for the rated motor speed. Inertia values calculated from the Ansys MAXWEL interface were used to calculate the retardation test curve. For the bearings, values from the documentation were used.

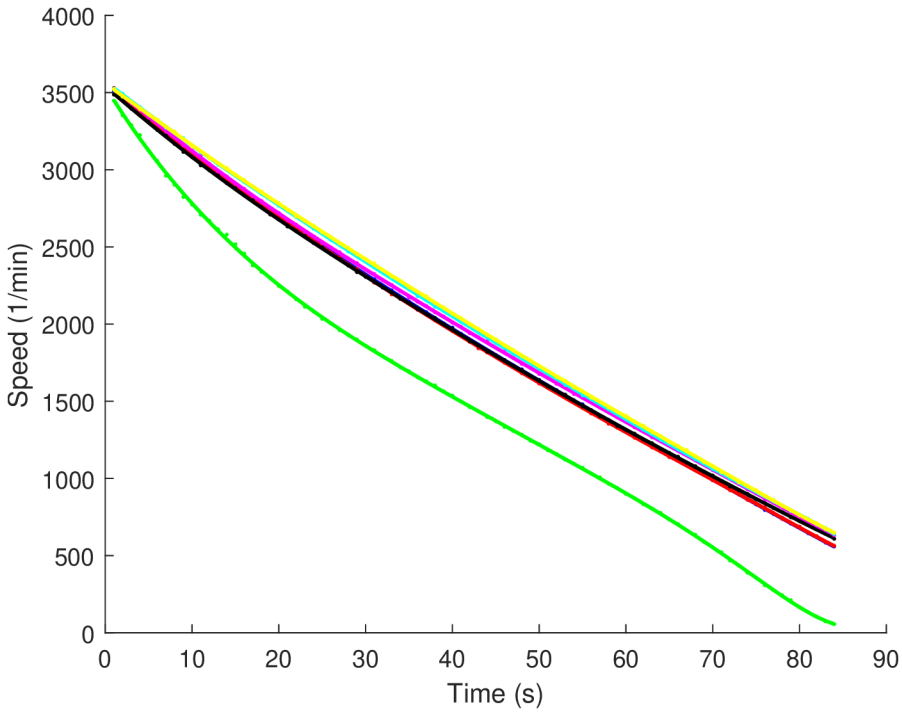

Figure 5.4: Characteristic describing the deceleration retardation curve.

The retardation test was performed from 3500 rpm several times to verify the measurement. The motor was preheated to approximately normal operating temperature

before performing the retardation tests. The retardation tests were performed while the motor was cooling to see the possible temperature dependence of the mechanical losses of the bearings. The green curve in the figures is an outlier in the middle of other almost identical tests. The different behavior can be caused, e.g. by some tensions in the motor during the cooling.

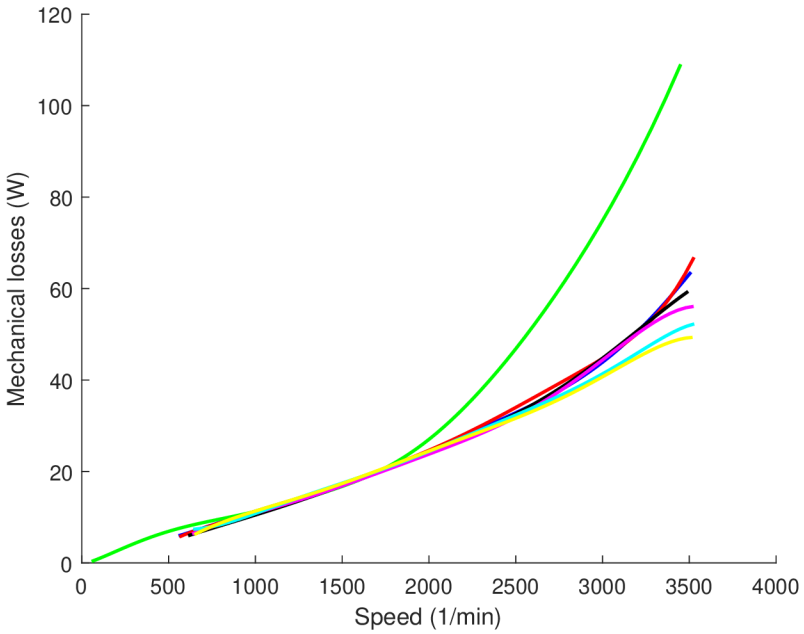

Figure 5.5: Mechanical losses characteristics depending on speed.

Figure 5.5 shows the calculated curves. The results of the retardation test did not show any consistent temperature dependence. Therefore, the green case was ignored, and the final mechanical loss values used in the further analysis are based on the remaining curves's average values at each speed. The MATLAB code allows to find the mechanical loss values for a defined velocity. The table 5.4 shows the value for the nominal motor speed.

5.3.2 Converter supply measurement

The retardation test was followed by the measurement of the motor with the frequency converter as a source. The first part with the frequency converter was to measure one working point P2, when the speed was half with full load. For this operating point, four switching frequencies were used, namely 2, 4, 8 and 12 kHz. The purpose was to observe the losses due to harmonics in comparison to the inverter losses. Measurements with different switching frequencies show the temperature difference in the table 5.5.

Table 5.5: Measured temperature values with different switching frequencies in test point P2 (50% speed, 100% torque).

		2 kHz	4 kHz	8 kHz	12 kHz
Stator slot	Temp. 1 (°C)	72.8	69.2	67.2	66.5
	Temp. 2 (°C)	72.5	69.0	67.0	66.3
	Temp. 3 (°C)	74.1	70.4	68.3	67.6
End winding - non drive end	Temp. 4 (°C)	74.5	70.9	68.7	68.0
	Temp. 5 (°C)	75.4	71.8	69.7	69.0
	Temp. 6 (°C)	77.4	73.4	71.1	70.4
Stator iron	Temp. 10 (°C)	64.6	61.6	59.9	59.2
	Temp. 11 (°C)	65.1	62.1	60.3	59.7
	Temp. 12 (°C)	69.5	66.1	64.1	63.5
End winding - drive end	Temp. 7 (°C)	78.2	74.1	71.7	71.0
	Temp. 8 (°C)	77.1	73.2	71.0	70.3
	Temp. 9 (°C)	76.1	72.3	70.1	69.3
Stator iron	Temp. 13 (°C)	68.3	65.0	63.1	62.4
	Temp. 14 (°C)	68.4	65.1	63.2	62.6
	Temp. 15 (°C)	71.5	67.9	65.8	65.1
Middle of stator iron	Temp. 16 (°C)	65.1	62.0	60.3	59.6
Rotor end ring	Temp. 17 (°C)	90.9	84.1	80.4	79.2
Rotor yoke	Temp. 18 (°C)	93.8	87.5	83.5	82.0

Later, the measurements were taken from load point 2 downward. Before the first measurement, the motor was allowed to warm up to operating temperature for one day. After the heat run, measurements were taken every day at an average local time of around 12:30. This method was chosen because of the variable conditions in the laboratory. The ventilation and lights in the laboratory were turned off overnight. In the morning, turning on the ventilation in the laboratory showed up in the temperature waveforms and in the measurements, so it was necessary to wait for the temperature to settle into equilibrium. Some measurements could be taken after several hours, but to standardize the measurements, a periodization was chosen every day. The measured values were written from the LABview interface in an excel csv format.

In the next figure 5.6 you can see the previous statement, where the total losses and also the heating of the machine are the highest at a switching frequency of 2 kHz, but for higher switching frequencies there is no less difference. While for the low frequencies of 2 kHz and 4 kHz the differences are somewhat large, between the higher frequencies of 8 kHz and 12 kHz the differences are very small.

The following figure shows the measured values for the working point P2 and the temperatures in 5.5.

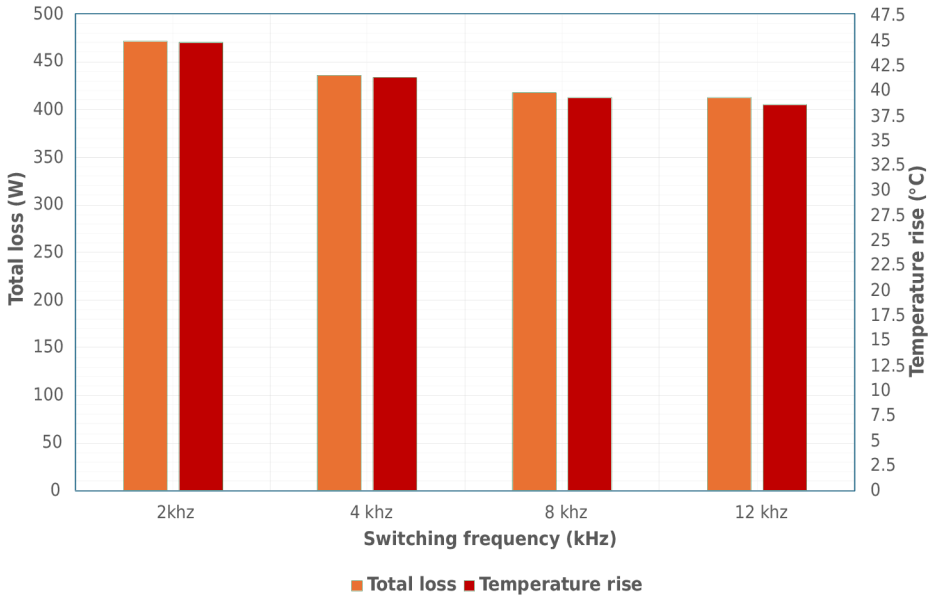

Figure 5.6: Comparison of total losses and temperature RISE for different switching frequencies at 50% speed and 100% load. The secondary and primary axes were selected to match the loss and temperature rise bars at 2 kHz.

The recorded electrical values for the full measurement of all loading points are in table 5.6. The temperature values recorded are in the following tables 5.7 and 5.5.

Table 5.6: Measured values for the converter supply.

	P1	P2	P3	P4	P5	P6	P7
U_{rms} (V)	260.4	230.0	173.9	263.2	113.7	229.5	169.2
I_{rms}(A)	10.4	10.4	10.4	7.5	7.4	6.6	6.5
P_1(W)	5032.1	2937.8	1614.1	2580.2	1498.3	835.2	449.5
S (W)	8126.0	7157.9	5441.3	5930.8	2523.1	4524.1	3282.8
Q (W)	6380.4	6527.2	5196.3	5340.1	2076.3	4446.3	3251.9
λ (-)	0.62	0.41	0.30	0.44	0.57	0.18	0.14
P_2 (W)	4502.0	2502.1	1246.6	2244.4	1251.5	625.3	313.0
n (rpm)	1337.8	726.5	361.5	1305.5	724.3	725.2	362.3
T (Nm)	-32.93	-32.89	-32.93	-16.42	-16.51	-8.23	-8.25
P_{loss} (W)	530.1	435.7	367.5	335.8	246.8	209.9	136.5
η (%)	89.47	85.17	77.23	86.99	83.53	74.87	69.64

Table 5.7: Measured temperature values for places in the motor for the converter supply.

		P1	P2	P3	P4	P5	P6	P7
Stator slot	Temp 1. (°C)	76.9	69.2	62.9	59.9	52.0	48.5	41.8
	Temp 2. (°C)	76.6	69.0	62.9	60.0	52.1	48.7	42.1
	Temp 3. (°C)	78.2	70.4	64.1	60.8	52.7	49.2	42.4
End winding - non drive	Temp 4. (°C)	78.0	70.9	64.8	60.1	52.7	48.9	42.5
	Temp 5. (°C)	79.1	71.8	66.0	60.6	53.1	49.2	42.8
	Temp 6. (°C)	80.6	73.4	67.2	61.8	54.1	50.2	43.4
Stator iron	Temp 10. (°C)	68.5	61.6	55.9	54.9	47.9	45.1	39.3
	Temp 11. (°C)	69.1	62.1	56.4	55.4	48.1	45.3	39.4
	Temp 12. (°C)	73.9	66.1	60.1	58.5	50.5	47.4	40.6
End winding - drive	Temp 7. (°C)	81.8	74.1	67.7	62.5	54.5	50.4	43.5
	Temp 8. (°C)	80.8	73.2	66.8	61.8	54.0	50.0	43.3
	Temp 9. (°C)	79.7	72.3	65.9	61.4	53.6	49.8	43.2
Stator iron	Temp 13. (°C)	72.3	65.0	59.2	57.5	49.9	46.9	40.6
	Temp 14. (°C)	72.6	65.1	59.1	57.8	50.1	47.0	40.7
	Temp 15. (°C)	75.8	67.9	61.7	59.8	51.5	48.3	41.6
Middle of stator iron	Temp 16. (°C)	68.9	62.0	56.4	55.2	48.1	45.3	39.5
Rotor end ring	Temp 17. (°C)	89.9	84.1	79.3	65.0	56.9	51.4	42.5
Rotor yoke	Temp 18. (°C)	93.8	87.5	82.0	68.6	60.1	54.5	45.2

Using the measured values from tables 5.6 and 5.7 the following figure 5.7.

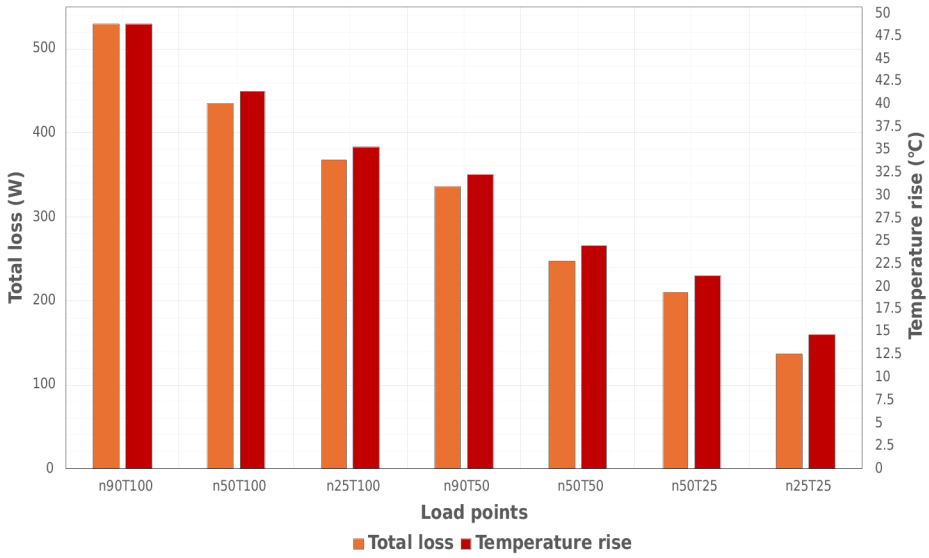

Figure 5.7: Comparison of total losses and temperature rise for load points PWM.

The figure 5.7 shows the comparison of total losses and motor heating in the temperature rise. Again, the ranges of the secondary and primary axes have been selected to match the loss and temperature rise bars at the first load point P1. It can be seen that the measurement results follow a linear trend. The seemingly linear trend is due to how the losses in this specific machine change between the operating points - in practice, basically a coincidence. This figure shows that the measurement results can be trusted. The losses and temperature rise in an electrical machine are expected to be proportional to each other under similar cooling conditions, and this figure clearly shows this dependence. However, in the case of these tests, the temperature rise seems to be a bit higher at lower speeds and loads relative to the determined losses. The table 5.7 shows the measured temperature values in certain parts of the machine. The categories in the table correspond to the 5.3 figure, where the measuring sensors are numbered and described. For a better display of the measured temperature values from the table 5.7 two images 5.8 and 5.9 are used. The bar chart is similar to the table, but it is easy to see where the highest temperatures are, and the 3D bar chart gives a better idea. The temperature value decreases with the difference in the load points. The highest temperatures were in the rotor yoke, and the lowest temperatures were in the stator iron.

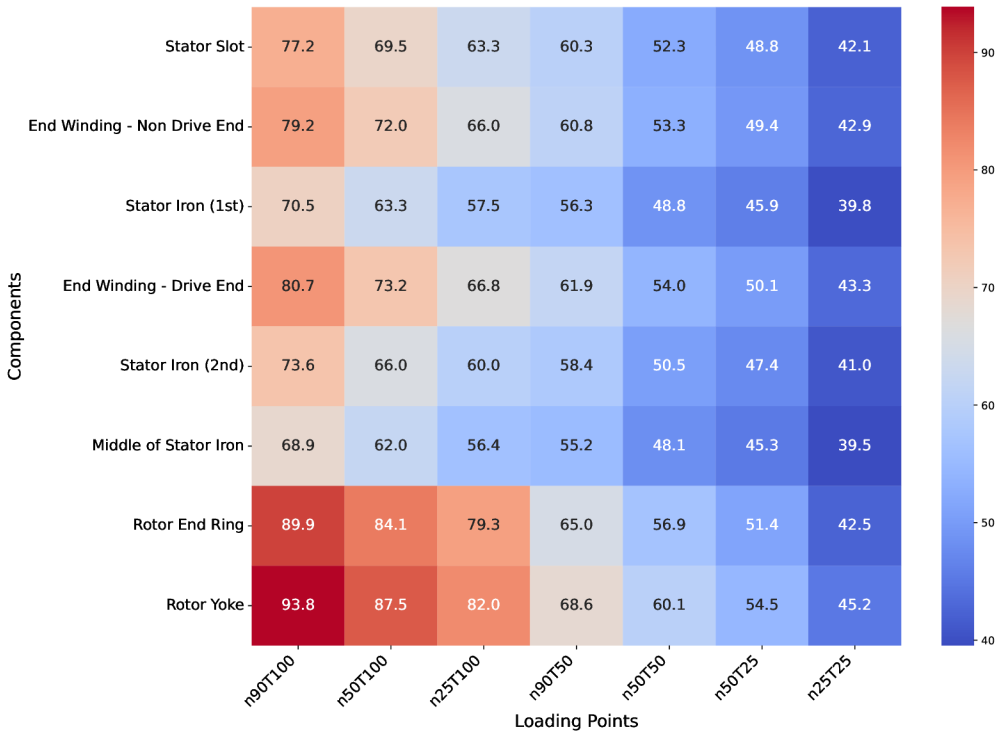

Figure 5.8: Heat map of average temperatures for converter across components and loading points.

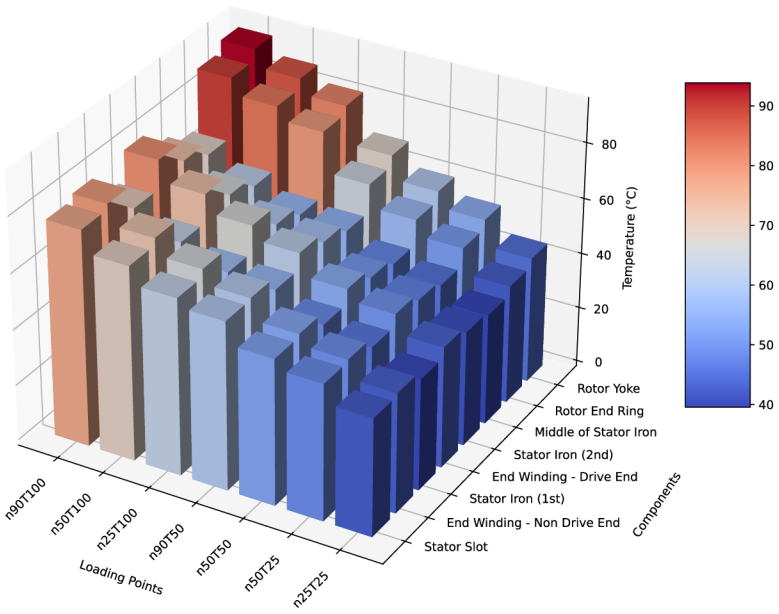

Figure 5.9: 3D bar chart of converter temperatures.

5.3.3 Generator supply measurement

Table 5.8: Measured electrical quantities used to compare the two measurements.

	P_{harmPD} (W)	I_{AVGfund} (A)	U_{hfund} (V)	f_{fund} (Hz)	Con-gen difference
Converter					U_{diff} (V)
n90T100	48.720	10.357	206.103	44.594	0.060
n50T100	65.796	10.316	116.837	25.297	0.507
n25T100	43.691	10.391	60.870	13.198	-0.18
n90T50	51.546	7.444	203.424	43.994	0.179
n50T50	66.436	7.364	113.682	24.597	-0.005
n50T25	67.525	6.468	112.838	24.397	0.002
n25T25	41.099	6.389	56.864	12.298	0.784
Generator					f_{diff} (Hz)
n90T100	1.21	10.37	206.04	44.599	-0.005
n50T100	**1.32**	**10.30**	**116.33**	**25.268**	-0.029
n25T100	**0.12**	**10.39**	**61.05**	**13.231**	0.033
n90T50	0.31	7.47	203.25	43.999	-0.005
n50T50	0.21	7.39	113.69	24.599	-0.002
n50T25	0.17	6.51	112.84	24.400	-0.003
n25T25	0.92	6.21	56.08	12.157	0.014

The same rules were applied as in the previous measurement. The measurements were taken at the same time of the day. Table 5.8 shows the necessary electrical quantities that had to be monitored to make the measurements comparable. The quantities that were matched to make the measurements comparable are the fundamental voltage and fundamental frequency (fund. voltage and fund. frequency determine the operating state of the motor, but fund. current can be slightly different). The frequency was controlled by FFT analysis of the voltage waveform during the measurement. In the first part of the measurements, the frequency values were wrongly set because only the fundamental values of the inverter voltage were checked, which were then fed into the sinusoidal power supply. After realizing this error, the magnitude of the fundamental frequency began to be considered as a reference. Some operating points had to be remeasured. Re-measured loading points are marked in bold.

Table 5.9: Measured temperature values for places in the motor for the generator supply.

		P1	P2	P3	P4	P5	P6	P7
Stator slot	Temp. 1 (°C)	72.7	63.0	59.4	56.1	46.9	43.3	38.8
	Temp. 2 (°C)	72.7	62.9	59.3	56.3	47.1	43.6	39.1
	Temp. 3 (°C)	73.9	64.0	60.1	57.0	47.5	43.8	39.1
End winding - non drive	Temp. 4 (°C)	74.0	64.6	61.4	56.4	47.5	43.7	39.3
	Temp. 5 (°C)	74.7	65.5	61.9	56.9	47.9	43.9	39.4
	Temp. 6 (°C)	76.3	66.7	63.4	57.7	48.7	44.6	40.1
Stator iron	Temp. 10 (°C)	65.0	56.4	53.1	51.8	43.6	40.8	36.8
	Temp. 11 (°C)	65.6	56.8	53.4	52.1	43.8	40.9	36.8
	Temp. 12 (°C)	69.8	60.2	56.6	55.1	45.7	42.4	37.8
End winding - drive	Temp. 7 (°C)	77.4	67.3	63.7	58.3	48.9	44.7	40.0
	Temp. 8 (°C)	76.4	66.6	63.1	57.8	48.6	44.5	40.0
	Temp. 9 (°C)	75.6	65.8	62.5	57.3	48.3	44.4	39.9
Stator iron	Temp. 13 (°C)	68.4	59.2	55.4	53.8	45.2	42.0	37.7
	Temp. 14 (°C)	68.7	59.4	55.9	54.2	45.3	42.2	37.8
	Temp. 15 (°C)	71.9	61.7	57.9	55.8	46.4	43.0	38.3
Middle of stator iron	Temp. 16 (°C)	65.4	56.7	53.3	52.0	43.8	41.0	36.9
Rotor end ring	Temp. 17 (°C)	84.1	74.9	73.3	59.1	48.9	43.0	37.2
Rotor yoke	Temp. 18 (°C)	87.9	77.8	76.3	62.7	51.9	45.8	40.0

Similarly to the frequency converter section, the 5.10 table shows the measured electrical quantities obtained from the generator measurements and the 5.9 table shows the measured temperatures at the defined locations. The magnitudes of the temperatures are lower compared to the frequency converter.

Table 5.10: Measured values for the generator supply.

	P1	P2	P3	P4	P5	P6	P7
U_{rms} (V)	206.10	116.86	60.88	203.32	113.71	112.89	56.78
I_{rms}(A)	10.37	10.33	10.41	7.47	7.40	6.51	6.42
P_1(W)	4981.66	2868.36	1569.90	2543.33	1433.55	767.58	409.27
S (W)	6411.60	3621.11	1900.63	4558.06	2523.13	2203.37	1092.66
Q (W)	4036.22	2210.15	1071.34	3782.48	2076.32	2065.33	1013.10
λ (-)	0.78	0.79	0.83	0.56	0.57	0.35	0.37
P_2 (W)	4505.13	2509.47	1249.27	2245.75	1252.09	624.83	313.25
n (rpm)	1305.65	727.64	362.33	1305.84	-723.83	725.39	361.69
T (Nm)	-32.93	-32.93	-32.92	-16.42	-16.51	-8.23	8.27
P_{loss} (W)	476.53	358.89	320.63	297.58	181.46	142.75	96.03
η (%)	90.43	87.49	79.58	88.30	87.34	81.40	76.54

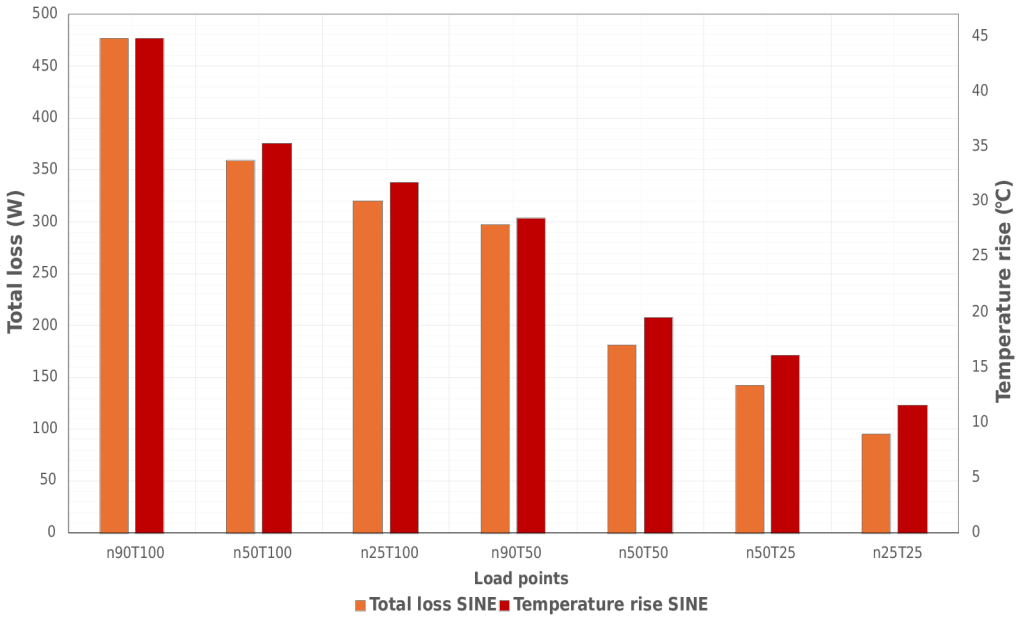

Figure 5.10: Comparison of total losses and temperature rise with different load points with generator supply.

Again as before, here is a figure showing the comparison of the total losses with motor warming based on the tables 5.9 and 5.10. The ranges of the secondary and primary axes have been selected to match the loss and temperature rise bars at the first load point P1. It can be seen that the measurement results follow the same trend as the converter supply.

To better display the table 5.9, two figures are plotted showing the distribution of the average temperatures in the motor structure for the specified sensor locations. As in the previous section, the heat map 5.11 shows a preview of where the highest and lowest temperatures are located. However, a 3D bar graph 5.12 is also provided to give a better idea, where, although the values are harder to see, the absolute magnitudes are better displayed. When comparing the two power supplies so far, there is little difference in temperatures, but the highest temperatures are in the same places. The rotor parts reach the highest temperatures. The largest temperature differences between the load points are related to the highest load point. As the load decreases, the specific high temperature points disappear and the heat in the motor is more evenly distributed.

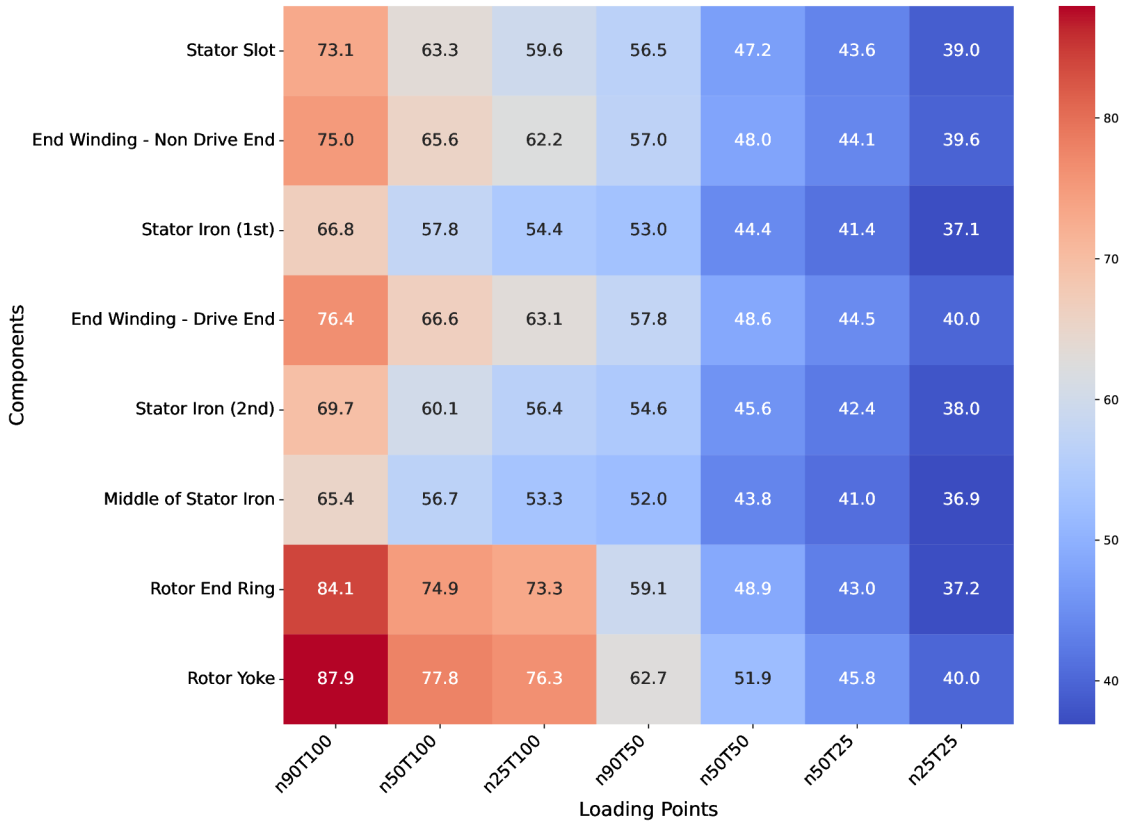

Figure 5.11: Heat map of average temperatures for generator across components and loading points.

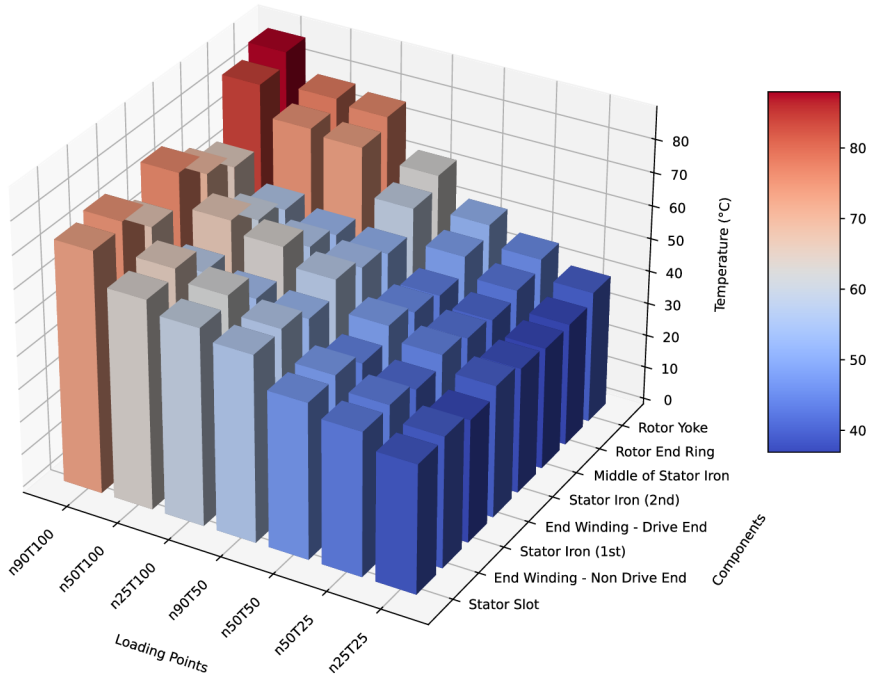

Figure 5.12: 3D bar chart of generator temperatures.

5.4 Comparison of measurements

This section shows a comparison of all differences for measurements with a PWM source and a sine source. First, a table 5.11 showing the comparison for average temperature rise, slip speed, total losses and the percentage difference that describes how much the temperature rise and total losses increased using the frequency converter compared to the generator.

Table 5.11: Comparison of both supplies.

		P1	P2	P3	P4	P5	P6	P7
Total loss (W)	Con	530.1	435.7	367.5	335.8	246.8	209.9	136.5
	Gen	476.5	358.9	320.6	297.6	181.5	142.8	96.0
Slip speed (rpm)	Con	32.2	32.5	34.5	14.3	14.1	6.8	6.6
	Gen	31.5	31.4	33.4	14.1	13.6	6.6	7.2
Temp. rise (°C)	Con	48.8	41.4	35.3	32.3	24.6	21.1	14.7
	Gen	44.8	35.3	31.8	28.5	19.6	16.0	11.6
Increase from sine to pwm (%)	$T_{\mathbf{rise}}$	11.2	21.4	14.6	12.8	36.0	47.1	42.1
	$P_{\mathbf{loss}}$	9.0	17.3	11.1	13.0	25.5	31.7	26.4

The following figure 5.13 shows a comparison of the total losses for two different

sources. It can be seen from the figure that the differences are around 50 W. The largest difference is for load point P2 with 50% speed and 100% torque and the smallest difference is for load point P4 with 90% speed and 50% torque.

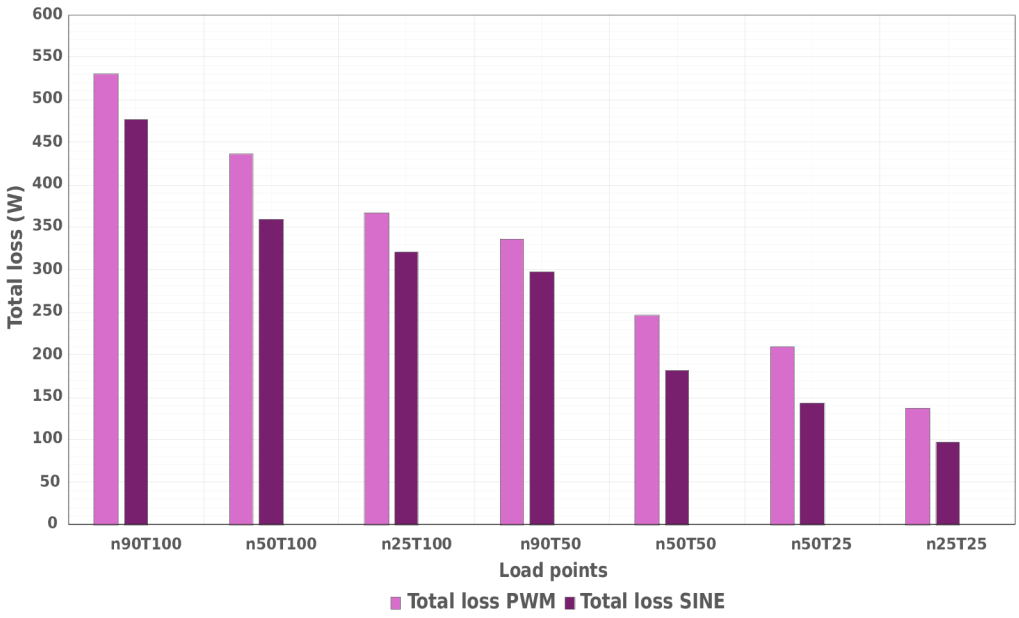

Figure 5.13: Total loss for different load points with two different supplies.

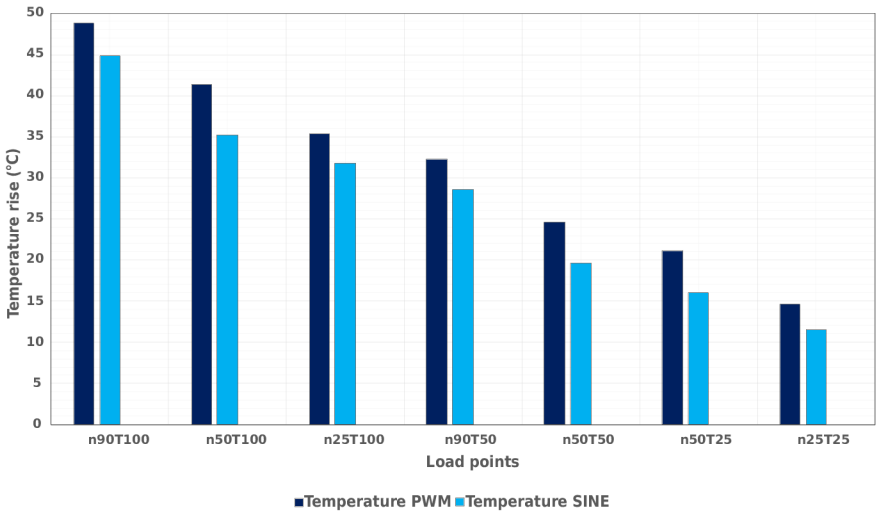

Figure 5.14: Temperature rise for different load points with two different supplies.

Then comparison of the temperature rise in figure 5.14. The graph corresponds to the total losses in the previous figure 5.13, where the largest and smallest total losses are also the largest and smallest temperature rise.

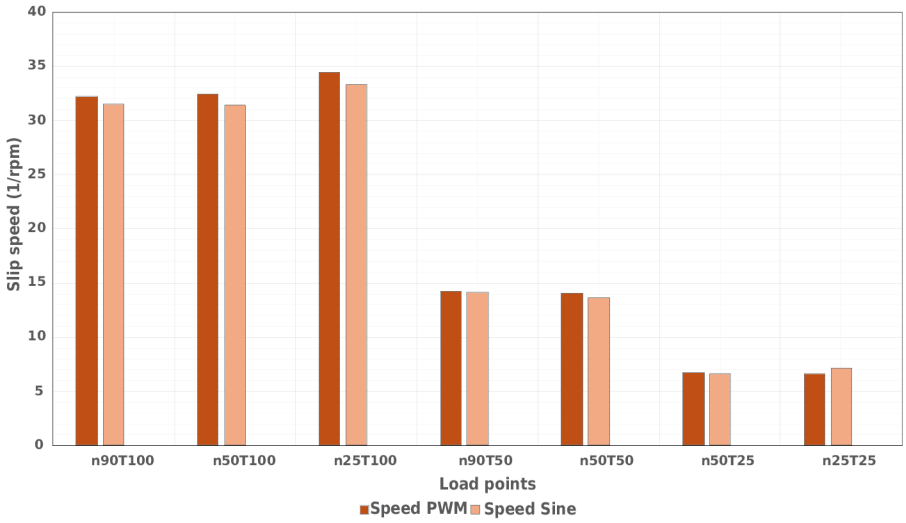

Figure 5.15: Comparison slip speed for different load points with two different supplies.

Figure 5.15 provides a display and comparison of slip speed. The speeds are very similar, but the measurements show that the slip speed is lower for the generator, which means lower slip and lower losses. A particular phenomenon occurs at the last operating point, where the slip speed of the converter is lower than that of the generator. That could be the result of a measurement error, where the generator voltage was lower, where in the table 5.8 the difference is 0.784 V.

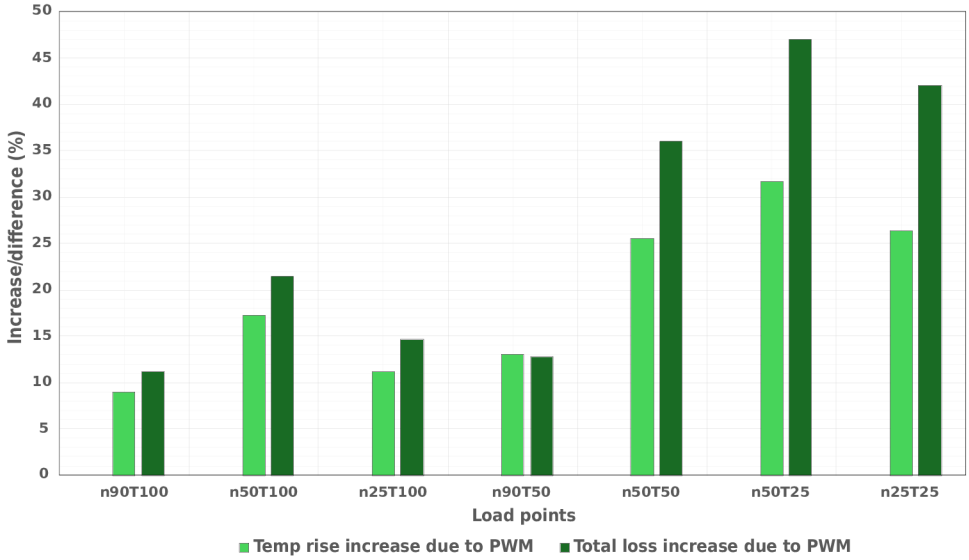

Figure 5.16: Increase in losses and temperature rise from SINE to PWM supply.

Figure 5.16 describes the increase in temperature rise and total losses from sinusoidal

power supply to PWM. Here, from the graph, we can see how low operating points with low load cause a larger percentage increase compared to higher operating points. The load point P2 (n50 % T100 %) is also relatively higher than the others. The following is a comparison of the two sources using the temperature difference and the relative temperature difference. First, a table 5.12 showing the average difference for selected locations in the machine. For better data visibility, two figures 5.17 and 5.18 are extracted from the table.

Table 5.12: Difference of converter and generator.

		P1	P2	P3	P4	P5	P6	P7
Stator slot	Temp. diff. (°C)	4.17	6.22	3.66	3.79	5.11	5.22	3.15
End winding - non drive	Temp. diff. (°C)	4.21	6.41	3.75	3.82	5.27	5.38	3.27
Stator iron	Temp. diff. (°C)	3.74	5.49	3.07	3.28	4.46	4.58	2.69
End winding - drive	Temp. diff. (°C)	4.28	6.63	3.74	4.11	5.46	5.55	3.35
Stator iron	Temp. diff. (°C)	3.91	5.95	3.64	3.78	4.87	4.96	3.03
Middle of stator iron	Temp. diff. (°C)	3.55	5.37	3.06	3.20	4.29	4.39	2.62
Rotor end ring	Temp. diff. (°C)	5.75	9.16	5.94	5.87	8.03	8.37	5.29
Rotor yoke	Temp. diff. (°C)	5.89	9.68	5.65	5.87	8.25	8.77	5.21

It can be seen from the figure that the biggest difference arises for load point P2 because it is the worst case for the motor current ripple.

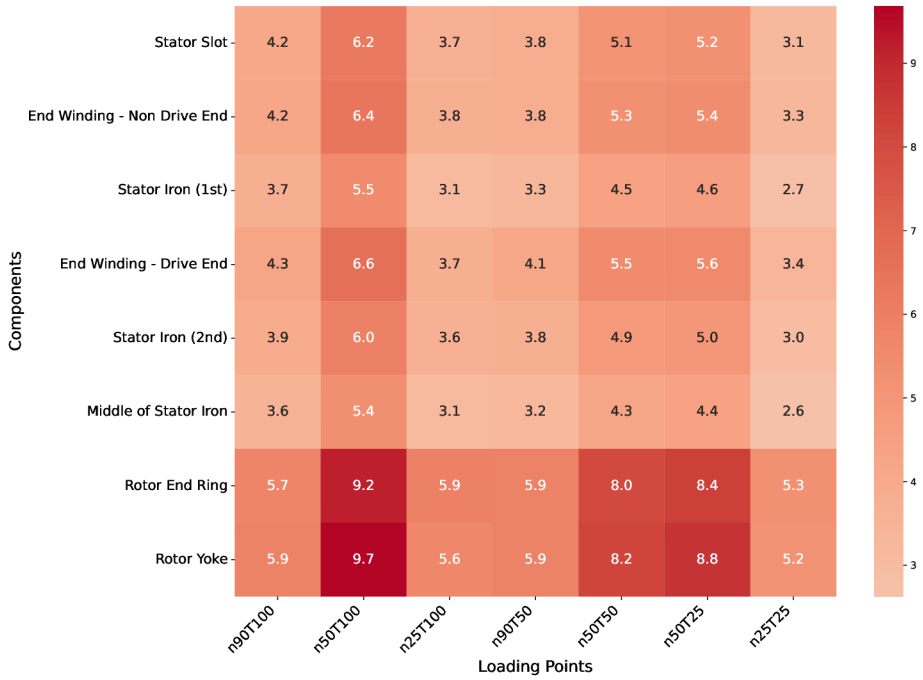

Figure 5.17: Temperature difference of supplies across components and loading points.

The other operating points with half the motor speed also show very high differences. The biggest difference is always for the places with the highest temperatures.

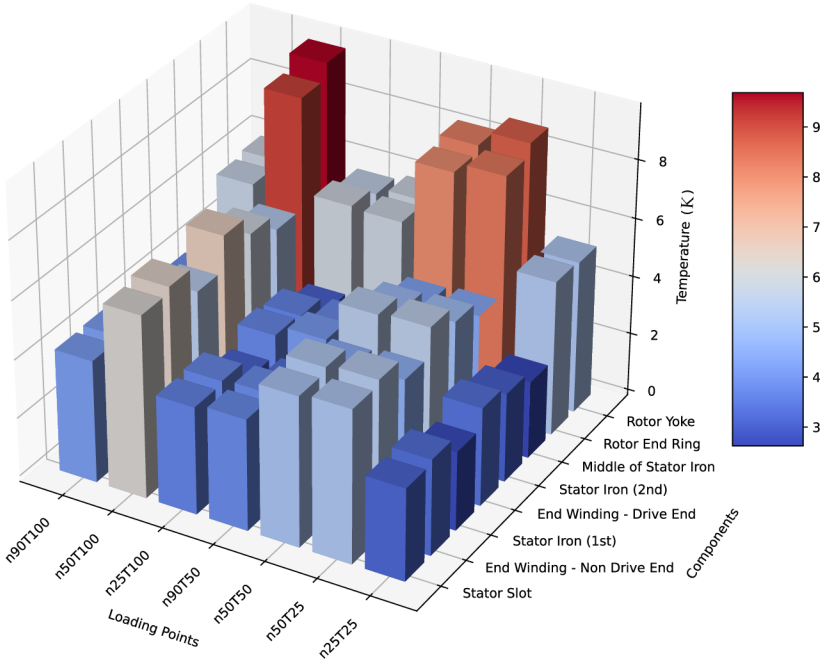

Figure 5.18: 3D bar chart of a temperature difference for two supplies.

The last part of this section compares the relative value of the difference between the frequency converter and the generator. The relative value is related to the higher measured values of the inverter.

Table 5.13: Relative difference of converter and generator

		P1	P2	P3	P4	P5	P6	P7
Stator slot	Rel. diff. (%)	5.39	8.95	5.79	6.29	9.77	10.70	7.47
End winding - non drive	Rel. diff. (%)	5.31	8.90	5.68	6.28	9.88	10.89	7.62
Stator iron	Rel. diff. (%)	5.29	8.67	5.34	5.84	9.13	9.97	6.76
End winding - drive	Rel. diff. (%)	5.31	9.06	5.59	6.63	10.11	11.09	7.74
Stator iron	Rel. diff. (%)	5.32	9.01	6.07	6.47	9.65	10.47	7.38
Middle of stator iron	Rel. diff. (%)	5.15	8.66	5.42	5.80	8.93	9.69	6.64
Rotor end ring	Rel. diff. (%)	6.39	10.90	7.50	9.03	14.12	16.28	12.45
Rotor yoke	Rel. diff. (%)	6.27	11.07	6.89	8.56	13.71	16.09	11.52

From the table 5.13 and figure 5.19 it can be seen that the largest relative differences are at the points with half speed but also at the lowest loading point. The largest differences are in the rotor, especially for the P6 operating point.

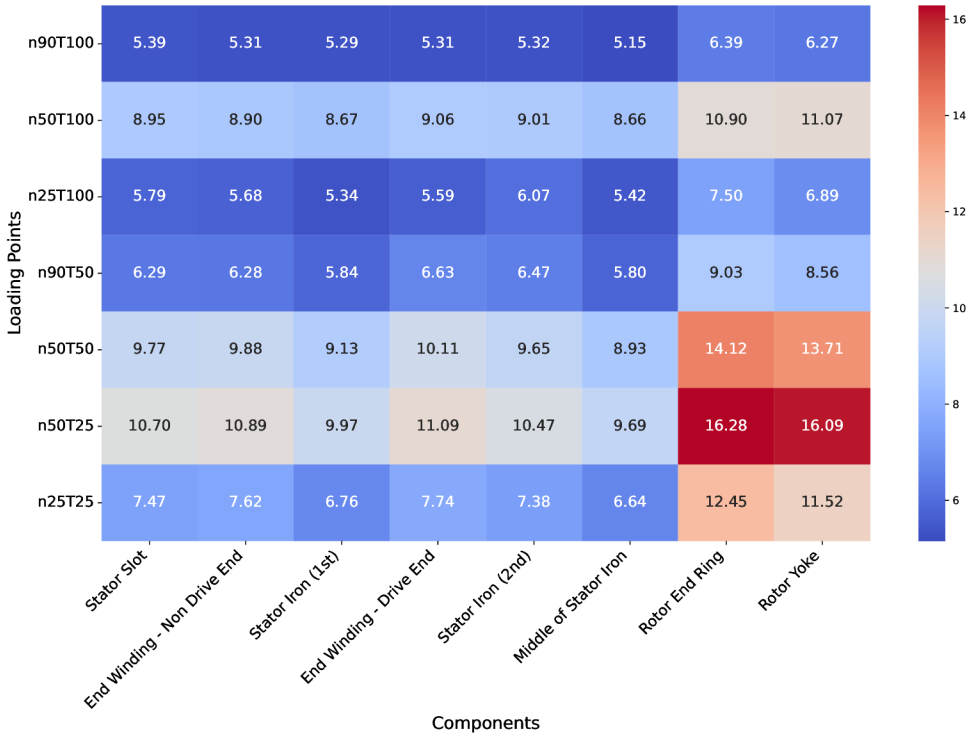

Figure 5.19: Heat map of relative temperature difference for two supplies across components and loading points.

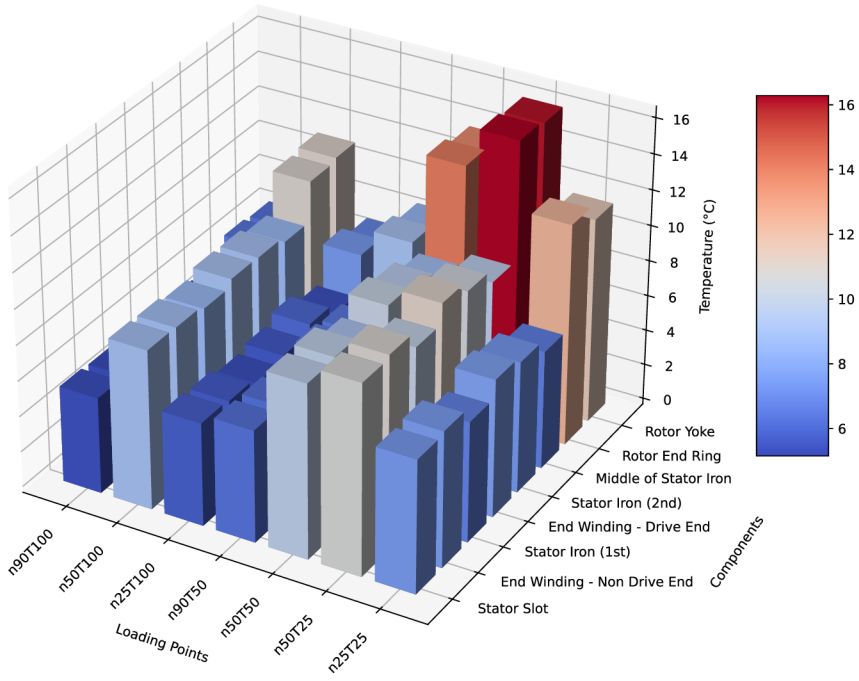

Figure 5.20: 3D bar chart of a relative temperature difference for two supplies.

It can be seen from the results that lower load points achieve higher deviations. However, the worst case occurs at load point P2, where a square wave voltage at modulation index of 0.5 causes the most ripple in current, and the ripple is lower at higher modulation index values and and also at lower modulation index values.

5.5 Comparison of measurement with simulation

The last section deals with the comparison of the measurement and simulation results. First, a comparison of the electrical quantities measured for the generator. Table 5.14 shows the comparison in absolute values, but for a better illustration, table 5.15 is shown here, where the values are given in relative magnitudes relative to the FEM.

Table 5.14: Comparison of measured and simulated electrical quantities for converter.

		n90T100	n50T100	n25T100	n90T50	n50T50	n50T25	n25T25
I_{rms} (A)	Meas.	10.40	10.37	10.43	7.51	7.40	6.57	6.47
	FEM	10.71	10.86	11.12	7.81	7.82	7.04	6.82
P_1 (W)	Meas.	5032.1	2937.8	1614.1	2580.2	1498.3	835.2	449.5
	FEM	5140.5	3045.5	1791.6	2650.6	1521.0	827.3	549.5
S (W)	Meas.	8126.0	7157.9	5441.3	5930.8	5122.82	4524.1	3282.8
	FEM	7764.4	6651.7	4705.0	5703.0	4707.6	4253.2	2740.4
Q (W)	Meas.	6380.4	6527.2	5196.3	5340.1	4898.8	4446.3	3251.9
	FEM	5819.3	5913.0	4350.1	5048.9	4455.3	4171.6	2684.4
λ (-)	Meas.	0.62	0.41	0.30	0.44	0.57	0.18	0.14
	FEM	0.66	0.46	0.38	0.47	0.32	0.20	0.20
P_2 (W)	Meas.	4502.0	2502.1	1246.6	2244.4	1251.5	625.3	313.0
	FEM	4526.4	2469.1	1204.0	2312.6	1231.3	594.7	364.8
n (rpm)	Meas.	1337.8	726.5	361.5	1305.5	724.3	725.2	362.3
	FEM	1301.3	725.3	348.8	1302.4	724.8	726.9	356.4
T (Nm)	Meas.	32.93	32.89	32.93	16.42	16.51	8.23	8.25
	FEM	33.2	32.50	32.96	16.96	16.22	7.81	9.77
P_{loss} (W)	Meas.	530.08	435.70	367.51	335.77	246.78	209.92	136.46
	FEM	685.94	625.80	619.79	390.03	325.25	257.47	207.43
η (%)	Meas.	89.47	85.17	77.23	86.99	83.53	74.87	69.64
	FEM	88.05	81.07	67.20	87.25	80.95	71.89	66.40

Table 5.15: Comparison of the simulation and measurement results. Positive values indicate that the measured value has been higher for converter.

	n90T100	n50T100	n25T100	n90T50	n50T50	n50T25	n25T25
Rel. inc. I_{rms} (%)	2.86	4.52	6.17	3.77	5.43	6.67	5.16
Rel. inc. P_1 (%)	2.10	3.54	9.91	2.66	1.49	-0.96	18.20
Rel. inc. S (%)	-4.66	-7.61	-15.65	-3.99	-8.82	-6.37	-19.79
Rel. inc. Q (%)	-9.65	-10.39	-19.45	-5.77	-9.96	-6.59	-21.14
Rel. inc. λ (%)	6.17	10.39	22.14	6.44	9.45	5.32	31.89
Rel. inc. P_2 (%)	0.54	-1.34	-3.54	2.95	-1.65	-5.14	14.21
Rel. inc. n (%)	-2.83	-0.16	-3.63	-0.24	0.07	0.24	-1.65
Rel. inc. T (%)	0.82	-1.20	0.09	3.18	-1.79	-5.45	15.59
Rel. inc. P_{loss} (%)	22.72	30.38	40.70	13.91	24.13	18.47	34.21
Rel. inc. η (%)	-1.67	-5.05	-14.92	0.30	-3.19	-4.14	-4.88

From the table 5.15 it can be concluded from the relative increase that the simulation was accurate for the current. For input power and output power, the deviations are also around 2-5 % except for the last operating point where the deviation is quite high. For apparent and relative power the differences are quite high, here the simulation was not very accurate. The power factor values coincide with the relative power, so the values are not completely accurate, but for the simulation they can be influenced by the rotor displacement and thus the air gap change. The output power values are very close except for the last operating point, the simulation was fairly accurate. These values are related to the relative torque increase, where at the last operating point the torque is inaccurate, which also creates a poor power output value. The same is true for the speed values. For these the simulation can be called reasonably accurate. For the total machine losses the simulation was very inaccurate and would require a thorough analysis. This is especially true for the losses with converter supply. The magnitudes of the efficiencies were reasonably accurate except for the third load point when the deviations are high. Simulation appears to be advantageous here.

In the second part of the section there is a comparison for the generator, here the same trend is followed. First the comparison in the table 5.16 and then for a better idea again the table with relative increase 5.17.

Table 5.16: Comparison of measured and simulated electrical quantities for generator.

		n90T100	n50T100	n25T100	n90T50	n50T50	n50T25	n25T25
I_{rms} (A)	Meas.	10.37	10.33	10.41	7.47	7.40	6.51	6.42
	FEM	10.47	10.57	11.02	7.62	7.50	6.79	6.55
P_1 (W)	Meas.	4981.7	2868.4	1569.9	2543.3	1433.5	767.6	409.3
	FEM	4960.5	2968.9	1756.0	2460.6	1488.4	772.6	457.9
S (W)	Meas.	6411.6	3621.1	1900.6	4558.1	2523.1	2203.4	1092.7
	FEM	6475.0	3703.1	2012.6	4647.1	2558.0	2297.4	1116.1
Q (W)	Meas.	4036.2	2210.2	1071.3	3782.5	2076.3	2065.3	1013.1
	FEM	4162.4	2212.0	981.6	3943.7	2080.1	2163.8	1018.0
λ (-)	Meas.	0.78	0.79	0.83	0.56	0.57	0.35	0.37
	FEM	0.77	0.80	0.87	0.53	0.58	0.34	0.41
P_2 (W)	Meas.	4505.1	2509.5	1249.3	2245.7	1252.1	624.8	313.2
	FEM	4502.7	2474.9	1201.0	2253.4	1275.3	618.4	312.1
n (rpm)	Meas.	1305.6	727.6	362.3	1305.8	723.8	725.4	361.7
	FEM	1302.1	720.2	348.2	1302.8	720.7	722.7	359.8
T (Nm)	Meas.	32.93	32.93	32.92	16.42	16.51	8.23	8.27
	FEM	33.02	32.81	32.94	16.52	16.90	8.17	8.28
P_{loss} (W)	Meas.	476.53	358.89	320.63	297.58	181.46	142.75	96.03
	FEM	605.65	557.12	593.69	322.35	275.49	211.16	177.09
η (%)	Meas.	90.43	87.49	79.58	88.30	87.34	81.40	76.54
	FEM	90.77	83.36	68.39	91.58	85.68	80.05	68.17

Comparing the simulation with the measurement, the table 5.17 shows that the simulation with the generator is slightly more accurate compared to the frequency converter. The relative differences are lower except for power consumption, total losses and efficiency. In the case of power, a higher deviation occurs for the two load points. For total losses, it is again shown that the given model was not sufficient to simulate the losses correctly, here a detailed analysis is needed. The simulation results for efficiency were not inaccurate. However, again a problem arises at the third and seventh load point where the error in the input power writes an error into the efficiency value.

Table 5.17: Comparison of the simulation and measurement results. Positive values indicate that the measured value has been higher for generator.

	n90T100	n50T100	n25T100	n90T50	n50T50	n50T25	n25T25
Rel. inc. I_{rms} (%)	0.99	2.24	5.56	1.93	1.37	4.12	2.11
Rel. inc. P_1 (%)	-0.43	3.39	10.60	-3.36	3.69	0.64	10.61
Rel. inc. S (%)	0.98	2.22	5.56	1.92	1.36	4.09	2.10
Rel. inc. Q (%)	3.03	0.08	-9.15	4.09	0.18	4.55	0.48
Rel. inc. λ (%)	-1.43	1.23	5.38	-5.48	2.38	-3.68	8.64
Rel. inc. P_2 (%)	-0.05	-1.40	-4.02	0.34	1.82	-1.04	-0.36
Rel. inc. n (%)	-0.27	-1.03	-4.06	-0.23	-0.44	-0.38	-0.52
Rel. inc. T (%)	0.28	-0.36	0.04	0.57	2.32	-0.66	0.16
Rel. inc. P_{loss} (%)	21.32	35.58	45.99	7.68	34.13	32.40	45.77
Rel. inc. η (%)	0.37	-4.95	-16.35	3.58	-1.94	-1.69	-12.27

Table 5.18 shows the percentages of how much the total losses increased from the generator to the inverter power supply. These values are compared between measurement and simulation.

Table 5.18: Comparison of relative increase in total losses from sine supply to PWM supply for different load points with simulation and measurement.

		Total loss	
		Simulation	Measurement
PWM-caused loss (%)	P1 (n90T100)	11.71	10.10
	P2 (n50T100)	10.98	17.63
	P3 (n25T100)	4.21	12.76
	P4 (n90T50)	17.35	11.37
	P5 (n50T50)	15.30	26.47
	P6 (n50T25)	17.99	32.00
	P7 (n25T25)	14.63	29.63

For load point 1, the simulation of relative increase is close, but it cannot be determined if this is a mere coincidence because the other load points do not match the accuracy.

Conclusion

The thesis dealt with the measurement and simulation of an induction machine with two types of power supply, namely a frequency converter and a generator. The first three chapters dealt with a literature research for an induction motor with a frequency converter and methods of measuring and evaluating its losses.

The fourth chapter starts by describing the creation of a model according to the given dimensions of the SEMTEC motor. The created model is shown in Figure 5.4. The properties of the model were set to replicate the real machine. The generator supply simulation was then performed for this model. Then there is explanation of the process of performing FFT analysis on the measured voltage waveform to obtain the necessary harmonics to construct the voltage equation. Here, it was necessary to limit the number of harmonics so that they could be inputted into the FEM software. This section is followed by the PWM simulation section and also a brief comparison with the generator simulation. The main differences between the two source simulations were mainly in the torque ripple and magnitude of losses, with the torque ripple being almost five times larger and the magnitude of the total losses increasing by 80 W for the first load point, mainly in the core losses.

The fifth chapter describes everything about measurement. First, a section on the methodology and how the measurements were carried out is presented. The first test included a retardation test to obtain mechanical losses. The results are given in Table 5.4. The following are measurement results with figures for two supplies. By comparing the measurements with each other, in the relative difference of the two supplies, it can be seen where the additional losses of the frequency converter are located compared to the generator sine supply. The main locations with additional losses include the rotor, stator slot, and end winding. Among the worst load points in terms of measured characteristics is load point P2, where the modulation index of 0.5 causes the most ripple in the current. Also, low load points, where speed and torque are low and the motor is in the worse operating zones. The last section compares the measurements and simulations together. Here, the simulation proved to be accurate enough for certain electrical quantities, but for the total machine losses the simulation was very inaccurate. It is very difficult to simulate the losses for a PWM power supply and would require much more detailed analysis and investigation.

Literature

[1] Čestmír Ondrušek. *Elektrické stroje*. Skriptum. Brno.

[2] Lassi Aarniovuori et al. "Measurement Accuracy Requirements for the Efficiency Classification of Converters and Motors". In: *2019 21st European Conference on Power Electronics and Applications (EPE '19 ECCE Europe)*. 2019, P.1–P.10. DOI: 10.23919/EPE.2019.8915560.

[3] Josef Škoda. "Five-phase induction machine". Master's thesis. Brno: Brno University of Technology, Faculty of Electrical Engineering, Communication, Department of Power Electrical, and Electronic engineering, 2020.

[4] Anibal T. De Almeida, Fernando J.T.E. T. E. Ferreira, and Joao A.C. Fong. "Standards for Efficiency of Electric Motors". In: *IEEE Industry Applications Magazine* 17.1 (2011), pp. 12–19. DOI: 10.1109/MIAS.2010.939427.

[5] Minhaj Zaheer et al. "Converter-Fed Induction Motor Finite Element Analysis With Different Time Steps". In: *2020 XI International Conference on Electrical Power Drive Systems (ICEPDS)*. 2020, pp. 1–7. DOI: 10.1109/ICEPDS47235.2020.9249341.

[6] E. Nicol Hildebrand and H. Roehrdanz. "Losses in three-phase induction machines fed by PWM converter". In: *IEEE Transactions on Energy Conversion* 16.3 (2001), pp. 228–233. DOI: 10.1109/60.937201.

[7] Lassi Aarniovuori et al. "Experimental Investigation of the Losses and Efficiency of 75 kW Induction Motor Drive System". In: *IECON 2019 - 45th Annual Conference of the IEEE Industrial Electronics Society*. Vol. 1. 2019, pp. 1052–1058. DOI: 10.1109/IECON.2019.8926814.

[8] Lassi Aarniovuori et al. "Measurements and Simulations of DTC Voltage Source Converter and Induction Motor Losses". In: *IEEE Transactions on Industrial Electronics* 59.5 (2012), pp. 2277–2287. DOI: 10.1109/TIE.2011.2161061.

[9] A. Boglietti et al. "Factors Affecting Losses in Induction Motors with Non-Sinusoidal Supply". In: *2007 IEEE Industry Applications Annual Meeting*. 2007, pp. 1193–1199. DOI: 10.1109/07IAS.2007.187.

[10] Jeong-Jong Lee et al. “Loss distribution of three-phase induction motor fed by pulsewidth-modulated inverter”. In: *IEEE Transactions on Magnetics* 40.2 (2004), pp. 762–765. DOI: 10.1109/TMAG.2004.825445.

[11] Minhaj Zaheer et al. “Comparison of Commercial and Open-Source FEM Software: A Case Study”. In: *IEEE Transactions on Industry Applications* 56.6 (2020), pp. 6411–6419. DOI: 10.1109/TIA.2020.3015827.

[12] Miroslav Lípa. “Calorimetric measurement of electrical machines”. Semestral thesis. Brno: Brno University of Technology, Faculty of Electrical Engineering, Communication, Department of Power Electrical, and Electronic engineering, 2023.

[13] Miroslav Lípa. “Losses in asynchronous machines supplied by a frequency converter”. Semestral thesis. Brno: Brno University of Technology, Faculty of Electrical Engineering, Communication, Department of Power Electrical, and Electronic engineering, 2024.

[14] Petr Fiala. “Induction motor powered from inverter”. Master’s thesis. Brno: Brno University of Technology, Faculty of Electrical Engineering, Communication, Department of Power Electrical, and Electronic engineering, 2015.

[15] Juha Pyrhönen, Valéria Hrabovcová, and R. Scott Semken. *Electrical machine drives control: An introduction.* John Wiley & Sons Ltd, 2016. ISBN: 9781119260455.

[16] Petr Bernat. “Negative effects of frequency converters on an induction motor”. Dissertation thesis. Ostrava: Technical University of Ostrava, Faculty of Electrical Engineering and Computer Science, Department of Electrical Power Engineering, 2006.

[17] Institute for Electrical Energy Conversion. *Part 5: Inverter-fed induction machines.* Selected part of the lectures. Darmstadt, Germany.

[18] Hannu Kärkkäinen. “Converter-fed induction motor losses: determination with IEC methods”. Master’s thesis. Lappeenranta, Finland: Lappeenranta University of Technology, LUT School of Energy Systems, Electrical Engineering, 2015.

[19] L. Aarniovuori et al. “DTC IM drive losses — Simulation and measurements”. In: *The XIX International Conference on Electrical Machines - ICEM 2010.* 2010, pp. 1–6. DOI: 10.1109/ICELMACH.2010.5608190.

[20] David Samec. “Scalar control of induction motor”. Bachelor thesis. Praha: České vysoké učení technické v Praze, Fakulta elektrotechniky, Katedra elektrických pohonů a trakce, 2023.

[21] Jan Kuřina. “Controlof synchronous servomotor with microprocessor platform Texas Instruments”. Master’s thesis. Praha: České vysoké učení technické v Praze, Fakulta strojní, Ústav mechaniky,biomechaniky a mechatroniky, 2019.

[22] Michal Vidlák. “Induction machine control techniques and models”. Master’s thesis. Brno: Brno University of Technology, Faculty of Electrical Engineering, Communication, Department of Power Electrical, and Electronic engineering, 2019.

[23] Lassi Aarniovuori et al. “Analysis of 37-kW Converter-Fed Induction Motor Losses”. In: *IEEE Transactions on Industrial Electronics* 63.9 (2016), pp. 5357–5365. DOI: 10.1109/TIE.2016.2555278.

[24] Lassi Aarniovuori et al. “Analytical Evaluation of High-Efficiency Induction Motor Losses”. In: *2019 IEEE International Electric Machines Drives Conference (IEMDC)*. 2019, pp. 1501–1507. DOI: 10.1109/IEMDC.2019.8785380.

[25] Dongdong Zhang et al. “Loss characteristic analysis of small and medium-sized induction motors fed by PWM inverter based on the experiment measurements”. In: *IECON 2017 - 43rd Annual Conference of the IEEE Industrial Electronics Society*. 2017, pp. 2053–2058. DOI: 10.1109/IECON.2017.8216345.

[26] Shaoshen Xue et al. “Iron Loss Model for Electrical Machine Fed by Low Switching Frequency Inverter”. In: *IEEE Transactions on Magnetics* 53.11 (2017), pp. 1–4. DOI: 10.1109/TMAG.2017.2696360.

[27] *IEC 60034-2-1: Rotating electrical machines - Part 2-1: Standard methods for determining losses and efficiency from tests (excluding machines for traction vehicles)*. ed. 2. International standard.

[28] *IEC 60034-2-3: Rotating electrical machines - Part 2-3: Specific test methods for determining losses and efficiency of converter-fed AC motors*. International standard.

[29] Minhaj Zaheer. “Evaluation of open-source FEM software performance in analysing converter-fed induction machine losses”. Dissertation. Lappeenranta, Finland: Lappeenranta–Lahti University of Technology LUT, School of Energy Systems, Department of Electrical Engineering, 2021.

[30] Shahab Khalghani. “Analytical loss calculation tool for an induction motor”. Master’s thesis. Lappeenranta, Finland: Lappeenranta University of Technology, LUT School of Energy Systems, Electrical Engineering, 2020.

[31] Sami Kanerva. “Simulation of Electrical Machines, Circuits and Control Systems Using Finite Element Method and System Simulator”. Dissertation. Espoo, Finland: Helsinki University of Technology, Department of Electrical and Communications Engineering, Laboratory of Electromechanics, 2005.

[32] Valéria Hrabovcová, Pavol Rafajdus, and Pavol Makyš. *Analýza elektrických strojů*. Žilina: EDIS-vydavatelské centrum ŽU, 2017. ISBN: 978-80-554-1323-5.

[33] Hannu Kärkkäinen and Lassi Aarniovouri. *Presentation from lectures, Efficiency determination methods*. Lecture presentation. Espoo, Finland, 2020.

[34] Pavel Ponomarev. *SEMTEC Report Elmer FEM - Induction Machine Tutorial*. May 2017. DOI: 10.13140/RG.2.2.18599.75688.

[35] Lassi Aarniovuori. *SEMTEC test motor datasheet*. Datasheet. Lappeenranta University of Technology, LUT School of Energy Systems, Electrical Engineering.

[36] Lassi Aarniovuori Hannu Kärkkäinen. *Experimental tests for simulation models verification*. Presentation. Lappeenranta University of Technology, LUT School of Energy Systems, Electrical Engineering.